

**IMAGE-BASED FLOW ANALYSIS AND FLUID  
STRUCTURE SIMULATION USING 3D COMPUTATIONAL  
MODELS OF MYOCARDIAL INFARCTION PATIENTS**

**CHAN BEE TING**

**FACULTY OF ENGINEERING  
UNIVERSITY OF MALAYA  
KUALA LUMPUR**

**2018**

**IMAGE-BASED FLOW ANALYSIS AND FLUID  
STRUCTURE SIMULATION USING 3D  
COMPUTATIONAL MODELS OF MYOCARDIAL  
INFARCTION PATIENTS**

**CHAN BEE TING**

**THESIS SUBMITTED IN FULFILMENT OF THE  
REQUIREMENTS FOR THE DEGREE OF DOCTOR OF  
PHILOSOPHY**

**FACULTY OF ENGINEERING  
UNIVERSITY OF MALAYA  
KUALA LUMPUR**

**2018**

**UNIVERSITY OF MALAYA**  
**ORIGINAL LITERARY WORK DECLARATION**

Name of Candidate: Chan Bee Ting

Matric No: KHA

Name of Degree: Doctor of Philosophy

Title of Project Paper/Research Report/Dissertation/Thesis ("this Work"):

Image-Based Flow Analysis and Fluid Structure Simulation using 3D Computational  
Models of Myocardial Infarction Patients

Field of Study: Biomedical Engineering

I do solemnly and sincerely declare that:

- (1) I am the sole author/writer of this Work;
- (2) This Work is original;
- (3) Any use of any work in which copyright exists was done by way of fair dealing and for permitted purposes and any excerpt or extract from, or reference to or reproduction of any copyright work has been disclosed expressly and sufficiently and the title of the Work and its authorship have been acknowledged in this Work;
- (4) I do not have any actual knowledge nor do I ought reasonably to know that the making of this work constitutes an infringement of any copyright work;
- (5) I hereby assign all and every rights in the copyright to this Work to the University of Malaya ("UM"), who henceforth shall be owner of the copyright in this Work and that any reproduction or use in any form or by any means whatsoever is prohibited without the written consent of UM having been first had and obtained;
- (6) I am fully aware that if in the course of making this Work I have infringed any copyright whether intentionally or otherwise, I may be subject to legal action or any other action as may be determined by UM.

Candidate's Signature

Date:

Subscribed and solemnly declared before,

Witness's Signature

Date:

Name:

Designation:

**IMAGE-BASED FLOW ANALYSIS AND FLUID STRUCTURE SIMULATION  
USING 3D COMPUTATIONAL MODELS OF MYOCARDIAL INFARCTION**

**PATIENTS**

**ABSTRACT**

Myocardial infarction (MI), or commonly known as heart attack, leads to high mortality and morbidity worldwide. Early detection of MI improves treatment strategy and increases patient's survival. Intraventricular blood flow dynamics has an incremental value in the evaluation of heart disease at an early stage because it changes accordingly in response to structural changes of the heart. Maladaptive intraventricular blood flow dynamics and excessive flow energetics were speculated as compensatory mechanisms to preserve ventricular function at the early stage of heart disease. However, several contradictory findings remain unexplained; the correlations between MI parameters and intraventricular flow variables were not quantitatively evaluated. This project aims to identify potential flow indicators and investigate the impact of MI characteristics on LV dysfunction in MI patients. To achieve this aim, phase contrast magnetic resonance (PC-MR) images of thirty MI patients and twenty healthy volunteers were analysed. A consistent measurement method for flow propagation velocity ( $V_p$ ) has been proposed to overcome the influences of different LV sizes and inflow jet directions. In image-based flow analysis, intraventricular flow variables including  $V_p$ , vortex parameters and flow energetic indices were evaluated. Among them, the vortex kinetic energy (KE) could potentially indicate LV dysfunction in MI patients. Generic 3D fluid-structure interaction models were developed to investigate the relationships between MI parameters and intraventricular flow related variables. The model analysis showed that strong flow acceleration, left ventricular mechanical dyssynchrony, and vortex-infarct interaction are predominant factors leading to excessive flow energy dissipation in MI. The high systolic KE flow fluctuation index ( $E'$ ) reflects energetic flow acceleration while low diastolic  $E'$

represents efficient diastolic filling flow. The correlation between systolic and diastolic  $E'$  indicates LV systolic-diastolic coupling mechanism.

Keywords: Myocardial infarction, vortex, dissipation, fluctuation, energetic

University of Malaya

**ANALISIS ALIRAN BERDASARKAN IMEJ DAN INTERAKSI CECAIR  
STRUKTUR SIMULASI DENGAN PENGGUNAAN 3D MODEL PENGIRAAN  
DARIPADA PESAKIT INFARKSI MIOKARDIUM**

**ABSTRAK**

Infarksi miokardium (MI) atau biasanya dikenali sebagai penyakit jantung menyebabkan kematian dan morbiditi dalam kadar yang tinggi di seluruh dunia. Pengesanan MI di peringkat awal membantu rawatan strategi yang berkesan dan memanjangkan hidup pesakit. Aliran darah dalam ventrikel menjadi semakin penting dalam pengesanan penyakit jantung di peringkat awal sebab ia bertindak balas atas perubahan struktur jantung. Ketidakesesuaian dinamik aliran darah dalam ventrikel dan tenaga aliran berlebihan telah dispekulasi sebagai mekanisme pampasan untuk mencapai fungsi ventrikel di peringkat awal penyakit jantung. Walau bagaimanapun, beberapa pencanggahan tidak diterangkan dan korelasi antara ciri-ciri MI dan pembolehubah dinamik aliran darah dalam ventrikel tidak dinilai secara kuantitatif. Projek ini bertujuan untuk mengenal pasti penunjuk aliran darah yang berpotensi dan faktor risiko yang menyebabkan disfungsi ventrikel kiri (LV) pada pesakit MI. Bagi mencapai tujuan tersebut, analisis telah dijalankan dengan penggunaan imej “phase contrast magnetic resonance” (PC-MR) daripada tiga puluh orang pesakit MI dan dua puluh orang sukarelawan yang sihat. Satu cara pengukuran  $V_p$  telah dicadangkan bagi mengatasi kesan-kesan saiz LV dan jet aliran masuk. Dalam analisis aliran, beberapa pembolehubah telah diukur termasuklah  $V_p$ , parameter-parameter vorteks dan energetik aliran. Antara pembolehubah tersebut, tenaga kinetik vorteks berpotensi untuk menunjukkan disfungsi LV pada pesakit MI. Model-model 3D infarksi dengan interaksi cecair struktur (FSI) direka untuk menyiasat hubungan antara ciri-ciri MI dan penunjuk aliran darah dalam ventrikel. Pecutan aliran yang kuat, mekanikal disynchorny LV, dan interaksi vorteks-infarksi adalah faktor-faktor utama yang menyebabkan pelepasan tenaga aliran yang

berlebihan dalam MI. Tenaga kinetik “flow fluctuation index” (E’) yang tinggi di systole berperanan sebagai pecutan aliran yang bertenaga manakala E’ yang rendah di diastole bercadangkan pengisian aliran darah yang berkesan di diastole. Hubungan antara E’ di systole dan diastole menunjukkan mekanisme gandingan LV antara systole dan diastole.

Kata kunci: Infarksi miokardium, vorteks, pelepasan, pergolakan, tenaga

University of Malaya

## ACKNOWLEDGEMENTS

First of all, I would like to thank my wonderful supervisor, Associate Professor Ir. Dr. Lim Einly, for her consistent supervision and guidance during my doctoral research. I am also grateful for her endless encouragement, support, and tolerance. I am thankful to have my co-supervisor, Associate Professor Dr. Socrates Dokos from the Graduate School of University of New South Wales (UNSW). His expertise and contribution, particularly in the computational modelling work, made this project go smoothly. I would like to thank him for his patience and guidance during my attachment in UNSW. My special gratitude goes to Associate Professor Dr. Yeoh Hak Koon, my ex-supervisor, who was involved in this project and co-supervised me for two years before leaving the Department of Chemical Engineering, University of Malaya. Dr. Yeoh was extremely helpful in every detail especially in the derivation and explanation of mathematical equations of fluid mechanics. I would like to thank Ir. Dr. Liew Yih Miin for her effort in the design of clinical study protocol and the reconstruction of patient-specific models. Many thanks to Dr. Amr Al-Abed (post-doctoral fellow in UNSW), Azam Ahmad Bakir (PhD student in UNSW) and Leong Chin Neng (PhD student in Asian Cardiac Engineering Lab) for the effective discussions regarding ventricular modelling works. I would like to offer my appreciation to Dr. Sridhar Ganiga Srinivasaiah (cardiologist), Professor Dr. Chee Kok Han (cardiologist) and Professor Dr. Yang Faridah Abdul Aziz (radiologist), Siti Salwa, Mohd Azwan (radiographers), Anita Chia Hui Ling, Nor Ashikin and Nur Wani (medical lab technologists) from University Malaya Medical Centre. Their great help in patient recruitment and scanning procedure are very much appreciated. Last but not least, my deepest gratitude goes to my husband, parents, siblings, best friends and colleagues in the Asian Cardiac Engineering Laboratory for their unconditional love and support during my PhD study.

## TABLE OF CONTENTS

Abstract .....	iii
Abstrak .....	v
Acknowledgements .....	vii
Table of Contents .....	viii
List of Figures .....	xii
List of Tables.....	xv
List of Symbols and Abbreviations.....	xvi
List of Appendices .....	xx
<b>CHAPTER 1: INTRODUCTION.....</b>	<b>1</b>
1.1 Motivation.....	1
1.2 Objectives .....	2
1.3 Thesis Scope .....	3
1.4 Thesis Outline.....	3
<b>CHAPTER 2: LITERATURE REVIEW.....</b>	<b>5</b>
2.1 Heart anatomy and physiology .....	5
2.2 Cardiac cycle .....	6
2.3 Myocardial infarction (MI).....	8
2.4 Heart Disease and Intraventricular Blood Flow Dynamics .....	11
2.4.1 Clinical flow analysis studies .....	11
2.4.2 Computational flow studies .....	13
2.5 Summary.....	15

**CHAPTER 3: IMAGE-BASED FLOW ANALYSIS OF LEFT VENTRICULAR  
FLOW PROPAGATION VELOCITY MEASUREMENT ..... 16**

3.1 Introduction..... 16

3.2 Literature review..... 16

3.3 Methodology..... 18

    3.3.1 Study group ..... 18

    3.3.2 Image Acquisition ..... 19

    3.3.3 Image Processing and Preparation ..... 20

    3.3.4 Vp Measurement Methods ..... 21

        3.3.4.1 Non-adaptive (NA) Method ..... 22

        3.3.4.2 Adaptive Positions (AP) Method ..... 22

        3.3.4.3 Adaptive Vectors (AV) Method..... 23

    3.3.5 Vp Acquisition ..... 23

    3.3.6 Strain Rate Analysis Using Cardiovascular Magnetic Resonance Feature  
        Tracking (CMR-FT) ..... 24

    3.3.7 Statistical Analysis ..... 25

3.4 Results ..... 25

3.5 Discussion..... 30

3.6 Conclusions ..... 33

**CHAPTER 4: IMAGE-BASED FLOW ANALYSIS OF INTRAVENTRICULAR  
FLOW VARIABLES ..... 34**

4.1 Introduction..... 34

4.2 Literature review..... 34

4.3 Methodology..... 36

    4.3.1 Study Population ..... 36

    4.3.2 Image acquisition ..... 37

4.3.2.1	Echocardiography.....	37
4.3.2.2	MRI	38
4.3.2.3	MRI image analyses .....	39
4.3.3	Statistical analysis .....	43
4.4	Results .....	43
4.5	Discussion.....	48
4.6	Conclusion .....	52

**CHAPTER 5: INVESTIGATION OF MYOCARDIAL INFARCTION AND INTRAVENTRICULAR FLOW VARIABLES USING 3D FLUID STRUCTURE SIMULATION ..... 53**

5.1	Introduction.....	53
5.2	Literature Review .....	53
5.3	Methodology.....	56
5.3.1	LV geometry.....	56
5.3.2	Electrophysiology.....	58
5.3.3	Solid mechanics.....	59
5.3.4	Excitation-contraction coupling .....	62
5.3.5	Fluid mechanics.....	62
5.3.6	Boundary conditions at inlet and outlet.....	62
5.3.7	Infarct models .....	64
5.3.8	Simulation models .....	66
5.3.9	Discretisation and implementation .....	67
5.3.10	3D assessment of flow energetic indices.....	69
5.3.11	Vortex identification and assessments.....	70
5.3.12	Myocardial assessment of Systolic Dyssynchrony Index (SDI) .....	71
5.4	Results .....	71

5.4.1.1	Assessment of LV dyssynchrony .....	71
5.4.1.2	Vortex evolution.....	72
5.4.1.3	Viscous energy dissipation.....	74
5.4.1.4	Analysis of flow energetic indices (DI, E' and W').....	76
5.4.1.5	Correlations among vortex, flow energetics and LVEF.....	77
5.5	Discussion.....	78
5.5.1	Clinical implications.....	82
5.6	Conclusion .....	83
<b>CHAPTER 6: CONCLUSION AND RECOMMENDATIONS .....</b>		<b>84</b>
6.1	Summary and conclusion.....	84
6.2	Recommendation for future studies.....	85
References .....		88
List of Publications and Papers Presented .....		102
Appendix .....		103

## LIST OF FIGURES

Figure 2.1: Anatomy of human heart (Applegate, 2011) .....	6
Figure 2.2: Pressure-volume loop during a cardiac cycle (Fung, 1997) .....	8
Figure 2.3: Progressive cell death (necrosis) in MI ( <i>Coronary Artery Disease</i> , 2015) ....	9
Figure 2.4: Evidence of MI (white region indicated by arrow) in late gadolinium enhancement MRI (Plein, Ridgway, & Greenwood, 2011) .....	10
Figure 3.1: LV landmark points and location of distance lines. MLT=Mitral Leaflet Tips. ....	21
Figure 3.2: The three proposed $V_p$ measuring techniques. Arrows at each measurement position indicate the velocity components (found along the full line) that will be used to calculate the mean forward flow. NA=Non-adaptive; AP=Adaptive Positions; AV=Adaptive Vectors.....	23
Figure 3.3: Measurement positions at 4 cm and one-half LV height (based on the AV method) for different LV sizes in a (a) healthy volunteer, (b) patient without dilated LV and (c) patient with dilated LV during flow deceleration. Colour map represents velocity magnitude in cm/s, with black streamline arrows representing flow direction and white arrows indicating all of the forward velocity components at the measurement positions .....	26
Figure 3.4: Measurement positions and intraventricular flow using the three $V_p$ measuring techniques in two post-infarct patients: (a) without dilated LV (EDV = 128 mL) and (b) with dilated LV (EDV = 300 mL). Colour map represents mean diastolic velocity magnitude in cm/s, with black streamline arrows representing flow direction and white arrows within the LV cavity indicating all forward velocity components at the measurement positions at peak E-wave. The resulting $V_p$ values for these two post-infarct patients are shown in (c) for no dilated LV (EDV = 128 mL) (left) and dilated LV (EDV = 300 mL) (right) .....	27
Figure 3.5: Summary of $V_p$ values at different measurement positions using the NA, AP and AV methods.....	29
Figure 3.6: The correlation between $SR_{IVR}$ and $V_p$ values obtained using the NA, AP and AV methods. The correlation coefficients are significant as the p-values are below the set threshold of 0.05. ....	30
Figure 4.1: Image axes of phase contrast MR image .....	39
Figure 4.2: Intraventricular flow patterns of a healthy subject, PNEF and PREF patients during diastole and systole. The flow directions were indicated by the purple arrow and	

arrows on the yellow velocity streamlines while the vortex appearance was indicated by the blue (clockwise) and red regions (counter-clockwise)..... 44

Figure 4.3: Comparison of intraventricular flow variables among the three subject groups. The box plots indicate the first to third quartiles and the midline in between indicates the median; the whiskers represent maximum and minimum values. Significant difference between the groups were indicated by **\*\***( $p < 0.01$ ) and **\***( $p < 0.05$ )..... 45

Figure 4.4: Correlations between  $E'$  and myocardial properties (a, b, d) as well as DI and flow variables (c, e) in MI patients. Significant correlations ( $p < 0.05$ ) were indicated by filled data points..... 47

Figure 4.5: Local distributions of (a) phase-averaged  $E'$  and (b) velocity in the LVOT plane of a healthy, PNEF and PREF subject. The profile of a single patient represents his/her respective groups. Vortex is indicated by the white circular regions in (a). The comparison of  $E'$  inside and outside of the vortical regions is shown in (c) with significant levels at  $p < 0.001$  (\*\*\*) and  $p < 0.05$  (\*). ..... 48

Figure 5.1: LV geometry and dimensions..... 57

Figure 5.2: Results of fibre orientation in (a) 3D LV geometry where the colour legend represents fibre angle, (b) fibre angle across the myocardium (myocardial location was indicated by the red line in LV geometry) ..... 60

Figure 5.3: Inflow velocity waveform at mitral valve of healthy LV ..... 63

Figure 5.4: Constructed infarct LVs with varying infarct size and multiplicity. The red and blue colours represent infarct and remote regions respectively, whilst colour in between the two indicates border zone. .... 65

Figure 5.5: Comparison of stress-strain curves under uniaxial tension along fibre direction for healthy and MI LV. .... 66

Figure 5.6: Flow chart of simulation process where  $n$  was 3 cycles in this study. .... 68

Figure 5.7: Endocardial Green-Lagrange fibre strain in healthy and infarct LV (REF-5+5) during end systole (a, b) and end diastole (c, d). Negative strain represents muscle fibre shortening while positive strain represents fibre lengthening. Black grid on endocardium indicates infarct. .... 72

Figure 5.8: Vortex evolution in healthy (a-d) and REF-10+10 (e-h) in LVOT view. The 3D vortex is visualised by magenta isosurfaces ( $\lambda_2 = -300 \text{ s}^{-2}$ ) and the colour map represents the magnitude of velocity streamline (m/s). .... 74

Figure 5.9: Vortex appearance with velocity streamlines in front view (a-c) and endocardial viscous EL (d-i) in REF-5+5, REF-10 and REF-10+10 during mid-systole. The endocardial viscous EL is shown in front view (d-f) and sagittal view (g-i). White

circular lines on endocardium indicates infarct region. Colour maps represent velocity magnitude (m/s) (top) and endocardial viscous EL (mW/mL) (bottom). Vortex is visualised by magenta colour isosurfaces ( $\lambda_2 = -300 \text{ s}^{-2}$ ) ..... 75

Figure 5.10: Percentage difference of intraventricular flow energetic indices (DI, E' and W') between healthy LV and each infarct model in systole (a) and diastole (b)..... 77

Figure 5.11: Relationships among E', LVEF and vortex during systole (a, b) and diastole (c, d). ..... 78

Figure B.1: Procedure to obtain angled velocity components: (a) reference line and one of its tilted directions; (b) parallel velocity components,  $V_\tau$  derived from velocity vectors,  $V$  at one-third measurement position. .... 107

University of Malaysia

## LIST OF TABLES

Table 3.1: Subject demographics .....	19
Table 4.1: Subject demographics .....	37
Table 4.2: Univariate and multivariate linear regression analyses for independent correlates of LVEF in patients (PNEF & PREF) .....	46
Table 5.1: Model settings in FSI simulation .....	67

University of Malaya

## LIST OF SYMBOLS AND ABBREVIATIONS

### List of Abbreviations

AP	:	Adaptive-Positions
AV	:	Adaptive-Vectors
BSA	:	Body surface area
CFD	:	Computational fluid dynamics
CMR-FT	:	Cardiovascular magnetic resonance feature tracking
CMMD	:	Colour M-mode Doppler
DBP	:	Diastolic blood pressure
echo-PIV	:	Echocardiographic Particle Imaging Velocimetry
ESV	:	End Systolic Volume
EDP	:	End Diastolic Pressure
EDV	:	End Diastolic Volume
EL	:	Energy loss
FSI	:	Fluid Structure Interaction
GLS	:	Global Longitudinal Strain
IBM	:	Immersed boundary method
RECVM	:	Regional Enhancement of Contractility at Viable Myocardium
IHD	:	Ischemic Heart Disease
IVR	:	Isovolumic relaxation
IVC	:	Isovolumic contraction
KE	:	Kinetic Energy
LAP	:	Left atrial pressure
LV	:	Left Ventricle
LVEF	:	Left Ventricular Ejection Fraction

LVMD	:	Left ventricular mechanical dyssynchrony
LVOT	:	Left Ventricular Outflow Tract
LVP	:	Left ventricular pressure
MI	:	Myocardial infarction
MLT	:	Mitral leaflet tips
MRI	:	Magnetic Resonance Imaging
NA	:	Non-Adaptive
PC-MRI	:	Phase Contrast Magnetic Resonance Imaging
PNEF	:	Patients with Normal Ejection Fraction
PREF	:	Reduced Ejection Fraction
Re	:	Reynolds number
SBP	:	Systolic blood pressure
SDI	:	Systolic Dyssynchrony Index
SI	:	Sphericity index
SR <sub>IVR</sub>	:	Isovolumic relaxation strain rate
SV	:	Stroke volume
SVR	:	Surgical ventricular restoration
TE	:	Echo Time
TR	:	Relaxation time
TPS-SD	:	Time-to-peak systolic standard deviation
V <sub>p</sub>	:	Flow propagation velocity
1D	:	One-dimensional
2D	:	Two-dimensional
3D	:	Three-dimensional
4D	:	Four-dimensional

## List of Symbols

$V_n$	:	orthogonal velocity components directed towards the apex (m/s)
$N$	:	total number of velocity components
$r$	:	Pearson's correlation coefficient
$\psi$	:	Stream function
$\omega$	:	Vorticity (1/s)
$\omega_0$	:	Phase-averaged vorticity (1/s)
$v_x$	:	Velocity component in x-direction (m/s)
$v_y$	:	Velocity component in y-direction (m/s)
$v_z$	:	Velocity component in z-direction (m/s)
$v_{x0}$	:	phase-averaged velocity in x-direction (m/s)
$v_{y0}$	:	phase-averaged velocity in y-direction (m/s)
$v_{z0}$	:	phase-averaged velocity in z-direction (m/s)
$\rho$	:	Blood density (kg/m <sup>3</sup> )
$\mu$	:	Blood viscosity (Pa.s)
$\nu$	:	Blood kinematic viscosity (m <sup>2</sup> /s)
$V$	:	Activation variable
$R$	:	recovery variable
$\underline{\underline{\sigma}}$	:	Conductivity tensor (S/m)
$\sigma_f$	:	conductivity along fibre direction (S/m)
$\sigma_s$	:	conductivity along sheet direction (S/m)
$\sigma_n$	:	conductivity along normal to sheet direction (S/m)
$\vec{F}$	:	fibre vector
$\vec{S}$	:	normal-to-sheet vector
$\vec{N}$	:	normal vector

$\Psi_s$	:	strain energy function
$T_a$	:	Active stress (kPa)
$\underline{\underline{T}}$	:	second Piola Kirchoff stress tensor (kPa)
$\underline{\underline{E}}$	:	Green-Lagrange strain tensor
$Q_{\text{mitral}}$	:	Volumetric flow rate at mitral valve (ml/s)
$Q_{\text{aorta}}$	:	Volumetric flow rate at aortic valve (ml/s)
$R_{\text{mitral}}$	:	Mitral valve resistance (mmHg·s·ml <sup>-1</sup> )
$R_{\text{aorta}}$	:	Aortic valve resistance (mmHg·s·ml <sup>-1</sup> )
$R_{\text{systemic}}$	:	Systemic vascular resistance (mmHg·s·ml <sup>-1</sup> )
$P_{\text{mitral}}$	:	Pressure at mitral valve (mmHg)
$P_{\text{aorta}}$	:	Pressure at aortic valve (mmHg)
$P_{\text{LV}}$	:	Pressure in LV (mmHg)
$P_{\text{systemic}}$	:	Systemic pressure (mmHg)
DI	:	Energy dissipation index
$E'$	:	Kinetic energy flow fluctuation index
$W'$	:	Vorticity flow fluctuation index

## LIST OF APPENDICES

Appendix A: Medical Ethics Approval .....	103
Appendix B: Determination of the Angled Velocity Components .....	106
Appendix C: Derivation of Stress Tensor .....	108

University of Malaya

## CHAPTER 1: INTRODUCTION

### 1.1 Motivation

Ischemic heart disease (IHD) is the leading cause of death worldwide (World Health Organization, 2015). IHD is characterised by the lack of blood supply to the heart muscles, which eventually leads to heart muscle injury. Prolonged ischemia can lead to heart muscle necrosis, which is commonly known as heart attack or Myocardial Infarction (MI). An early detection of MI can improve the treatment strategy and prolong patient's survival.

Minor changes in the geometry and myocardial wall deformation immediately affect the intraventricular blood flow dynamics. Hence, intraventricular blood flow has been proposed to be an early indicator of progressive alteration in cardiac function before evident irreversible modifications in tissues occur. Various flow-related parameters, including flow propagation velocity ( $V_p$ ) (Garcia et al., 1997; González-Vilchez et al., 2002; Khouri, Maly, Suh, & Walsh, 2004), vortex (Bermejo et al., 2014; Hong et al., 2008; Pedrizzetti, La Canna, Alfieri, & Tonti, 2014) and flow energetics (Agati et al., 2014; Elbaz et al., 2017; Zajac et al., 2015) have been proposed as markers for left ventricular (LV) dysfunction. However, potential flow indicators of LV dysfunction in MI patients remains to be further investigated. Moreover, measurement methods of several flow variables, in particular  $V_p$ , have raised concerns due to varying LV size and inflow jet directions among patients.

Detailed investigations on the relationship between MI parameters and intracardiac flow related variables could provide further insights into the mechanism leading to the deterioration in LV pumping efficiency in these patients. Due to the high variability in patient characteristics and the existence of various confounding factors, investigation on the impacts of individual MI parameters on LV dysfunction in these patients through

clinical studies is restricted. To overcome this problem, fluid-structure interaction (FSI) model has emerged as a useful tool to study the pathophysiology of heart disease. Despite the existence of various computational models for the LV, only a few studies (Domenichini & Pedrizzetti, 2011; Khalafvand, Ng, Zhong, & Hung, 2012; Watanabe, Sugano, Sugiura, & Hisada, 2004) have investigated the impact of MI on intracardiac flow dynamics. However, none of these studies have investigated the correlation between infarct properties, left ventricular mechanical dyssynchrony (LVMD) as well as the regional enhancement of contractility at the viable myocardium area (RECVVM) with vortex and flow energetics variables in MI patients.

## **1.2 Objectives**

The main objective of this thesis is to discover the potential flow indicators that could reflect LV abnormality in MI patients at an early stage of heart disease as well as to determine the relationship between individual MI parameters with the intraventricular flow variables. The specific aims and scope of the thesis are as follows:

- i. To explore the measurement methods of flow propagation velocity ( $V_p$ ) in PC-MR images of healthy subjects and MI patients whose LV size and directions of inflow jet are different.
- ii. To quantify and analyse the intraventricular flow variables (including  $V_p$ , vortex parameters and flow energetics) using image-based analysis and investigate their relationship with LV function to identify potential flow indicators for heart dysfunction.
- iii. To study the impact of infarct parameters on intraventricular flow variables using generic 3D FSI model for MI investigation.

### 1.3 Thesis Scope

The focus of this thesis is on the analysis of intraventricular flow variables, particularly  $V_p$ , vortex and flow energetic indices in MI patients. Thirty MI patients and twenty healthy individuals were recruited as subjects. All subjects went through phase contrast magnetic resonance imaging (PC-MRI) and transthoracic echocardiographic examinations at Universiti Malaya Medical Centre. The collected images were post-processed and analysed. The acquired flow results were compared between the groups of healthy subjects and MI patients in order to identify the potential flow indicator of LV dysfunction as a consequence of MI. The impacts of each MI parameters (i.e. infarct size, infarct multiplicity, LVMD, and RECV) on the intraventricular flow variables were studied using the developed FSI model.

### 1.4 Thesis Outline

This thesis consists of six chapters. **Chapter 2** includes the general literature review that provides the background of the cardiovascular system and MI. Clinical and computational analyses on the intraventricular flow dynamics and its relevance to heart disease are also covered in this chapter. In the next two chapters, the original research studies based on image-based flow analysis were reproduced. Among the analysed flow variables, the measurement method of the vortex and flow energetic indices are well defined, but not for  $V_p$ . Hence, **Chapter 3** explores the  $V_p$  measurement methods using PC-MRI data acquired from nine healthy subjects and nine MI patients with different LV sizes and inflow jets. The best  $V_p$  measuring method was later being used in the analysis of intraventricular flow for all subjects in **Chapter 4**, which presents the investigation of intraventricular flow variables (i.e.  $V_p$ , vortex and flow energetics), that carry the information of the LV function of twenty healthy subjects and thirty MI patients. Following the identification of potential flow indicator in this chapter, FSI simulation is subsequently implemented to study the impact of individual MI parameters on the

intraventricular flow. **Chapters 5** describes the development of FSI model that can be used to investigate MI parameters, particularly the infarct size, infarct multiplicity, LVMD, and RECV. Chapters 3, 4 and 5 share the same framework. Each chapter begins with a brief introduction, followed by a literature review, methodology, results, discussion, and conclusion. Finally, the significant findings and recommendations for future studies of this thesis are concluded in **Chapter 6**.

University of Malaya

## CHAPTER 2: LITERATURE REVIEW

This chapter gives a general review and background introduction on topics related to cardiovascular hemodynamics and abnormality. The chapter starts with a description on the heart anatomy and physiology as well as the cardiac cycle. It continues with the introduction of MI disease. A summary of the previous findings on intraventricular blood flow dynamics in healthy and abnormal LV using either clinical studies or computational studies are presented. Considering the significance of intraventricular blood flow dynamics in cardiac health assessment, this thesis focusses on the investigations of potential flow indicator that contribute to LV dysfunction in MI as well as the MI parameters that are associated with the intraventricular blood flow.

### 2.1 Heart anatomy and physiology

The structure of the heart is illustrated in Figure 2.1. The heart consists of four chambers i.e. two atria and two ventricles each at the left and right sides. There are heart valves located between the atrium and the ventricle as well as between the ventricle and the blood vessels in order to prevent backflow. The oxygenated blood from the lung enters the left atrium through the pulmonary veins and passes through the mitral valve into the LV. LV pumps the oxygenated blood to the systemic circulation through the aorta, with the aortic valve preventing backflow of blood from the aorta back into the LV. From the systemic circulation, deoxygenated blood flows back into the right atrium and passes through the tricuspid valve into the right ventricle. The right ventricle is responsible for pumping deoxygenated blood back into the lung through the pulmonary artery, with the pulmonary valve acting to prevent backflow into the right ventricle.

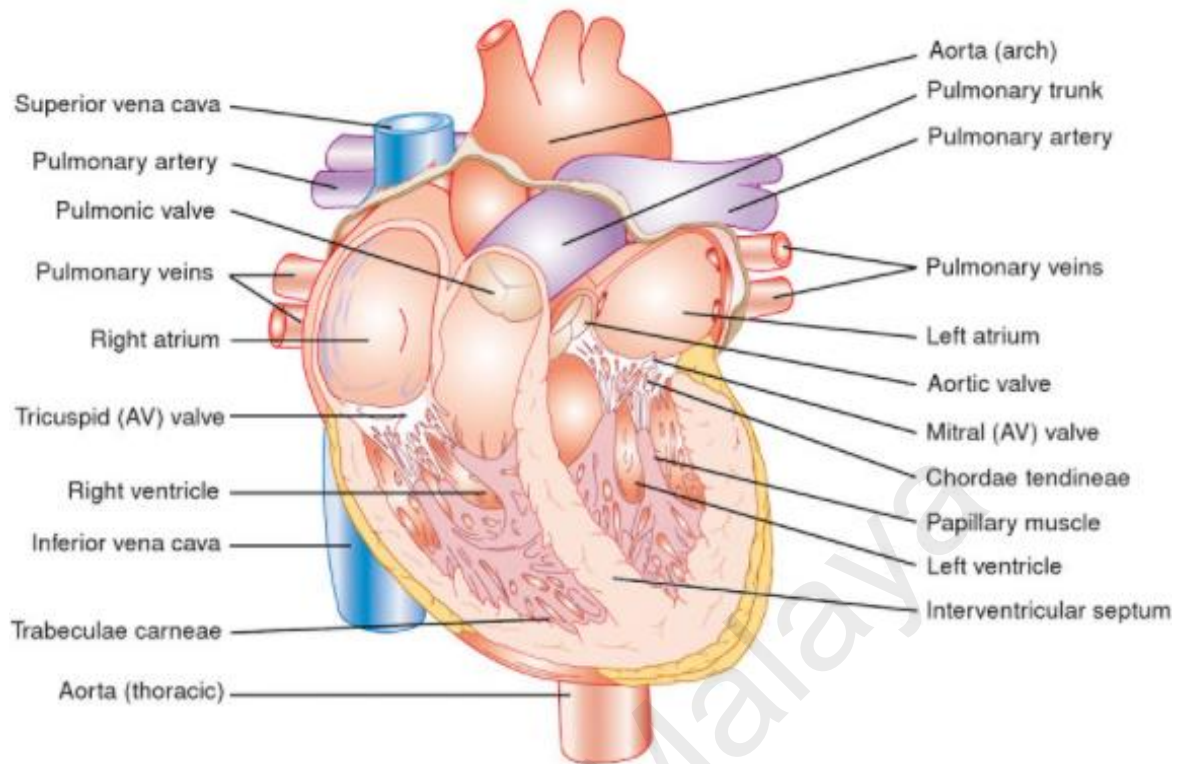


**Figure 2.1: Anatomy of human heart (Applegate, 2011)**

Among the heart chambers, the LV has the thickest heart muscle because it is the most vital chamber that predominantly determines the heart function. The heart muscle (from the innermost to the outermost layer) is composed of the endocardium, the myocardium, and the epicardium, where the myocardium is the thickest muscle layer. Heart muscle comprises fibres which are orientated linearly from the endocardium to the epicardium, with fibre angle ranging from +60 to -60 degrees relative to the circumferential alignment of the LV, as measured by the diffusion-tensor MRI (Hsu, Muzikant, Matulevicius, Penland, & Henriquez, 1998; Scollan, Holmes, Winslow, & Forder, 1998; Wu & Wu, 2009).

## 2.2 Cardiac cycle

Cardiac cycle describes the sequence of events in a single heartbeat. A cardiac cycle which consists of the systole (LV contracts) and the diastole (LV relaxes) phases is completed within a duration of less than a second. The cardiac cycle can be further divided

into four phases: isovolumic relaxation (IVR), filling, isovolumic contraction (IVC) and ejection. IVR and filling are diastolic events while IVC and ejection are systolic events. During IVR, heart muscle relaxes and LV pressure drops. Both mitral and aortic valves remain closed and LV volume remains constant. When the LV pressure drops to a level lower than the left atrial pressure (LAP), the mitral valve opens to allow blood to fill the LV. This happens during the filling phase. The filling phase is sub-divided into rapid filling, diastasis, and atrial contraction. During rapid filling, blood accelerates into the LV and then decelerates due to the increment of LV pressure. This is reflected by the first peak of the filling curve (E-wave) which contributes the largest filling volume. Subsequently, diastasis, which involves a very small amount of the incoming blood flow, occurs when the LV pressure approaches the LAP. During the second peak of the filling curve (A-wave), blood is driven again into the LV by atrial contraction. The mitral valve closes when the LV pressure equals the LAP, signifying the end of the filling phase. The LV volume at the end of diastole is known as the end diastolic volume (EDV). During IVC, heart muscle contracts, causing an increase in the LV pressure. LV volume remains constant as both mitral and aortic valves remain closed. When the LV pressure exceeds aortic pressure, the heart continues to contract to eject blood out of the LV into the aorta. Once the LV pressure is lower than the aortic pressure, the aortic valve is closed. The LV volume at the end of systole is known as the end systolic volume (ESV). The events in a cardiac cycle are characterised by the pressure-volume loop, as shown in Figure 2.2.

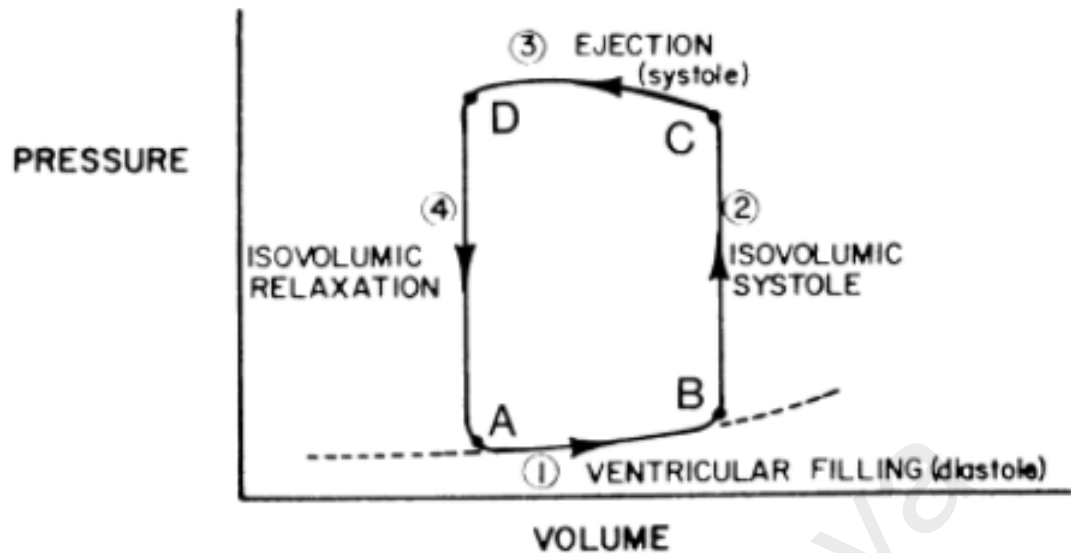
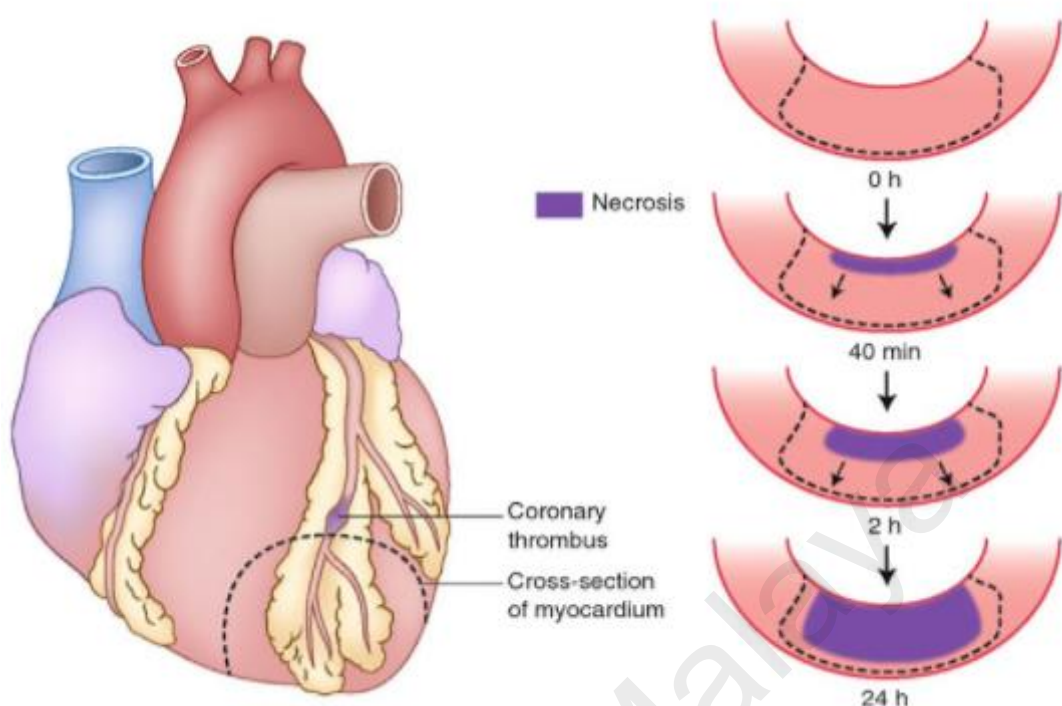


Figure 2.2: Pressure-volume loop during a cardiac cycle (Fung, 1997)

### 2.3 Myocardial infarction (MI)

IHD occurs when the coronary blood vessels are blocked by plaques. As plaques continuously build up in the coronary artery (atherosclerosis), there is a limited supply of oxygen-rich blood to the heart muscle, thus leading to heart muscle injury. IHD must be treated earlier in order to prevent progressive heart failure. IHD may lead to heart attack or MI, one of the most common cardiovascular diseases in the world (World Health Organization, 2015). MI happens when the coronary artery is totally blocked and lead to heart muscle death (necrosis or infarct), as illustrated in Figure 2.3. The necrotic region initiates at endocardium and spreads transmurally across the heart muscle. The infarct area spreads progressively if it remains untreated. The common symptoms of MI include chest pain, shortness of breath, dizziness, nausea, fatigue, sweating and irregular heartbeat. MI can be recognized through an electrocardiogram, blood tests, and imaging modalities such as chest X-ray, echocardiogram, angiogram and magnetic resonance imaging (MRI).



**Figure 2.3: Progressive cell death (necrosis) in MI (*Coronary Artery Disease, 2015*)**

In order to assess cardiac morphology and functionality as a consequence of MI, echocardiogram and MRI are the most common non-invasive cardiac imaging modalities used. Two-dimensional (2D) echocardiogram has been used in the clinical routine for its simplicity, efficacy, and stability. Apart from the cardiac dimension, heart wall motion is assessed through a series of cine frames in echocardiogram and cine MRI. Late gadolinium enhanced MRI is used to characterise infarct where the bright region indicates infarcts or scar tissue (Figure 2.4).

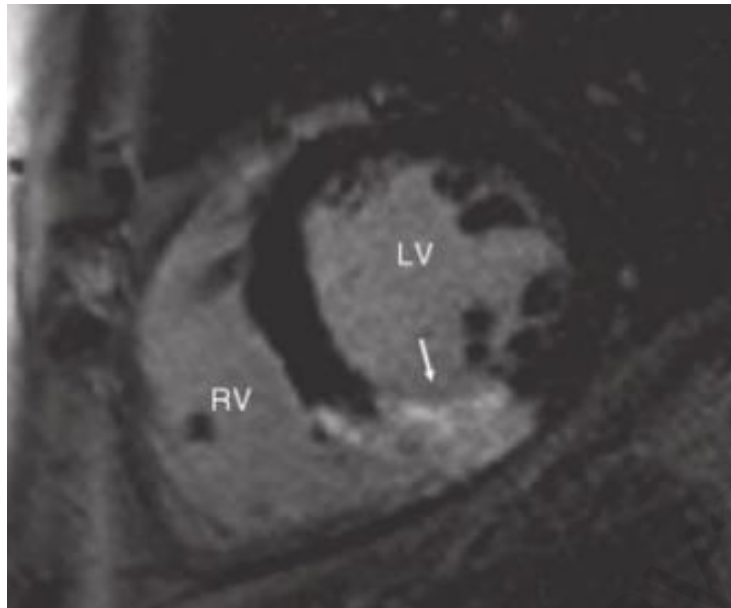


**Figure 2.4: Evidence of MI (white region indicated by arrow) in late gadolinium enhancement MRI (Plein, Ridgway, & Greenwood, 2011)**

The appearance of the infarct region could weaken regional systolic wall motion, diastolic relaxation (Roes et al., 2007; Zafari, Reddy, Jeroudi, & Garas, 2012) and LVMD due to inhomogeneous myocardial movement (Sato et al., 2017). LV remodelling, which is associated with an enlarged LV and reduced LVEF, is the most common complications of MI which leads to progressive heart failure (Cohn, Ferrari, & Sharpe, 2000).

The treatments for MI patients include medications (such as aspirin, beta-blockers, ACE inhibitors, thrombolytics, and anticoagulants) as well as surgical procedure, such as percutaneous coronary intervention and coronary artery bypass surgery, which attempt to restore blood flow in the blocked arteries to the LV. In post-MI patients, an operative method named as surgical ventricular restoration (SVR) aims to reduce the enlarged LV volume by restoring the enlarged spherical LV to its elliptical geometry. The outcome of SVR was shown to be effective in increasing patients' survival (Athanasuleas et al., 2004) and improving the intraventricular flow dynamics (Doenst et al., 2009).

## **2.4 Heart Disease and Intraventricular Blood Flow Dynamics**

As blood flow in the LV is immediately affected by minor changes in the surrounding conditions such as geometry and myocardial deformation, intraventricular blood flow is a natural early indicator of progressive alterations in LV function before evident irreversible modifications in tissues occur. Thus, intraventricular blood flow plays important roles in early detection of heart disease and prediction of heart disease progression (Hong, Kim, Pedrizzetti, & Vannan, 2013). In recent years, there has been widespread interest in the analysis of intraventricular flow pattern.

### **2.4.1 Clinical flow analysis studies**

The most common non-invasive tools used for inspecting intraventricular blood flow are PC-MRI, echocardiographic and particle image velocimetry techniques. Through detailed examination of the human cardiac flow fields, a distinctive entity with rotating motion, or known as vortex rings, has been discovered in the intracardiac blood flow (Kilner et al., 2000; Kim et al., 1995). The vortex develops during diastolic filling, with the streaming blood rolling-up in the LV due to an increase in the apical pressure, forming a recirculating structure. The diastolic vortex persists into systole and finally diminishes at the end of systole (Pasipoularides, Shu, Shah, Womack, & Glower, 2003).

Optimal vortex formation has been proposed as a measure of cardiac health (Gharib, Rambod, Kheradvar, Sahn, & Dabiri, 2006). Extensive studies have investigated the appearance of intraventricular vortex in healthy subjects and patients with cardiovascular disease. Generally, distinctive vortex appearance and flow dynamics were observed in abnormal LVs. For instance, as compared to the healthy subjects, larger vortex was observed in patients with dilated heart (Arvidsson et al., 2016) while slower vortex evolution was observed to occur in heart disease patients (Zhang et al., 2013). Lower  $V_p$  was noted in MI patients (Houliand et al., 2002). On the other hand, vortex penetrated less

deeply into the LV cavity of patients with apical LV thrombus (Son et al., 2012). To date, intraventricular vortex has been proposed to have beneficial roles in assisting closure of the mitral valve (Bellhouse, 1972; Kim et al., 1995), aiding flow redirection towards the outflow tract during systole (Kilner et al., 2000; Sengupta et al., 2007) and facilitating filling during diastole (Bermejo et al., 2014). Moreover, the strong recirculating motion of the vortex was seen as a mechanism for helping blood mixing and thus preventing thrombus formation (Pasipoularides et al., 2003; Son et al., 2012). The diastolic vortex was suggested to act as KE reservoir in systolic-diastolic coupling (Kanski et al., 2015; Nucifora et al., 2010; Steding-Ehrenborg et al., 2015).

Due to high variability among patients' characteristics or measurement methods, contradicted findings with regards to the role and diagnostic value of the vortex have been reported. For example, while some studies (Hong et al., 2008) have observed weaker vortex in patients with systolic dysfunction, stronger vortex were reported in other studies (Bermejo et al., 2014). Several studies have also raised questions regarding the role of vortex as a KE reservoir because the KE content in the diastolic vortex was found to be insignificant as compared with the total KE in the LV (Bermejo et al., 2014; Carlsson, Heiberg, Toger, & Arheden, 2012; Kim et al., 1995).

In addition to vortex, the intraventricular flow energetics have also received immense interest in recent decades for its potential ability to identify cardiac abnormality. The intraventricular KE content and its changes (Carlsson et al., 2012; Eriksson, Bolger, Ebbers, & Carlhäll, 2012; Kanski et al., 2015), KE flow fluctuation (Agati et al., 2014; Dyverfeldt et al., 2008; Zajac et al., 2015) as well as viscous energy dissipation (Agati et al., 2014; Elbaz et al., 2017; Honda et al., 2017; Stugaard et al., 2015) are among the properties of flow energetics which have been investigated. Overall, heart disease patients with impaired systolic function were found to have lower KE content, higher degrees of

flow fluctuation and viscous energy loss (EL) than healthy individuals. However, recently, opposite findings have been presented: while patients with preserved systolic function had excessive flow energetics, patients with impaired systolic function had much lower flow energetics than healthy subjects (Agati et al., 2014). Limitations of the imaging modalities such as their sensitivity to flow velocity, spatial and temporal resolutions can also contribute to inconsistent findings (Chan et al., 2018; Hong et al., 2013)

The discrepancies among various studies with regards to flow variables had motivated further investigations into the correlation among vortex, flow energetics and LV functional measurements (Agati et al., 2014; Akiyama et al., 2017; Carlsson et al., 2012; Nucifora et al., 2010; Zajac et al., 2015). Nevertheless, due to the high variability in patient characteristics as well as the existence of various confounding factors, it is difficult to ascertain the effect of individual factors on the flow-related variables.

#### **2.4.2 Computational flow studies**

Computational modelling technique has emerged as useful tools in cardiovascular medicine as it presents the ability to capture the complex and multifactorial cause and effect relationships that link underlying pathophysiological mechanisms (Morris et al., 2016). This, in turn, provides the capacity to derive indicators that are not directly observable but play a key mechanistic role in the disease process. Computational fluid dynamics (CFD) models allow the assessment of regional velocity and pressure by solving Navier-Stokes and continuity equations which govern incompressible fluid motion.

Numerous CFD models have been developed in order to disclose the mechanisms behind differences in the intraventricular flow pattern (Long et al., 2008; Saber et al., 2003), vortex (Baccani, Domenichini, Pedrizzetti, & Tonti, 2002; Nguyen et al., 2015;

Schenkel et al., 2009) and flow energetics (Chnafa, Mendez, & Nicoud, 2016; Khalafvand, Hung, Ng, & Zhong, 2015; Mangual et al., 2013) among different individuals. The effects of individual factors such as LV geometry (Baccani et al., 2002), regional wall abnormalities (Domenichini & Pedrizzetti, 2011) and asymmetry in the entering flow jet (Pedrizzetti & Domenichini, 2005) on intraventricular vortex evolution and energy dissipation have been studied using the CFD approach. Furthermore, CFD model has also been used as a tool to predict the effectiveness of the SVR treatment (Doenst et al., 2009).

However, CFD models ignore the two-way interaction between blood flow and myocardial wall mechanics, which constitutes energy exchange in driving cardiovascular transport (Cheng, Oertel, & Schenkel, 2005). On the other hand, realistic FSI models, which consider the blood-wall momentum transfer, are able to provide information on how alterations in the myocardial mechanics translate into cardiovascular blood flow (Nordsletten et al., 2011). The FSI method can be further classified into fictitious FSI and realistic FSI methods. Fictitious FSI method is also known as the Immersed boundary method (IBM), in which the myocardial wall is simplified into elastic fibres that are not fitted to coordinate curves and is immersed in the blood. On the other hand, realistic FSI couples both the CFD and structural solver to simulate both heart wall and blood flow domains simultaneously (Doost, Ghista, Su, Zhong, & Morsi, 2016). Although realistic FSI is more complicated and numerically expensive, it provides more accurate fluid-structure solution.

Compared to the IBM heart models (Gao, Carrick, Berry, Griffith, & Luo, 2014; Peskin, 1977), the realistic FSI method is more commonly used to investigate the relation between intraventricular flow and myocardium through the resulting regional velocity vectors and pressure distribution in the LV chamber (Arefin & Morsi, 2014; Cheng et al.,

2005; Nordsletten et al., 2011; Watanabe et al., 2004). To date, only a few FSI models have been developed. These models have been used for several applications: (i) to understand the mechanical efficiency in MI patients (Watanabe et al., 2004) ; (ii) to elucidate the intraventricular flow mechanism in DCM cases (Chan et al., 2013) as well as (iii) to evaluate the efficacy of surgical procedures in patients with Tetralogy of Fallot (Tang, Yang, Geva, & Pedro, 2010).

## **2.5 Summary**

Intraventricular flow dynamics play crucial roles in indicating cardiac health and discovering disease at an early stage. Early detection of MI through intraventricular flow dynamics may help to prevent disease deterioration. Various flow-related variables have been proposed to reveal the LV abnormality, predominantly Vp, vortex and flow energetics. However, potential flow indicators for MI remain to be investigated. In addition, complicated patients' characteristics motivate the development of computational models to investigate the impact of individual MI parameters on the intraventricular blood flow. Despite the existence of various computational LV models, only a few studies (Domenichini & Pedrizzetti, 2011; Khalafvand et al., 2012; Watanabe et al., 2004) have explored the intracardiac flow dynamics in MI patients. Furthermore, the relation between MI parameters with intraventricular flow-related variables has not been thoroughly understood particularly using an FSI approach.

## **CHAPTER 3: IMAGE-BASED FLOW ANALYSIS OF LEFT VENTRICULAR FLOW PROPAGATION VELOCITY MEASUREMENT**

### **3.1 Introduction**

This chapter investigated several Vp measurement methods using PC-MRI and assessed the discrepancies in Vp results due to varying inflow jet directions and LV sizes. Three Vp measuring techniques were suggested and the Vp values acquired using these methods were compared. Vp measurement was performed on nine healthy volunteers and nine MI patients at four measurement positions, respectively at one-third, one-half, two-thirds and the conventional 4cm distances from the mitral valve leaflet (MLT) into the LV.

### **3.2 Literature review**

Cardiac diastolic dysfunction is a common cardiac condition and contributes to high mortality rates (Halley, Houghtaling, Khalil, Thomas, & Jaber, 2011; Mooi, Chin, Ahmad, & Jalalian, 2012). Although invasive measurement of the cardiac pressure-volume relationship serves as the gold standard of diastolic function assessment, this technique has limited clinical applicability. There are a multitude of non-invasive measurements of diastolic function that are used in routine clinical practice, such as E/A ratio, mitral flow velocities, deceleration time, isovolumetric relaxation time and indices from speckle tracking echocardiography (Flachskampf et al., 2015; Nagueh et al., 2009). However, ambiguous outcomes can be attained due to preload dependency of some of these measurements (Ie et al., 2003; Ogunyankin, 2011). This has subsequently led to the introduction of the Vp measure as the diastolic relaxation index due to its preload-independent characteristics (Garcia et al., 1997; González-Vilchez et al., 2002; Khouri et al., 2004).

V<sub>p</sub> refers to the propagation of the maximum velocity across specific locations during early diastole (De Boeck et al., 2005). A slow V<sub>p</sub> reflects abnormal LV relaxation. Conventionally, V<sub>p</sub> measurement is determined from CMMD echocardiography, as the slope of the isovelocity contour, which spreads from the MLT to 4 cm distance into the LV cavity (Garcia, Thomas, & Klein, 1998). This V<sub>p</sub> determination technique has recently been validated by using PC-MRI (Calkoen et al., 2015; van den Boogaard, Marsan, Bax, de Roos, & Westenberg, 2013). However, this conventional V<sub>p</sub> measurement only captures LV flow in a single linear dimension and therefore only a single directional velocity component could be examined. Since the position of the maximum velocity across the inflow stream diameter is known to vary (Houliind et al., 2002), the use of CMMD limits the true measurement of maximum velocity, not only in healthy LVs in which flow is known to be redirected at the two-thirds of the LV site (Long et al., 2008) but also in dilated LVs, in which swirling inflow jets had been observed (D'cruz & Sharaf, 1991). Consequently, conventional V<sub>p</sub> measurement, based on the assumption that flow propagates along a single direction, is likely to be inadequate for diastolic function assessment.

As a step away from such 1D measurement, Houliind et al. (2002) investigated V<sub>p</sub> using PC-MRI across several 2D measurement positions. The V<sub>p</sub> was calculated as the ratio of the distance between measurement positions (i.e. 4 cm) to the time delay, the latter referring to the time difference between the occurrence of peak velocity at each measurement position along a reference line. However, these observations were based on a single peak velocity at the measurement position, which may be subject to measurement errors caused by noise or flow disturbances. The use of mean peak velocity as a metric may reduce the error with an appropriate orientation of the measurement position and the directional angle of the velocity components. This metric has yet to be reported in

conjunction with diastolic dysfunction assessment and therefore warrants further investigation.

An additional factor that has evaded attention is the diversity of LV sizes amongst subject groups and populations (Chahal et al., 2012), as well as medical conditions such as LV hypertrophy (Ching, Chia, Chong, & Jalalian, 2014). Vp measurements at a fixed distance of 4 cm from the MLT are likely to be made at different relative positions among individual LVs, at which very different flow patterns may prevail. As such, Vp measurement at a fixed distance may not be the best choice. To date, this has yet to be scrutinized.

To overcome the aforementioned deficiencies, in this study, the potential use of three different Vp measurement methods were proposed, investigated and compared. These methods use the mean velocity instead of point velocity along a line, vary the location of the measurement position relative to LV length, and account for the orientation of the line at the measurement position. There is further a choice of which velocity component to take in relation to the line marking the measurement position. The measurement methods were validated with myocardial strain rate acquired from cardiovascular magnetic resonance feature tracking (CMR-FT), which has previously been shown to accurately assess myocardial deformation (Buss et al., 2015; Moody et al., 2015).

### **3.3 Methodology**

#### **3.3.1 Study group**

Nine post-infarct patients were recruited in this study. Exclusion criteria were unstable angina, atrial fibrillation, tachycardia (>100 bpm at rest) and moderate or worse valvular regurgitation or stenosis, as study has reported that Vp could not be used as an indicator for LV relaxation in these patients (De Boeck et al., 2005). Nine healthy volunteers were also recruited as healthy subjects to establish the baseline. The subject demographics are

summarised in Table 3.1. Inclusion criteria for healthy subjects were no prior history, symptoms or medication for cardiovascular disease, as well as normal cardiac function as indicated in an echocardiographic examination. The scan was done by using iE33 ultrasound machine (Phillips Medical Systems, Andover, MA, USA) with S5-1 Sector Array transducer. Subjects with contraindications to MRI, including claustrophobia and ferrous implants, were also excluded. Written informed consent was obtained from all subjects prior to participation in this study. The research was approved by the medical ethics committee of the University Malaya Medical Centre (Ref: 989.75).

**Table 3.1: Subject demographics.**

	Healthy group (n=9)	Patient group (n=9)	p-values
Male (female)	4 (5)	9 (0)	-
Age	50±8	58±7	p=0.074
Heart rate (bpm)	72±9	73±11	p=0.541
<b>ESV (mL)*</b>	<b>34±11</b>	<b>119±74</b>	<b>p=0.004</b>
<b>EDV (mL)*</b>	<b>92±20</b>	<b>168±70</b>	<b>p=0.002</b>
<b>LVEF (%)*</b>	<b>64±6</b>	<b>35±19</b>	<b>p=0.006</b>
E/A ratio	1.2±0.3	1.4±0.7	p=0.574
Diastolic function			-
• Normal filling	9	0	-
• Impaired relaxation	0	3	-
• Pseudonormal filling	0	3	-
• Restrictive filling	0	3	-

ESV = End systolic volume. EDV = End diastolic volume. LVEF = Left ventricular ejection fraction.  
\*p<0.05 was the level of significance between healthy group and patient group.

### 3.3.2 Image Acquisition

Images were acquired using a 1.5T MRI scanner (SignaHDxt 1.5T, GE Healthcare, WI, USA) and all subjects were lying in the supine position. An eight-channel cardiac coil was placed on the patient's chest. Four-chamber acquisition was performed with cardiac gated, multi-breath-hold Fast Cine Phase Contrast sequence which enables shorter scan times through prospective gating and segmented k-space and by retrospectively reconstructing images throughout the entire cardiac cycle. The acquisition parameters were: TR = 6.2–6.5 ms, TE = 3.2–3.5 ms, flip angle = 25°, in-plane pixel resolution =

1.37 × 1.37 mm, acquisition matrix = 256 × 256 pixels, slice thickness = 8mm and number of cardiac time frames = 20. The temporal resolution was 25–26 ms. Velocity encoding was performed in three spatial directions with 150 cm/s maximum velocity encoding. For  $V_p$  measurement validation, multi-breath-hold steady-state free precession short-axis cine image stack (repetition time, TE = 1.6 ms, echo time, TR = 3.7 ms, flip angle = 55°, number of slices = 10 – 15) were acquired using accelerated imaging (Array Spatial Sensitivity Encoding Technique or ASSET). A set of 6 multi-breath-hold LA cine images radially oriented around the centre of the LV chamber at uniform angular intervals, which contain both 2- and 4-chamber views, were also prescribed with the same acquisition parameters by using the first short-axis slice at the base for planning.

### 3.3.3 Image Processing and Preparation

The artefact compensation for possible phase errors and masking of random noise was performed (Walker et al., 1993). The LV endocardial contours were manually segmented from the magnitude image of 2D PC-MRI using Segment software (v1.9 R3216, Medviso, AB) (Heiberg et al., 2010). The segmented images are further processed as described below to enable the extraction of  $V_p$ .

Three landmark points, i.e. the apical point and two points on the mitral edges, were marked on the modulus image during the early filling (peak E-wave), as shown in Figure 3.1. The MLT level was located via the indicated geometric construction at about 2 cm beneath the mitral edge points (Houliand et al., 2002). An 8 cm long MLT line was drawn at this position, which was sufficient to fully span the local width of the LV chamber. Subsequently in this thesis, the LV height is defined as the distance between the mid-point of the MLT line and the apex point. In addition to the conventional distance line at 4 cm depth from the mid-point of the MLT line, three other 8 cm long distance lines were positioned at fractional heights (i.e.  $\frac{1}{3}$ ,  $\frac{1}{2}$  and  $\frac{2}{3}$ ) of the LV (Figure 3.1).

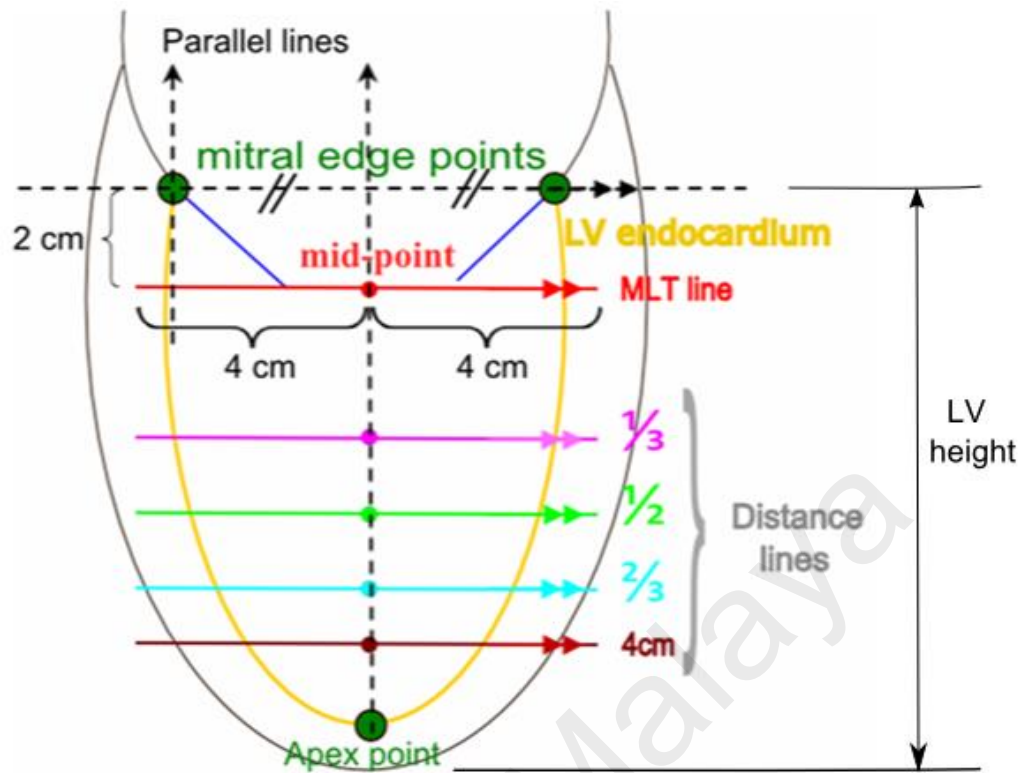


**Figure 3.1: LV landmark points and location of distance lines. MLT=Mitral Leaflet Tips.**

### 3.3.4 V<sub>p</sub> Measurement Methods

Three V<sub>p</sub> measuring techniques are suggested in this study namely the non-adaptive (NA) method, the adaptive-positions (AP) method, and the adaptive-vectors (AV) method. These V<sub>p</sub> measuring techniques differ in the measurement positions and the directional angle of velocity components at each measurement position. Details of the methods are elaborated below.

For all methods, the orientation of “MLT-inflow” was decided according to the inflow direction at the MLT level. This position was determined by tilting the MLT line about its mid-point, until a maximum mean velocity at peak E-wave was obtained. For this purpose, the orthogonal velocity components at each tilted MLT line were evaluated. Only the orthogonal velocity components directed towards the apex were considered,

whereas velocity components in the opposite direction or back flow were excluded in the analysis. The average of orthogonal velocity components was defined as the mean forward flow, calculated according to Equation 3.1.

$$\text{Mean forward flow} = \frac{\sum_{i=1}^N V_{n_i}}{N} \quad (3.1)$$

where  $i$  represents number of points,  $V_n$  represents the orthogonal velocity components directed towards the apex at each tilted MLT line, and  $N$  represents the total number of velocity components.

The “MLT-inflow position” was the tilted MLT line which produced the maximum mean forward flow.

#### 3.3.4.1 Non-adaptive (NA) Method

The distance lines at  $\frac{1}{3}$ ,  $\frac{1}{2}$ ,  $\frac{2}{3}$  and 4 cm positions from the MLT, were aligned beneath and parallel to the MLT-inflow (Figure 3.2a). These oriented distance lines are referred to as measurement positions. At each measurement position, we obtained the mean forward flow from the orthogonal velocity components.

#### 3.3.4.2 Adaptive Positions (AP) Method

As curved inflow jet may cause underestimation of peak velocity by using the NA method, the AP method was therefore proposed. The distance lines were aligned perpendicularly to the local direction of the inflow jet instead of being parallel to the MLT-inflow. By tilting about the mid-point of each distance line, the measurement positions were identified by searching for the angle that produced a maximum mean velocity during peak E-wave (Figure 3.2b). At each position, the mean forward flow was obtained from the orthogonal velocity components.

### 3.3.4.3 Adaptive Vectors (AV) Method

The AV method represents an alternative option to trace the nonlinear inflow jet. Similar to the NA method, the measurement positions were parallel to the MLT-inflow. However, the mean forward flow was determined by angled velocity components (details in Appendix B) that produced the maximum mean forward velocity (Figure 3.2c), instead of from the orthogonal velocity components. A notable difference of this method is that the search process for the velocity component was repeated at each diastolic phase.

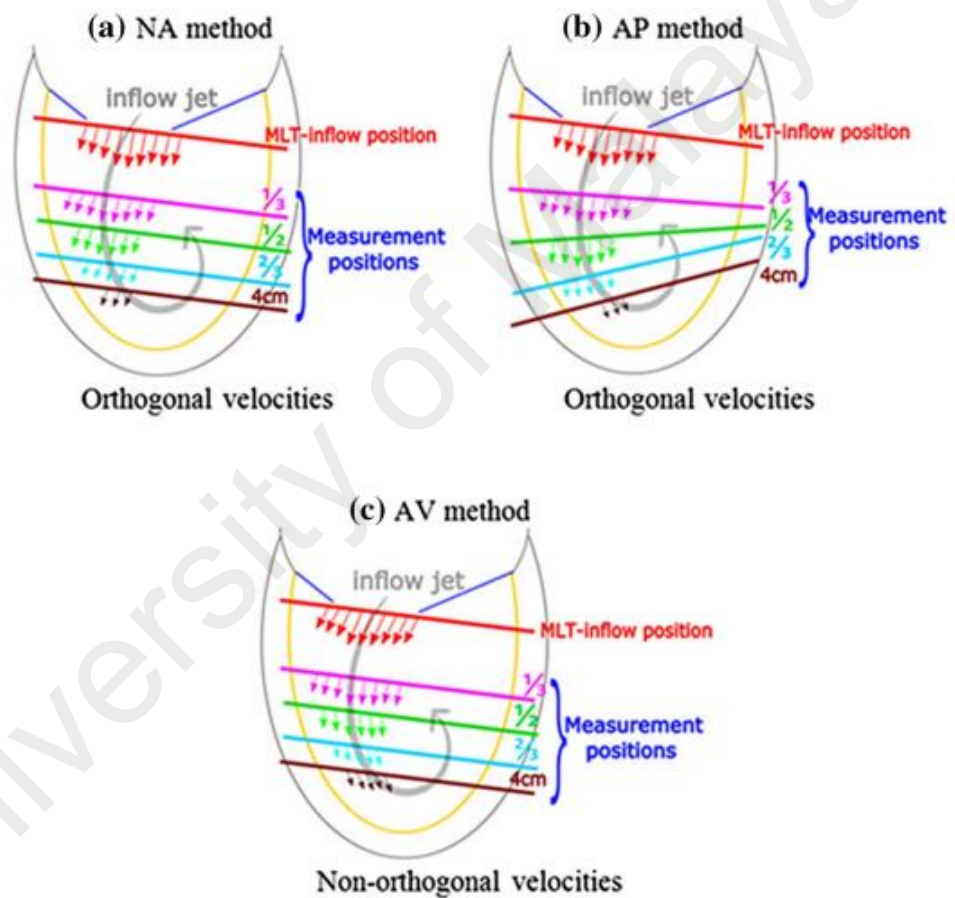


**Figure 3.2: The three proposed Vp measuring techniques. Arrows at each measurement position indicate the velocity components (found along the full line) that will be used to calculate the mean forward flow. NA=Non-adaptive; AP=Adaptive Positions; AV=Adaptive Vectors.**

### 3.3.5 Vp Acquisition

For all methods, the mean forward flow calculated using Equation (3.1) was computed by fixing the measurement positions in place throughout the diastolic phase. This produces a velocity-time curve, or more specifically the mean forward flow velocity

across diastolic phases for each measurement position. The velocity-time curves were then fitted by using third order polynomials. The maximum point-wise error of the velocity-time curve fitting was within 10 percent.

For all three methods,  $V_p$  was calculated using Equation 3.2.

$$V_p = \frac{\text{Distance from MLT (cm)}}{\text{Time Delay (s)}} \quad (3.2)$$

where time delay is defined as the time difference between the E-wave peak at each measurement position and that at the MLT-inflow position.  $V_p$  was to be obtained from all measurement positions and reported for all subjects. The algorithms for calculating  $V_p$  were programmed using MATLAB (vR2012a, Mathworks, Natick, MA) without optimization, on Intel(R) Core (TM) i7-2600 CPU @3.40 GHz computer. The average computation time was recorded.

### **3.3.6 Strain Rate Analysis Using Cardiovascular Magnetic Resonance Feature Tracking (CMR-FT)**

CMR-FT was performed using Tissue Tracking cvi<sup>42</sup> (Circle, Calgary, Canada). In both short-axis and long-axis cine images, the endocardial and epicardial borders were delineated in all cardiac phases with the initial contour set at end-diastole and the contours were manually corrected where required. The myocardial strain rate was automatically calculated by the tissue tracking algorithm in Tissue Tracking cvi<sup>42</sup> (Schuster et al., 2015). As three-dimensional (3D) myocardial deformation has better accuracy and reproducibility than 2D (Nesser et al., 2009; Seo et al., 2009), peak 3D longitudinal isovolumic relaxation strain rate ( $SR_{IVR}$ ) of each segment in the short-axis stack and the 6 radial long-axis images was calculated in the present study. Global 3D peak strain rates, defined as the average  $SR_{IVR}$  during isovolumic relaxation in all LV segments were then

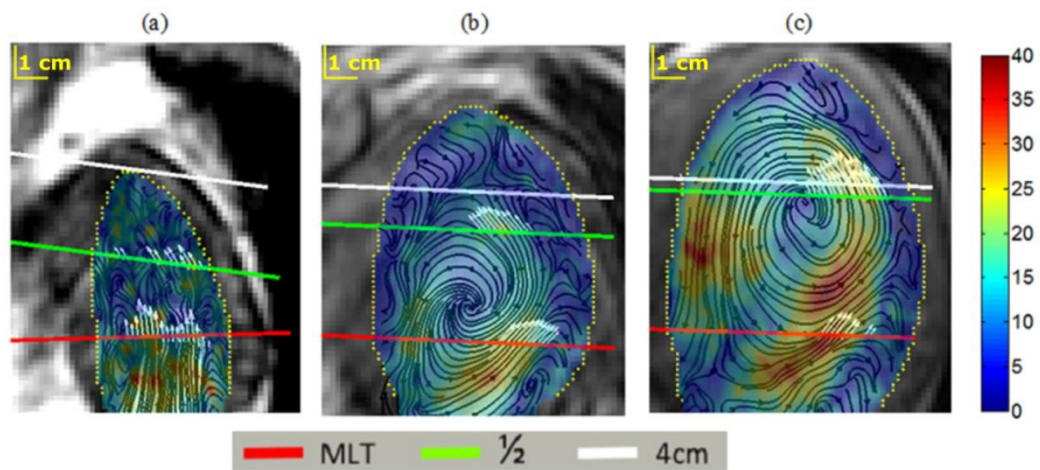
derived and used to indicate LV relaxation (Hashimoto et al., 2003; Kasner et al., 2010) for correlation with the proposed Vp measurements.

### **3.3.7 Statistical Analysis**

Statistical analysis was performed using the Statistical Package for Social Sciences (SPSS v22.0, SPSS Inc., USA). The Shapiro-Wilk test was used to test for normality. Vp values between healthy and patient groups were compared using the non-parametric Mann-Whitney U-test. The correlation between Vp values and  $SR_{IVR}$  was determined via Pearson's correlation coefficient,  $r$ . The level of significance (p-value) was set at 0.05 in all analyses.

## **3.4 Results**

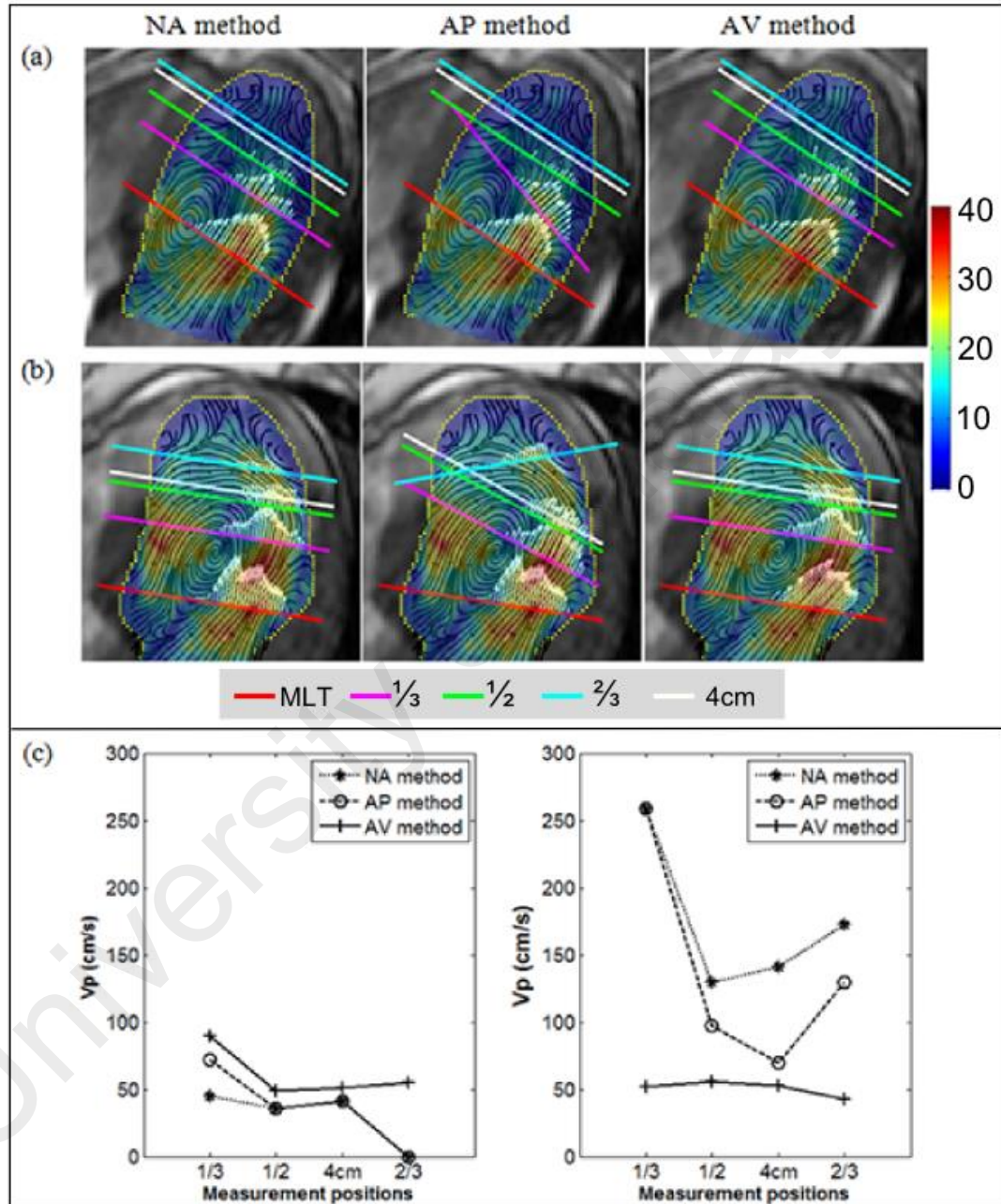
Figure 3.3 illustrates the impact of different LV sizes. Since the healthy volunteers and post-infarct patients had different LV sizes, the various measurement positions were located at different LV levels. For the healthy volunteer shown in Figure 3.3a, the 4 cm position was located outside of the LV cavity, preventing any Vp measurement to be obtained. For the post-infarct patient with LV dilatation (Figure 3.3b), the fixed 4 cm depth was located at the apical area where the Vp is not measurable due to flow reversal. Nevertheless, for the patient with a dilated LV (Figure 3.3c), the 4 cm depth was close to the one-half measurement position, both of which were located at mid-LV and allowed Vp to be quantified.



**Figure 3.3: Measurement positions at 4 cm and one-half LV height (based on the AV method) for different LV sizes in a (a) healthy volunteer, (b) patient without dilated LV and (c) patient with dilated LV during flow deceleration. Colour map represents velocity magnitude in cm/s, with black streamline arrows representing flow direction and white arrows indicating all of the forward velocity components at the measurement positions**

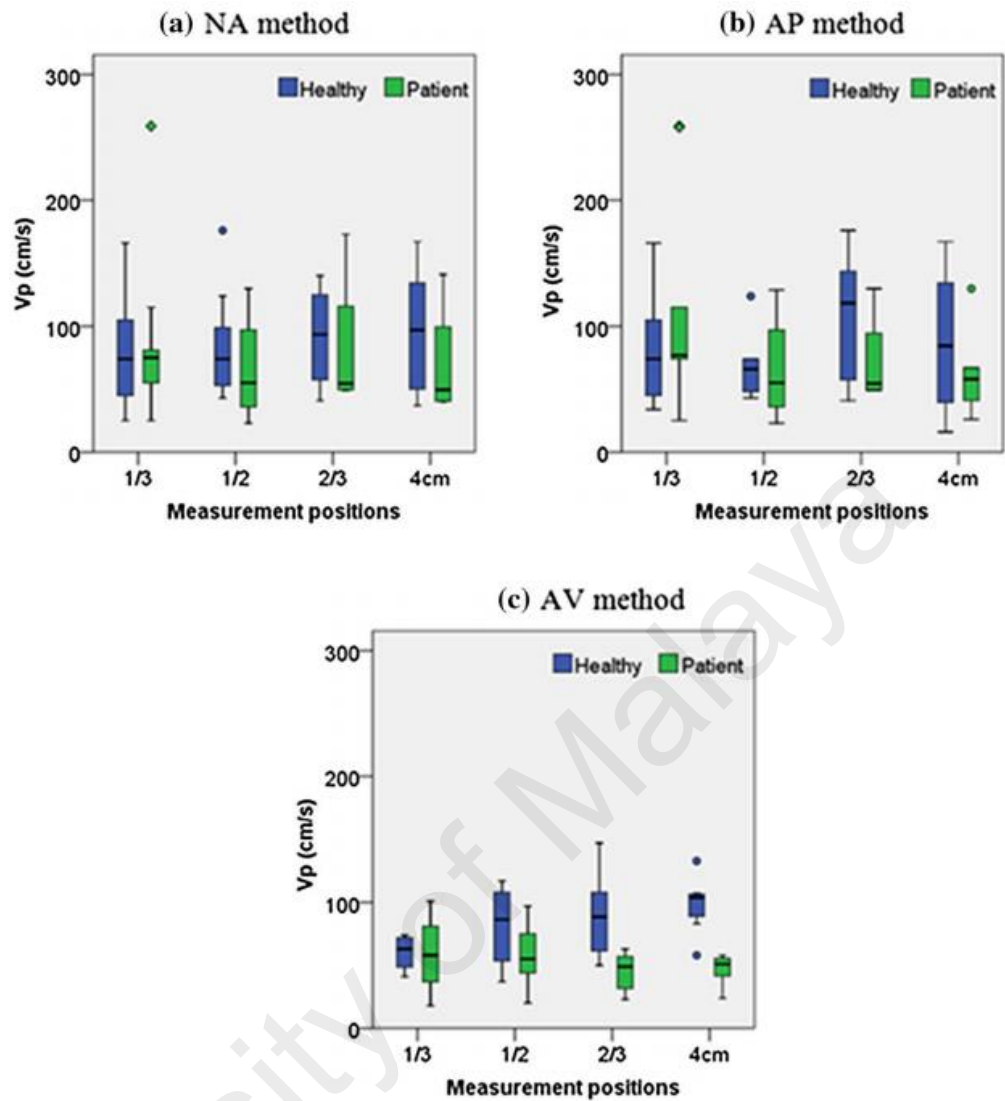
For cases in which  $V_p$  values could be determined, the differences seen in each  $V_p$  measurement method are detailed in Figure 3.4. It shows a comparison between two post-infarct patients, each having different LV volumes i.e. without dilated LV (EDV = 128 mL) vs. with dilated LV (EDV = 300 mL). From the echocardiographic examination, both patients were diagnosed with abnormal LV relaxation and were classified in the restrictive filling group. In further analysis of myocardial relaxation, these two patients also had abnormally low  $SR_{IVR}$  of 1.29 %/s and 1.31 %/s respectively. As seen in Figure 3.4a, the inflow jet travelled straight down from the mitral valve towards the apex of the patient without dilated LV. All three  $V_p$  measuring methods have the measurement positions as well as the velocity components for the calculation of mean forward flow directed approximately in the same path along the inflow jet. In contrast, a curved inflow jet occurs in the LV chamber of the patient with dilated LV (Figure 3.4b). Only velocity components in the AV method were able to follow the direction of the inflow jet. The patient without dilated LV demonstrated a rather consistent  $V_p$  values for all measurement positions (Figure 3.4c: left). On the contrary, a fluctuating and abnormally high  $V_p$  (~250 cm/s compared to an expected value of below 120 cm/s (Houliind et al., 2002)) was acquired in

the patient with dilated LV by using both the NA and AP methods (Figure 3.4c: right). For this particular patient, only the AV method produced consistently low Vp values at all measurement positions.



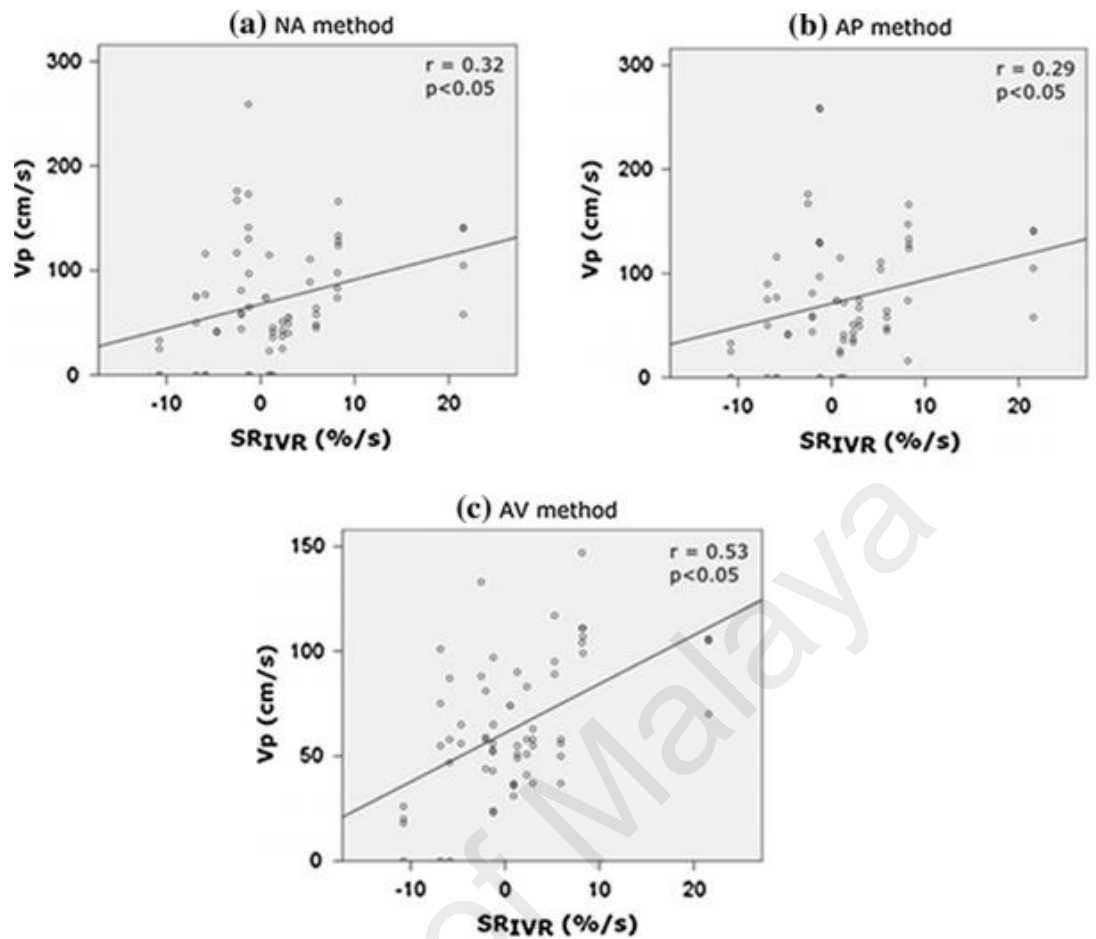
**Figure 3.4: Measurement positions and intraventricular flow using the three Vp measuring techniques in two post-infarct patients: (a) without dilated LV (EDV = 128 mL) and (b) with dilated LV (EDV = 300 mL). Colour map represents mean diastolic velocity magnitude in cm/s, with black streamline arrows representing flow direction and white arrows within the LV cavity indicating all forward velocity components at the measurement positions at peak E-wave. The resulting Vp values for these two post-infarct patients are shown in (c) for no dilated LV (EDV = 128 mL) (left) and dilated LV (EDV = 300 mL) (right)**

Figure 3.5 consolidates the analysis of  $V_p$  at each measurement position using the three suggested  $V_p$  measuring techniques. The NA and AP methods showed inconsistent  $V_p$  values across measurement positions as evidenced by the large standard deviations and the presence of outliers ( $1.5 \times$  interquartile range) in both subject groups. The extremely high  $V_p$  values (i.e. outliers) in Figure 3.5a and Figure 3.5b were contributed by a post-infarct patient with dilated LV, in whom the curvy inflow jet was observed. A healthy volunteer was also identified as one outlier in both the NA and the AP methods due to overestimation of  $V_p$  from its slightly slanted inflow path. On the other hand, the AV method showed a more consistent trend of  $V_p$  values across different measurement positions with smaller standard deviations (Figure 3.5c). Using the AV method, notable  $V_p$  difference was observed between healthy volunteers and post-infarct patients at the measurement positions of one-half ( $81 \pm 31$  vs.  $58 \pm 25$  cm/s), two-thirds ( $89 \pm 32$  vs.  $45 \pm 15$  cm/s) and 4 cm ( $98 \pm 23$  vs.  $47 \pm 13$  cm/s), though no statistically significant results ( $p < 0.05$ ) were obtained due to the small number of subjects. Regardless of the  $V_p$  measurement methods,  $V_p$  at two-thirds and 4 cm measurement positions were unobtainable from 45% (4 out of 9) of post-infarct patients and 20% (2 out of 9) of healthy volunteers.



**Figure 3.5: Summary of Vp values at different measurement positions using the NA, AP and AV methods.**

Figure 3.6 indicates the correlation between Vp values obtained from the three Vp measuring techniques with  $SR_{IVR}$ . Vp values from NA and AP methods were weakly related to  $SR_{IVR}$  ( $r = 0.32$ ,  $p < 0.05$ ;  $r = 0.29$ ,  $p < 0.05$ ) whereas the strongest correlation was found between Vp values from the AV method and  $SR_{IVR}$  ( $r = 0.53$ ,  $p < 0.05$ ) (Figure 3.6c).



**Figure 3.6: The correlation between SRIVR and Vp values obtained using the NA, AP and AV methods. The correlation coefficients are significant as the p-values are below the set threshold of 0.05.**

### 3.5 Discussion

The results showed that Vp measurements were highly dependent on the inflow jet direction (Figure 3.4). In the NA method, the measurement positions were parallel to the MLT-inflow and the mean forward flow was acquired from velocity components orthogonal to the measurement positions. However, for LVs with a curved inflow jet, the orthogonal velocity components poorly represented the nature of the inflow jet, especially at distal measurement positions (Figure 3.4b: left), causing high fluctuations in the Vp values from one position to another. The AP method, on the other hand, determined the measurement positions based on the initial frame (peak E-wave) and these measurement positions were maintained throughout the diastolic phases, to obtain a consistent Vp calculation (Figure 3.4b: middle). As the incoming flow has yet to reach the distal part of

LV at the peak E-wave instant, the placement of measurement positions based on the peak of E-wave did not allow us to ascertain the accurate pathway of the inflow jet. This pathway only became obvious at later diastolic phases. Unlike the NA and the AP methods, the velocity components in the AV method was selected according to the direction of the inflow jet and updated at each diastolic phase (Figure 3.4b: right); therefore, this method was able to better track the peak velocity along the pathway of the inflow jet. Further, for the two post-infarct patients who had restrictive filling pattern, their  $V_p$  values are expected to be comparable in magnitude as gauged from their  $SR_{IVR}$  data. This expectation was corroborated only by measurements with the AV method (Figure 3.4c).

For a post-infarct patient with severe LV dilatation and restrictive filling, the  $V_p$  values estimated using the NA and the AP methods were abnormally high as compared to the AV method (Figure 3.3b). As reported in a previous PC-MRI study using a larger group of patients ( $n=46$ ), the  $V_p$  acquired from patients with restrictive filling was shown to have values below 120 cm/s (Houliand et al., 2002). Using this value as a reference, the NA and AP methods might have inaccurately measured the  $V_p$  values and indicated erroneously normal relaxation for patients with restrictive filling. This had been further supported by the preliminary group analysis (Figure 3.5). By using the NA and AP methods, an inconsistent  $V_p$  trend across the measurement positions was also observed in both groups of subjects in addition to abnormally high  $V_p$  values in some of the patients. On the contrary, the AV method demonstrated a more consistent  $V_p$  trend across the measurement positions and significantly differentiated the healthy group from the post-infarct patient group. This significant difference was observed at all measurement positions except at one-third of LV level. The superiority of the AV method was further supported by its strongest correlation with  $SR_{IVR}$  (Figure 3.6), which has been used as a well-established marker for diastolic function (Chen et al., 2014; Nagueh et al., 2009;

Wang, Khoury, Thohan, Torre-Amione, & Nagueh, 2007) In the present study, we have chosen to use  $SR_{IVR}$  derived from CMR-FT instead of the more commonly used speckle tracking echocardiogram as the latter modality was subjected to low inter-observer reproducibility (Kempny et al., 2012; Kowallick et al., 2014). Most importantly, the accuracy of CMR-FT derived strain rates has been validated against gold standard measurements such as invasive pressure measurement (Hor et al., 2010) as well as cardiac tagged image analysis (Gaasch & Zile, 2011).

Since LV sizes vary with cardiac health (Stewart et al., 2011) and between healthy ethnic groups (Chahal et al., 2012),  $V_p$  values at a number of distances away from MLT had been inspected. At the one-third measurement position, the short traveling distance of the inflow jet from the MLT produced unsteady flow propagation. This had been demonstrated by another study that the  $V_p$  measured close to MLT was unable to accurately identify the diastolic dysfunction (Stewart et al., 2011). In addition to the low temporal resolution of PC-MRI, a negligible or zero-time delay was frequently encountered at one-third measurement position, making the estimation of  $V_p$  impossible. The conventional fixed 4 cm distance is also considered inappropriate for characterizing  $V_p$  because this position could be located outside the LV of Asian subjects, unlike the LV sizes of Caucasians as reported in previous studies (Chahal et al., 2012). In addition, the inflow jet does not commonly reach the distal measurement positions, notably the 4 cm measurement position, in most of the MI patients with apical infarction due to the presence of stagnant flow at the apical regions (Van Dantzig, Delemarre, Bot, Koster, & Visser, 1995). This again defeated any  $V_p$  measurement. The same also happened at the two-thirds measurement position, but involving a smaller number of patients. These suggest that the one-half measurement position is more appropriate and feasible for  $V_p$  determination, not only because notable difference was found between the subject groups

(Figure 3.5c), but also because the inflow jet typically passes through mid-LV (Son et al., 2012).

In a clinical setting, the analysis of Vp using any of the methods above is a relatively fast process. Beyond the standard manual segmentation of the 4-chamber image and determination of the MLT line which are necessary in all MRI-based methods, the automated extraction of the Vp results along a given distance line took an average of only 25 s.

### **3.6 Conclusions**

Vp measurement is not a straight-forward matter because of the heterogeneity of inflow pattern and LV size between individuals, which strongly affect the availability and the interpretation of results. It will be challenging for the conventional Vp measurement using CMMD to capture the intricacies found in this work. Conceivably, using multiple CMMD scans along different lines might help to compensate for the data. The use of PC-MRI is possibly a better alternative, especially in serial assessments of diastolic improvement. For patients who are unable to go through an MRI scan, the use of colour Doppler echocardiographic scan with recently developed vector flow mapping technique (Garcia et al., 2010) could be an alternative. With the higher dimensional spatial-temporal data, it is recommended the use of a novel AV method for a more consistent Vp measurement based on mean forward flow, at the midway distance between the MLT-inflow and the apex.

## CHAPTER 4: IMAGE-BASED FLOW ANALYSIS OF INTRAVENTRICULAR FLOW VARIABLES

### 4.1 Introduction

This chapter evaluated the intraventricular flow variables including  $V_p$ , vortex and flow energetic in twenty healthy subjects and thirty MI patients with varying degree of LVEFs. The correlations among the important variables as well as their associations with LV pumping efficiency were also examined.

### 4.2 Literature review

Intraventricular flow dynamics is a potential indicator for heart abnormality as it may be a sign of maladaptive cardiac function before a remarkable structural change takes place (Pedrizzetti et al., 2014). The intracardiac vortex has been reported to be beneficial in facilitating the filling and mixing of blood during diastole (Bermejo et al., 2014; Pasipoularides, 2015) while aiding flow redirection towards the outflow tract during systole (Kilner et al., 2000; Sengupta et al., 2007). Recent studies have also looked at flow-energetic indices, such as energy dissipation (Elbaz et al., 2017; Zhong et al., 2016) and KE fluctuation (Dyverfeldt et al., 2008; Zajac et al., 2015), which may reflect intraventricular flow efficiency.

It is believed that abnormal fluid dynamics in post-infarct patients, triggered by temporal inhomogeneity in myocardial contractions between viable and infarcted segments, can significantly contribute to the progression of cardiac inefficiency leading to heart failure. In a recent study of flow-energetics in post-infarct patients using 2D echo-PIV (Agati et al., 2014), patients with small infarcts and preserved LVEF were observed to have high fluctuations in vorticity and KE, which were associated with excessive DI levels. The authors hypothesised that this phenomenon was a compensatory mechanism to maintain LVEF, which nevertheless, would favour adverse remodelling at a later stage.

In other studies using phase-contrast magnetic resonance imaging (PC-MRI) (Dyverfeldt, Sigfridsson, Kvitting, & Ebbers, 2006), high KE fluctuations, indicated by turbulent KE, were observed in patients with aortic valve diseases (Dyverfeldt et al., 2008) and dilated cardiomyopathy (Zajac et al., 2015). The high LV KE fluctuations were believed to be the cause of maladaptive flow dynamics, and thus, inefficient LV function. While most studies suggested that KE fluctuations would lead to negative consequences, a recent image-based computational fluid dynamics study, which was performed at much finer spatial resolution than existing imaging techniques, had instead, reported a substantial amount of turbulent KE in healthy LVs (Chnafa et al., 2016). Contrary to previous studies, the authors suggested that LV flow turbulence was beneficial in preventing blood aggregation at low shear rates (Einav & Bluestein, 2004) while triggering the mechano-sensitive feedback between blood flow and myocardial wall (Pasipoularides, 2015). In view of these contradictory findings, it remains inconclusive whether the fluctuations in flow-energetic indices were indicative of negative compensatory mechanism, or purely a measurable consequence of dynamic velocity conditions in the LV.

The absence of a coherent vortical arrangement in the patient's LV is believed to be the cause of flow turbulence, thus leading to an increase in DI (Pedrizzetti & Domenichini, 2005; Sengupta et al., 2007). In MI patients, this is believed to be caused by the infarct segments that introduced temporal disequilibrium in the overall myocardial wall motion. Over the last decade, numerous studies have demonstrated the relationship between impaired LV function (measured by LVEF) and abnormal vortex dynamics in MI patients (Domenichini & Pedrizzetti, 2011; Fukuda et al., 2014; Nucifora et al., 2010; Zhang et al., 2013). Despite the various hypotheses linking abnormal vortex dynamics and contraction inhomogeneity with flow-energetic indices in the LV, limited studies have looked into their correlations to understand the mechanism leading to deterioration

in LVEF function. Gürel et al. (2016) found that patients with left bundle branch block had significantly higher apical transverse motion (indicating conduction delay) and vortex energy dissipation (relative strength, vortex relative strength and vortex pulsation) compared with healthy subjects. Based on their findings, they suggested that the increase in vortex energy dissipation was a result of wall-motion dyssynchrony, which disturbed the vortical flow arrangement as well as the transfer of KE during the cardiac cycle in LV. Agati et al. (2014) observed no significant difference in vortex intensity between healthy subjects and post-infarct patients. However, substantially higher vortex fluctuation, KE fluctuation and DI were observed in post-infarct patients with preserved EF. Despite contraction inhomogeneity been suggested to be the cause, no assessment with regards to this had been conducted in their study.

### **4.3 Methodology**

#### **4.3.1 Study Population**

The study population comprised 20 healthy subjects and 30 patients who had ST elevation MI (Table 4.1). The patients were further classified into two groups based on their LVEF. Patients with normal ejection fraction (PNEF) had LVEF  $\geq$  50 percent while patients with reduced ejection fraction (PREF) had LVEF  $<$  50 percent. The exclusion criteria for the patients were unstable angina, atrial fibrillation, tachycardia ( $>$ 100 bpm at rest) and severe valvular regurgitation or stenosis. Healthy subjects had no history of cardiovascular disease and had normal cardiac function as confirmed by echocardiographic examination. Subjects with contraindications to MRI, including claustrophobia and ferrous implants, were excluded. Written informed consent was obtained from all subjects prior to participation in this study. The research was approved by the University of Malaya Medical Centre medical ethics committee (Ref: 989.75).

**Table 4.1: Subject demographics**

	Healthy subjects (n=20)	PNEF (n=14)	PREF (n=16)	Group comparison (P-values)
Gender (male: female)	11:9	11:3	15:1	-
Age	50±8	54±11	56±7	0.071
BSA (m <sup>2</sup> )	1.8±0.2	1.8±0.1	1.7±0.2	0.492
SBP (mmHg)	119±7	137±26	126±16	0.094
DBP (mmHg)	75±7	81±10	72±11	0.124
Heart rate (bpm)	70±10	71±9	72±15	0.731
LVEF (%) <sup>††</sup>	70±9	65±11	36±9	<0.001
LVESV (mL) <sup>††</sup>	25±15	24±12	83±46	<0.001
LVEDV (mL) <sup>††</sup>	81±42	68±29	125±60	0.019
SV (mL)	56±28	44±21	42±19	0.307
GLS (%) <sup>*†</sup>	-16±2	-13±3	-10±2	0.000
TPS-SD (ms)*	71±14	102±39	90±20	0.012
Number of infarct segments <sup>††*</sup>	-	4±3	8±2	<0.001
Infarct size (%) <sup>††*</sup>	-	8±8	21±11	<0.001
NYHA class	-	1.6±0.5	1.9±0.6	0.400
Dyslipidaemia (%)	-	77	44	0.132
Hypertension (%)	-	77	56	0.351
Smoking (%)	-	69	40	0.201
Diabetes mellitus (%)	-	62	69	0.746
Infarct related coronary artery (%)				
Left anterior descending	-	64	94	0.179
Left circumflex	-	14	38	0.294
Right coronary artery	-	36	50	0.525

PNEF, patients with normal ejection fraction; PREF, patients with reduced ejection fraction; BSA, Body surface area; SBP, Systolic blood pressure; DBP, Diastolic blood pressure; LVEF, Left ventricular ejection fraction; LVESV, Left ventricular end systolic volume; LVEDV, Left ventricular end diastolic volume; SV, Stroke volume; GLS, Global longitudinal myocardial strain; TPS-SD, Standard deviation of time-to-peak systolic strain.

<sup>†</sup>significant difference between Healthy vs. PREF

<sup>††</sup>significant difference between PNEF vs. PREF

\*significant difference between Healthy vs. PNEF

## 4.3.2 Image acquisition

### 4.3.2.1 Echocardiography

Transthoracic 2D echocardiographic examination was performed on all subjects with iE33 ultrasound machine (Phillips Medical Systems, Andover, MA, USA) with S5-1 Sector Array transducer. The myocardial contraction and LV dyssynchrony were assessed from three apical long-axis views in 2D Speckle-Tracking Echocardiography. GLS was

acquired from the average segmental peak systolic strain in a 17-segment model. The LV dyssynchrony was evaluated by standard deviation of time-to-peak systolic strain (TPS-SD). To minimize operator error, the procedures were performed by three experienced sonographers and the average values were obtained for GLS and TPS-SD readings.

#### 4.3.2.2 MRI

Cine MRI was performed using a 1.5T MRI scanner (SignaHDxt, GE Healthcare, WI, USA) with the subjects in supine position. An eight-channel cardiac coil was placed on the patient's chest. The ESV, EDV and LVEF were acquired from motion-corrected 3D geometrical models reconstructed based on short axis and long axis of the cine MRI images of the LV (Liew et al., 2015). Cine MRI image acquisition protocol was the same as reported in a previous study (Liew et al., 2015).

PC-MRI was performed using a three-chamber acquisition protocol with multi-breath-hold 2D Fast Cine Phase-Contrast sequence, which enables shorter scan times through prospective gating and segmented k-space. The images were retrospectively reconstructed throughout the entire cardiac cycle. Velocity encoding (VENC) was 150 cm/s with a TR of 6.2–6.5 ms resulting in 20 reconstructed phases. TE was 3.2–3.5 ms, flip angle was 25°, acquisition matrix was 256 × 256 pixels, in which the in-plane pixel resolution was 1.37 mm × 1.37 mm and slice thickness was 8 mm.

Delayed-enhancement MRI (DE-MRI) was performed using 20° flip angle, 256 × 256 pixels acquisition matrix, in which the in-plane pixel resolution was 1.37 mm × 1.37 mm and slice thickness was 8 mm. Images were acquired 8 minutes after the injection of gadolinium as the contrast agent and close to end-systole. Visualisation and quantification of infarct size were manually performed by a qualified radiologist. The infarct size was defined as the percentage ratio of scar mass to total LV mass.

### 4.3.2.3 MRI image analyses

Artefact compensation to mask out phase errors and random noise was performed (Walker et al., 1993). The LV endocardial contours in three-chamber view from all 20 cardiac phases were manually segmented from the magnitude 2D PC-MRI images using Segment software (v1.9 R3216, Medviso, AB) (Heiberg et al., 2010).

The vorticity,  $\omega$ , was derived from 2D velocity field in Equation 4.1,

$$\omega(x, y, t) = \frac{\partial v_x}{\partial y} - \frac{\partial v_y}{\partial x} \quad (4.1)$$

where  $v$  represents in-plane velocity,  $x$  corresponds to the image in-plane horizontal axis and  $y$  corresponds to the in-plane vertical axis (Figure 4.1).

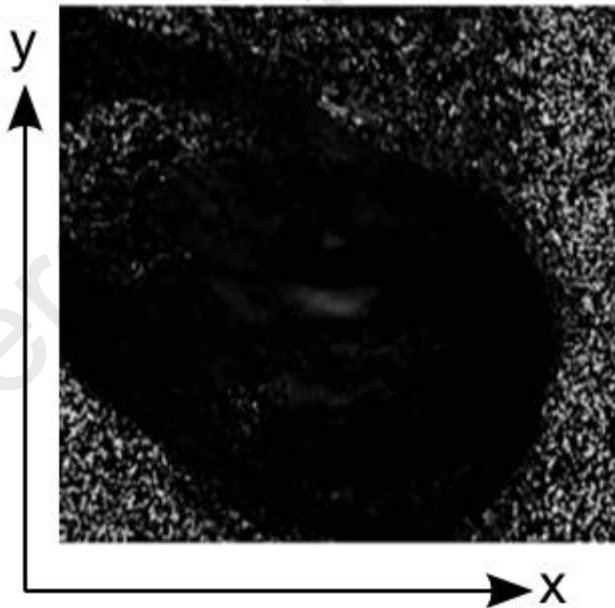


**Figure 4.1: Image axes of phase contrast MR image**

Stream function,  $\psi$ , is estimated from vorticity using Poisson's equation (Equation 4.2),

$$\nabla^2 \psi = -\omega \quad (4.2)$$

with homogeneous boundary conditions applied to the borders of the image and LV wall. The flow pattern was then obtained from phase-averaged or steady-streaming stream function presented in (Agati et al., 2014; Hong et al., 2008). The vortical region was defined as flow region with steady-streaming stream function values of greater than 60% of the maximum.

The vortex flow parameters included area, circulation, sphericity, Reynolds number (Re) and KE were calculated. Vortex area was defined as the vortical region normalised by the LV end-diastolic area (Equation 4.3),

$$\text{Vortex area} = \frac{\int_{\text{vortex}} S_{ss} \, dx dy}{\int_{LV} S_{ED} \, dx dy} \quad (4.3)$$

where  $S_{ss}$  is the pixel area of steady-streaming flow ( $m^2$ ) and  $S_{ED}$  is the pixel area at end diastole. Vortex circulation was the vorticity integral in vortical region ( $m^2/s$ ) normalised by the absolute vorticity integral within the LV ( $m^2/s$ ) (Agati et al., 2014), as shown in Equation 4.4,

$$\text{Vortex circulation} = \frac{S_{\text{vortex}} \int_{\text{vortex}} \omega_{ss} \, dx dy}{S_{LV} \int_{LV} |\omega_{ss}| \, dx dy} \quad (4.4)$$

where  $\omega_{ss}$  is the steady-streaming vorticity ( $1/s$ ),  $S_{\text{vortex}}$  is the total area of vortical region ( $m^2$ ) and  $S_{LV}$  is the total area of LV of steady-streaming flow ( $m^2$ ). Vortex sphericity was the vortex width-to-length ratio (Hong et al., 2008) (Equation 4.5).

$$\text{Vortex sphericity} = \frac{\text{vortex width}}{\text{vortex length}} \quad (4.5)$$

Vortex Reynolds number (Re) was the steady-streaming vorticity integral in vortical region ( $\text{m}^2/\text{s}$ ) normalised by the kinematic viscosity of blood,  $\nu$  ( $\text{m}^2/\text{s}$ ), as shown in Equation 4.6,

$$\text{Vortex Re} = \frac{S_{\text{vortex}} \int_{\text{vortex}} \omega_{\text{ss}} \, dx dy}{\nu} \quad (4.6)$$

where  $\nu$  was set to  $3.3 \times 10^{-6} \text{ m}^2/\text{s}$  (Agati et al., 2014). Vortex KE ( $\text{mJ}/\text{m}$ ) was the steady-streaming kinetic energy,  $\text{KE}_{\text{ss}}$ , contained in the vortical region ( $\text{mJ}$ ) normalised by the vortex radius,  $r_{\text{vortex}}$ , ( $\text{m}$ ) (Bermejo et al., 2014) in steady-streaming flow, as shown in Equation 4.7.

$$\text{Vortex KE} = \frac{\int_{\text{vortex}} \text{KE}_{\text{ss}} \, dx dy}{(r_{\text{vortex}})_{\text{ss}}} \quad (4.7)$$

All the vortex measurements were dimensionless except vortex KE. The  $V_p$  ( $\text{m}/\text{s}$ ) was evaluated by using the AV method at  $\frac{1}{2}$  measurement position as proposed in Chapter 3.

The DI, E' and W' were calculated as dimensionless indices (Agati et al., 2014). The DI described the KE loss due to frictional forces within blood flow and was calculated using Equation 4.8 (Agati et al., 2014).

$$\text{DI} = \frac{T_c \int \int \text{EL} \, dx dy dt}{\int \int \text{KE} \, dx dy dt} \quad (4.8)$$

In the DI formulation, KE ( $\text{kg}/\text{ms}^2$ ) is defined as in Equation 4.9,

$$\text{KE} = \frac{\rho}{2} (v_x^2 + v_y^2) \quad (4.9)$$

and EL is the energy dissipation rate by friction (Bird, Stewart, & Lightfoot, 2002) (kg/ms<sup>3</sup>) calculated by using Equation 4.10,

$$EL = \rho\nu \left\{ \begin{array}{l} 2\left(\frac{\partial v_x}{\partial x}\right)^2 + 2\left(\frac{\partial v_y}{\partial y}\right)^2 + \dots \\ \left(\frac{\partial v_x}{\partial y} + \frac{\partial v_y}{\partial x}\right)^2 \dots \\ -2\left(\frac{\partial v_x}{\partial x} + \frac{\partial v_y}{\partial y}\right)^2 \end{array} \right\} \quad (4.10)$$

where  $\rho$  is the blood density (1050 kg/m<sup>3</sup>),  $\nu$  is kinematic viscosity (3.3×10<sup>-6</sup> m<sup>2</sup>/s) (Agati et al., 2014),  $T_c$  is the cardiac cycle duration (s),  $v_x$  and  $v_y$  are in-plane velocity components (m/s). The  $E'$  and  $W'$  represent the degree of fluctuations and are calculated by using Equations 4.11 and 4.12 (Agati et al., 2014),

$$E' = \frac{\frac{\rho}{2} \int \int_{T LV} \left[ (v_x - v_{x0})^2 + (v_y - v_{y0})^2 \right] dx dy dt}{\int \int_{T LV} KE dx dy dt} \quad (4.11)$$

$$W' = \frac{\int \int_{T LV} (\omega - \omega_0)^2 dx dy dt}{\int \int_{T LV} \omega^2 dx dy dt} \quad (4.12)$$

where  $\omega$  is the vorticity (1/s),  $v_{x0}$ ,  $v_{y0}$  and  $\omega_0$  are the steady-streaming (phase-averaged) velocity (m/s) and vorticity (1/s). The integral was computed as sum of values while the differential was computed as subtraction of values in space. In the following, “flow variables” refer to the aforementioned intraventricular flow energetic indices as well as

vortex flow parameters. The algorithms for calculating flow variables (Equations 4.1 to 4.12) were programmed using MATLAB (vR2012a, Mathworks, Natick, MA).

### **4.3.3 Statistical analysis**

Statistical analysis was performed using Statistical Package for Social Sciences (SPSS v22.0, SPSS Inc., USA). All continuous data were reported as mean  $\pm$  standard deviation and categorical variables were expressed in percentages. The three groups were compared using the Kruskal-Wallis test and post-hoc analysis was used to determine significant difference between groups.

For each subject group, the comparison of E' inside and outside of vortical region was analysed using the Mann-Whitney U test. The relationships between flow-energetic indices, myocardial movement and vortex parameters were analysed using the Pearson correlation test. Determinants of LVEF were assessed by univariate and multivariate linear regression analyses. P-values less than 0.05 were considered to be statistically significant.

## **4.4 Results**

The intraventricular flow patterns demonstrated by a healthy subject, a PNEF and another PREF are shown in Figure 4.2. During diastole, blood filled the LV through the mitral valve, and subsequently rolled-up forming two counter-rotating vortex rings near the LV base as a result of the interaction between the E-wave and flow residing in the LV. Unlike the relatively symmetrical vortex pairs shown in the healthy subject and the PNEF, a pair of asymmetrical vortex rings was observed in PREF. During systole, a substantial amount of flow was ejected through the aortic valve in both healthy and PNEF subjects, with the appearance of a clockwise vortex adjacent to the left ventricular outflow tract (LVOT). On the contrary, a large systolic vortex remained in the mid LV of the PREF, who was unable to eject an adequate flow volume.

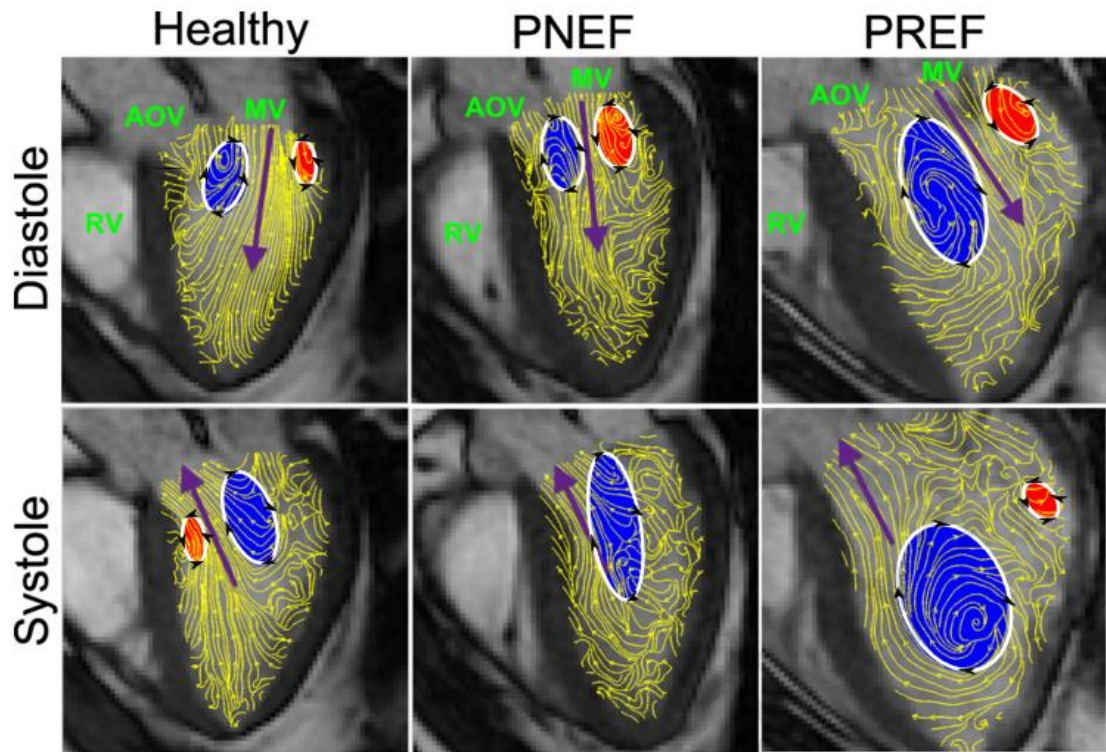


**Figure 4.2: Intraventricular flow patterns of a healthy subject, PNEF and PREF patients during diastole and systole. The flow directions were indicated by the purple arrow and arrows on the yellow velocity streamlines while the vortex appearance was indicated by the blue (clockwise) and red regions (counter-clockwise).**

The characteristics of healthy subjects, PNEF and PREF groups are in Table 4.1. Although ischemia and LV dyssynchrony were observed in PNEF group, they had similar LV volumes and LVEF to healthy subjects. Meanwhile, substantial LV dilatation (enlarged ESV and EDV) and myocardial injury (large infarct size) were noted in PREF group.

Figure 4.3 shows the boxplots of flow-energetic indices (DI,  $E'$  and  $W'$ ), vortex parameters (area, circulation, sphericity index,  $Re$  and  $KE$ ) and  $V_p$  among healthy subjects, PNEF and PREF groups. Overall, the three groups showed significant difference in  $E'$  ( $p < 0.001$ ), vortex area ( $p = 0.003$ ), vortex  $Re$  ( $p = 0.045$ ) and vortex  $KE$  ( $p = 0.003$ ). The PREF group had significantly lower  $E'$  ( $0.58 \pm 0.07$ ) and vortex  $KE$  ( $290 \pm 116$  mJ/m), but a larger vortex area ( $0.14 \pm 0.04$ ) than healthy subjects ( $E'$ :  $0.68 \pm 0.07$ ; vortex  $KE$ :  $445 \pm 144$  mJ/m; vortex area:  $0.10 \pm 0.03$ ) and PNEF ( $E'$ :  $0.68 \pm 0.07$ ; vortex  $KE$ :  $485 \pm 181$

mJ/m; vortex area:  $0.09 \pm 0.02$ ). The vortex Re in PREF group ( $1917 \pm 323$ ) was significantly higher than healthy subjects ( $1575 \pm 381$ ) but not PNEF group ( $1718 \pm 269$ ).

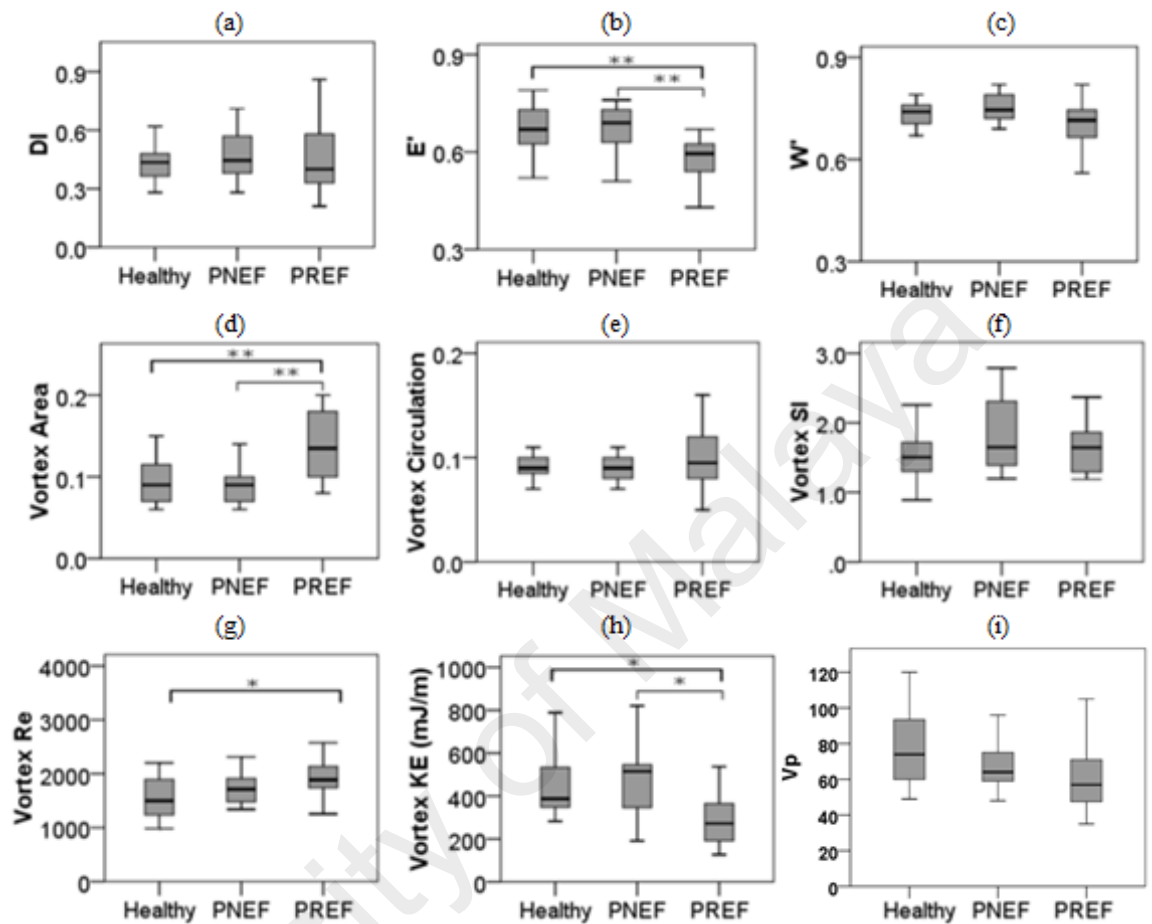


**Figure 4.3: Comparison of intraventricular flow variables among the three subject groups. The box plots indicate the first to third quartiles and the midline in between indicates the median; the whiskers represent maximum and minimum values. Significant difference between the groups were indicated by \*\*( $p < 0.01$ ) and \*( $p < 0.05$ ).**

In patients, the determinants of LVEF were investigated among myocardial properties and flow variables (Table 4.2). The measurements of GLS, infarct size, KE fluctuation index ( $E'$ ), vortex area and vortex KE were significantly correlated with LVEF in univariate analysis. In multivariate analysis, only infarct size and vortex KE were independently associated with LVEF and could explain 71.3 percent of the variation in LVEF (Table 4.2).

**Table 4.2: Univariate and multivariate linear regression analyses for independent correlates of LVEF in patients (PNEF & PREF)**

	Univariate		B	Multivariate	R <sup>2</sup>
	r	p-value		p-value	
<b>GLS (%)</b>	<b>-0.538</b>	<b>0.003</b>			<b>0.713</b>
TPS-SD (ms)	0.097	0.624			
<b>Infarct size (%)</b>	<b>-0.717</b>	<b>&lt;0.001</b>	<b>-0.576</b>	<b>&lt;0.001</b>	
DI	-0.023	0.904			
<b>E'</b>	<b>0.606</b>	<b>&lt;0.001</b>			
W'	0.361	0.050			
<b>Vortex area</b>	<b>-0.553</b>	<b>0.002</b>			
Vortex circulation	-0.118	0.535			
Vortex SI	0.145	0.444			
Vortex Re	-0.306	0.121			
<b>Vortex KE (mJ/m)</b>	<b>0.678</b>	<b>&lt;0.001</b>	<b>0.434</b>	<b>0.002</b>	
Vp (cm/s)	0.110	0.564			

GLS, Global longitudinal strain; TPS-SD, standard deviation of time-to-peak systolic strain; DI, energy dissipation index; E', KE fluctuation index; W', vorticity fluctuation index; r, Pearson correlation coefficient; B, standardized regression coefficient.

As the altered myocardial properties in MI patients were previously suggested to be associated with intraventricular flow turbulence (Agati et al., 2014), the correlations of flow fluctuation (characterised by E') with myocardial contractility (indicated by GLS), infarct size and inhomogeneous contraction (indicated by TPS-SD) were, therefore, examined. The results showed that E' was significantly correlated with GLS ( $r = -0.45$ ,  $p = 0.016$ ) as well as infarct size ( $r = -0.61$ ,  $p < 0.001$ ) as illustrated in Figure 4.4a and Figure 4.4b. However, no correlation was observed between E' and TPS-SD (Figure 4.4d).

In addition, the relationship between energy dissipation (characterised by DI) and E', as reported in a previous echo-PIV study (Agati et al., 2014), was further investigated using PC-MRI, in which no association was observed between the two parameters (Figure 4.4e). The proposed beneficial roles of intracardiac vortex in minimizing energy dissipation, thus helping LV ejection (Pedrizzetti & Sengupta, 2015), was demonstrated by the significant negative correlation between DI and vortex KE ( $r = -0.44$ ,  $p = 0.021$ ) in Figure 4.4c.

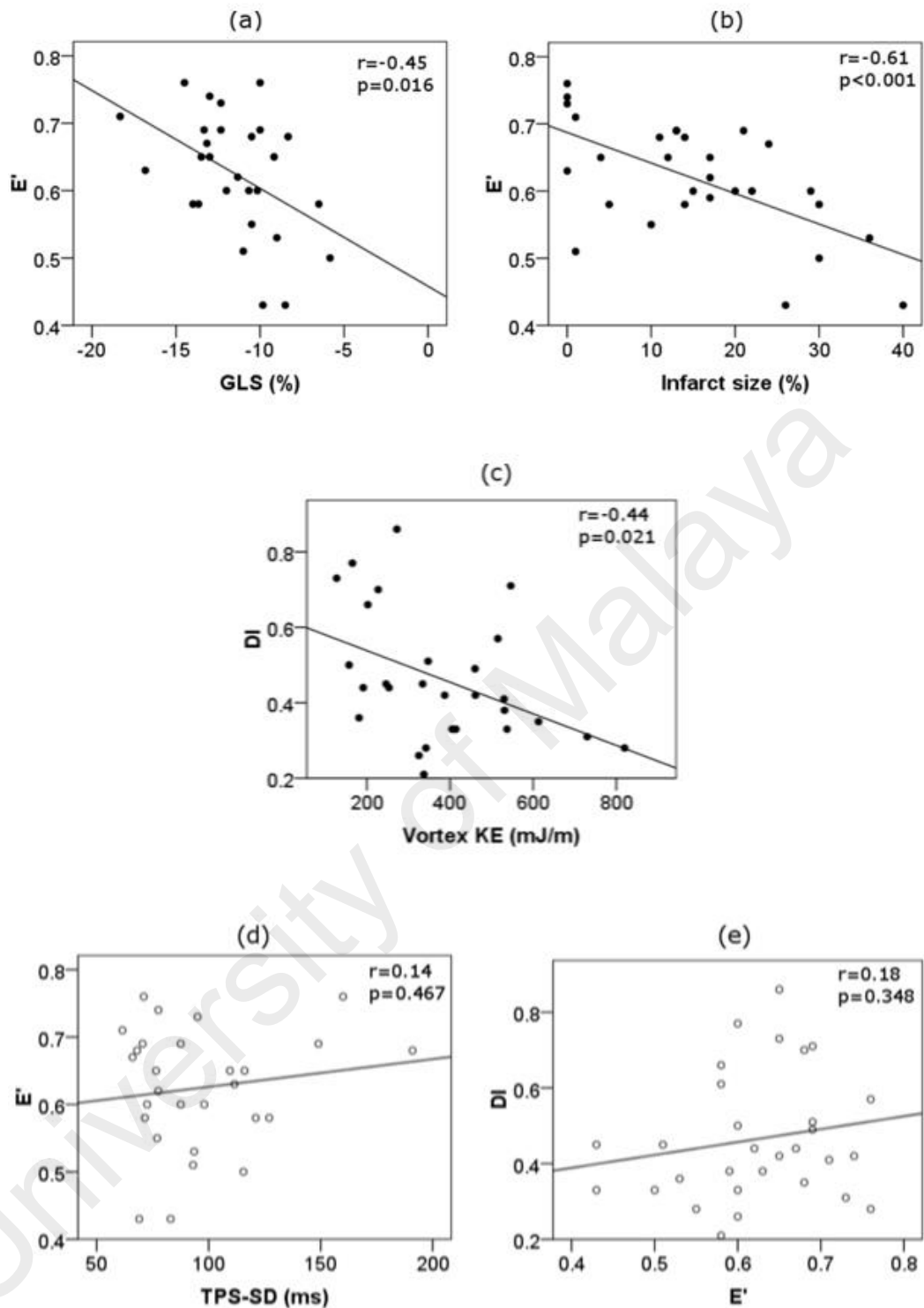


**Figure 4.4: Correlations between  $E'$  and myocardial properties (a, b, d) as well as DI and flow variables (c, e) in MI patients. Significant correlations ( $p < 0.05$ ) were indicated by filled data points.**

As shown in Figure 4.5a, healthy subjects and PNEF group had high  $E'$  that was concentrated inside the vortical region near the LVOT. The regions with concentrated high  $E'$  coincided with high velocity as illustrated in Figure 4.5b. As shown in Figure

4.5c,  $E'$  inside the vortical region was significantly higher than that outside for healthy subjects ( $0.77 \pm 0.08$  vs.  $0.65 \pm 0.07$ ,  $p < 0.001$ ) and for PNEF ( $0.75 \pm 0.13$  vs.  $0.65 \pm 0.06$ ,  $p = 0.012$ ). Whereas for PREF, high  $E'$  was seen along the shear layer outside the vortex. There was no significant difference of  $E'$  inside and outside the vortical regions ( $0.62 \pm 0.11$  vs.  $0.56 \pm 0.07$ ,  $p > 0.05$ ).

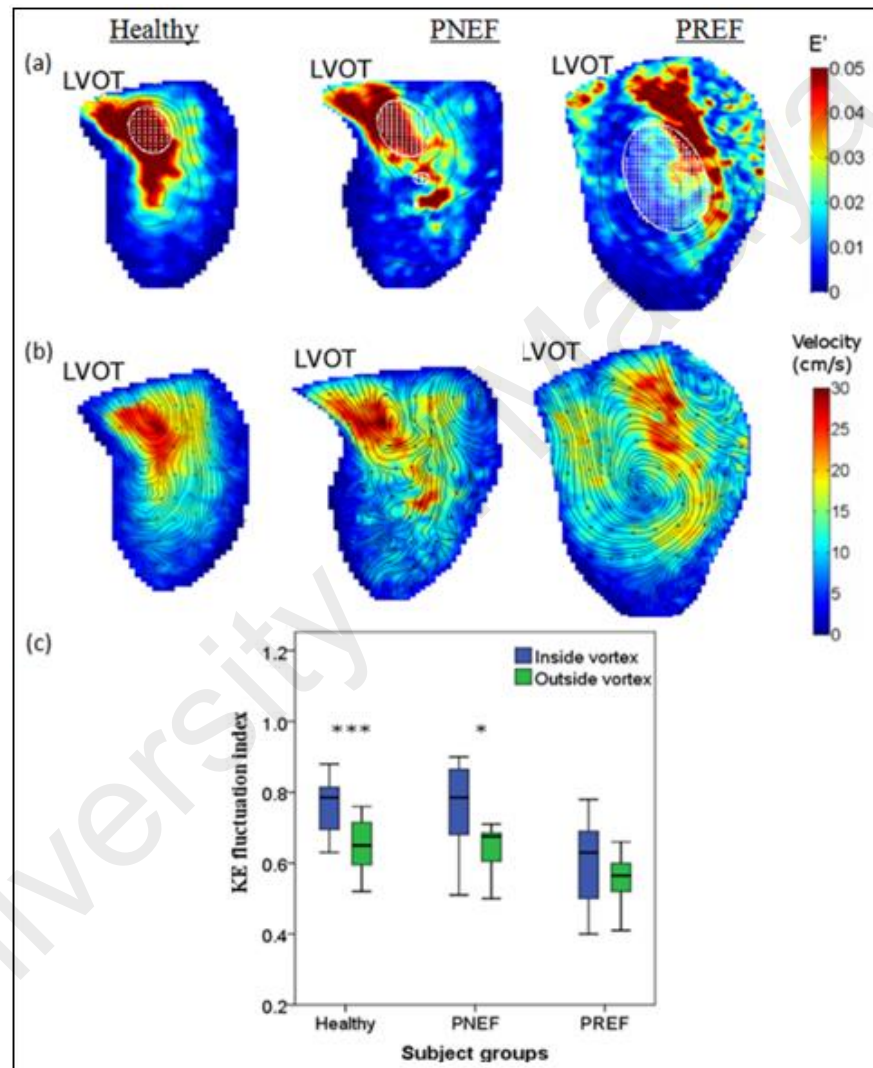


**Figure 4.5: Local distributions of (a) phase-averaged  $E'$  and (b) velocity in the LVOT plane of a healthy, PNEF and PREF subject. The profile of a single patient represents his/her respective groups. Vortex is indicated by the white circular regions in (a). The comparison of  $E'$  inside and outside of the vortical regions is shown in (c) with significant levels at  $p < 0.001$  (\*\*\*) and  $p < 0.05$  (\*).**

#### 4.5 Discussion

To date, 2D PC-MRI has been commonly used for the assessment of cardiovascular flow patterns (Charonko, Kumar, Stewart, Little, & Vlachos, 2013; Kim et al., 1995;

Sundareswaran et al., 2012; Wong et al., 2009). The results of intraventricular flow patterns (Figure 4.2) are in agreement with previously reported findings (Charonko et al., 2013; Kilner et al., 2000; Kim et al., 1995). This is the first study to investigate the intraventricular flow-energetic indices in healthy subjects and MI patients using PC-MRI. Among the key findings were the absence of a significant difference in flow-energetic indices between healthy subjects and PNEF group, and a substantial reduction of  $E'$  in PREF group. The present findings contradicted an echo-PIV study, which found significantly higher flow-energetic indices ( $DI$ ,  $E'$  and  $W'$ ) in the PNEF group compared with healthy subjects (Agati et al., 2014). The discrepancy could be due to the different imaging modalities used. In particular, PC-MRI adopted in the present study is known to be more accurate for high LV velocities (both healthy and PNEF groups have high intraventricular flow velocities) compared with echo-PIV (Hong et al., 2013; Sengupta et al., 2012). Although PC-MRI has a relatively low temporal resolution as compared to echo-PIV, this does not critically affect the key findings as the key variables involved in the present study were computed on each frame individually and phase-averaged results were acquired subsequently. A follow-up study with identical subjects using both PC-MRI and echo-PIV will be helpful to cross-check this hypothesis.

In addition to magnitudes, the spatial distribution of  $E'$  was also quite similar in both the healthy and PNEF groups. Strong acceleration and deceleration of blood was observed near the LVOT, which disturbed the retained blood volume, thus leading to a vigorous flow in the LV. Subsequently, high  $E'$  was found near the LVOT as well as inside the vortex core region. This phenomenon was absent in PREF group, most likely due to damaged heart muscles at critical locations, thus impairing the effectiveness of the contraction process.  $E'$  inside the vortex core was significantly higher than outside in healthy volunteers as well as the PNEF group, but not in the PREF cohort. Seen together, these results suggest that the magnitude and spatial distribution of flow-energetic indices

could identify PREF patients, but are insufficient to distinguish the PNEF group from healthy subjects.

Amongst the MI patients, there was no direct correlation between the levels of flow fluctuation (characterised by  $E'$ ) with DI. In univariate and multivariate analyses, only infarct size and vortex KE were independently associated with LVEF. After excluding the PREF group, the results were similar except that only vortex KE remained significantly correlated with LVEF. There are two key implications of these findings:

Firstly, it is suspected that the high level of flow fluctuations (reflected by DI,  $E'$  and  $W'$ ) observed in both healthy and PNEF subjects were mainly measurable consequences of dynamic velocity conditions in the LV, instead of reflections of negative compensatory mechanisms to help LV ejection. This is further supported by a recent simulation study, known to possess a much finer spatial resolution and accuracy compared with existing imaging modalities, which also demonstrated substantial flow fluctuation in healthy LV (Chnafa et al., 2016). Considering the sensitivities of flow-energetic indices to varying measurement methods with different spatial resolutions and accuracies, more detailed studies using computer simulations and subject follow-up are required to ascertain the role of flow fluctuation in the progression of LV dysfunction.

Interestingly, although  $E'$  in MI patients was not correlated with LVEF,  $E'$  was found to be significantly correlated with GLS and infarct size. In this aspect, the results in this study agree with those reported by Agati et al. (2014). As substantial flow irregularity (high  $E'$ ) was seen in the PNEF but not PREF group, the authors hypothesised that  $E'$  was associated with the homogeneity in myocardial contraction as well as magnitude of flow velocity. Nevertheless, for MI patients, using TPS-SD as an indicator for myocardial dyssynchrony, it was found that this was not the case. Instead of contraction inhomogeneity, the myocardial contraction strength itself (indicated by GLS) affected  $E'$ .

This may explain why the results did not observe an increase in  $E'$  in the PNEF group compared with healthy subjects, even though the former demonstrated a significant degree of contraction inhomogeneity. The results question the applicability of  $E'$  in determining progressive LV failure in MI patients at an early stage.

Second, this study hypothesise that vortex KE may be useful to maintain LV function. This supports the statement in a previous study that the appearance of a vortex in normal LV helps to minimize EL via dissipation and promotes LV ejection (Pedrizzetti & Domenichini, 2005). A high LVEF is believed to be achieved by an energetic vortex (with high vortex KE) that induces a low pressure region in the LV, and subsequently draws intraventricular blood flow towards the LVOT. Amongst the MI patients (PNEF and PREF), an increase in vortex KE was associated with a significant reduction in DI. This is the direct consequence of two effects to the definition of DI (Equation 4.8). First, the denominator (KE in LV, which includes KE inside and outside of the vortex) rises with increasing velocities in the vortex. Second, the stronger flow in the bulk will reduce velocity gradients as fluctuation approaches, thus reducing the numerator (frictional dissipation rate in LV) of Equation 4.8. In other words, while the KE in LV rises, the fraction that is dissipated as heat as indicated by DI drops. However, the correlation is expected as the vortex KE will surely correlate negatively with a quantity involving the reciprocal of the sum of itself and the KE outside the vortex.

Previous studies had suggested that abnormal vortex appearance and evolution could lead to excessive energy dissipation, myofiber work and oxygen consumption (Pedrizzetti & Domenichini, 2005). Despite the postulated vortex roles in helping flow redirection and systolic ejection (Kilner et al., 2000; Pedrizzetti & Domenichini, 2005; Watanabe, Sugiura, & Hisada, 2008), only a few studies had looked into the relationship between

vortex measurements and LVEF (Fukuda et al., 2014; Nucifora et al., 2010; Zhang et al., 2013).

The results showed no difference in the vortex parameters between the healthy subjects and PNEF group, which concurs with a previous echo-PIV study (Agati et al., 2014). However, in PNEF cohort with substantially dilated LVs, a significantly increased vortex area and vortex  $Re$  were noticed. This is in agreement with previous findings which suggested that a dilated LV provides a larger space for the vortex to grow in size (Bermejo et al., 2014; Chan et al., 2013).

#### **4.6 Conclusion**

This study systematically collates and correlates all commonly used flow-variables with performance indices of LVEF function in MI patients. It narrowed down the pool of candidate indices to  $E'$  and vortex KE, which correlated with GLS and LVEF, respectively. The vortex KE, in particular, could be scrutinized as an alternative to LV performance. The quantitative data also enabled a few hypotheses to be supported or refuted, for example, in interpreting the relationship between  $E'$  and LVEF. The inability to distinguish PNEF from healthy subjects, however, calls for more discerning indices, possibly beyond using flow variables.

# CHAPTER 5: INVESTIGATION OF MYOCARDIAL INFARCTION AND INTRAVENTRICULAR FLOW VARIABLES USING 3D FLUID STRUCTURE SIMULATION

## 5.1 Introduction

This chapter investigated the impact of individual MI parameters on the intraventricular flow variables in healthy and MI patients using generic 3D FSI models. The association between individual MI parameters (i.e. infarct size, infarct multiplicity, LVMD and RECV) and intraventricular variables was also studied.

## 5.2 Literature Review

MI is a common cardiovascular disease where intraventricular blood flow dynamics will change with the presence of myocardial deformation (Hong et al., 2013). Thus, intracardiac flow dynamics have been proposed to be used as an indicator of infarction at the early stage (Hong et al., 2013; Pedrizzetti et al., 2014). Among the various flow-related parameters, the analysis of distinct vortices and excessive flow-energetics (energy dissipation and flow fluctuation indices) has been proposed for diagnosis of cardiac abnormality and early risk stratification of MI patients (Agati et al., 2014; Nucifora et al., 2010).

With MI occurrence, LVMD develops due to inhomogeneity in myocardial contraction. In an echo-PIV study, the substantial changes in flow-energetics observed in PNEF have been suggested to be a consequence of LVMD (Agati et al., 2014). LVMD causes multiple conflicting intraventricular vortices, and thus, the LV requires extra effort (dissipating energy) to maintain LVEF. As such, the extensive energy dissipation and flow fluctuation indices have been postulated as compensatory mechanisms of PNEF patients in preserving cardiac function (Agati et al., 2014). However, a recent quantitative study using PC-MRI has observed the opposite of what it was suggested, where there was

no correlation between flow-energetics and LVMD, but flow fluctuation was moderately correlated with infarct size (Chan et al., 2018). It has to be noted that besides MI, excessive flow fluctuations were also noticed in healthy (Chnafa et al., 2016) and dilated cardiomyopathy patients (Mangual et al., 2013; Zajac et al., 2015), who did not have LVMD and infarcts. This indicates that the phenomenon may be triggered by other cardiovascular factors.

The inconsistent observations may also be due to variation of study subjects, who may have inconsistent degrees of impairment in systolic and diastolic function. The high level of flow-energetics in a cardiac cycle can be influenced by its systolic or diastolic phase (Mangual et al., 2013; Wang et al., 2016). Hence, the evaluation of flow-energetics in a full cardiac cycle (Agati et al., 2014; Chan et al., 2018; Chnafa et al., 2016) may mask its corresponding impact during systole and diastole. Another possible reason for the discrepancies is the different modalities used in the studies. Compared with the echo-PIV study (Agati et al., 2014), the use of flow MRI (Chan et al., 2018; Zajac et al., 2015) is more accurate for high velocities as demonstrated in healthy and PNEF patients, whereas the CFD model (Chnafa et al., 2016; Mangual et al., 2013) can provide much finer spatial resolution, which surpasses the limitations of existing imaging modalities.

The investigation of individual MI parameters in clinical studies may pose a challenge because of high variability in patient characteristics and various confounding factors. However, with the advancement of technology, computational models have emerged as a useful tool not only for the study of LV pathophysiology (Doost et al., 2016), but also to investigate the impact of individual risk factors in heart disease (Chan et al., 2013). CFD studies have been conducted to investigate the intraventricular flow pattern in MI (Domenichini & Pedrizzetti, 2011; Khalafvand et al., 2012). A distinct vortex evolution and dynamics have been observed as a consequence of abnormal LV geometry

(Khalafvand et al., 2012) and impaired myocardial wall movement (Domenichini & Pedrizzetti, 2011). However, if the material properties of the myocardial wall are not taken into consideration, determining the accurate intraventricular pressure can become a challenge because blood flow is dependent on the myocardial structure (Cheng et al., 2005). Additionally, the correlation between abnormal wall characteristics and intraventricular flow is impossible to determine from CFD studies.

Cardiac computational incorporating FSI allows better assessment of momentum transfer between wall movement and blood flow, making it more feasible for MI investigation. Only two FSI models were noted being used to explore myocardial wall mechanism and intraventricular flow patterns in MI (Gao et al., 2014; Watanabe et al., 2004). These studies focused on the structural analysis of an inhomogeneous myocardial fibre strain in MI and one study, using a patient-specific model of myocardial tissue assessment, observed that more mechanical energy has been wasted in large infarcts (Watanabe et al., 2004). Although intraventricular flow variables have been proposed as potential indicators of MI in an early stage (Pedrizzetti et al., 2014), only the general intraventricular flow pattern has been studied (Gao et al., 2014; Watanabe et al., 2004). The impact of MI parameters on intraventricular vortex and flow-energetics has not been thoroughly explored and discussed.

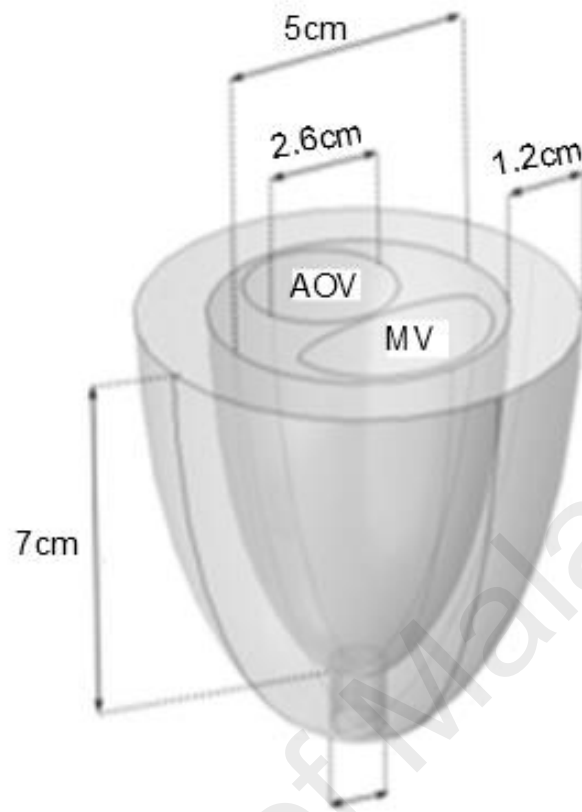
In this study, the levels of systolic and diastolic flow-energetic indices in healthy and MI subjects are investigated using 3D electro-FSI simulation. Apart from that, the association of individual MI parameters (i.e. infarct size, infarct multiplicity, LVMD, and RECV) with intraventricular vortex as well as flow-energetic indices are also studied.

### **5.3 Methodology**

#### **5.3.1 LV geometry**

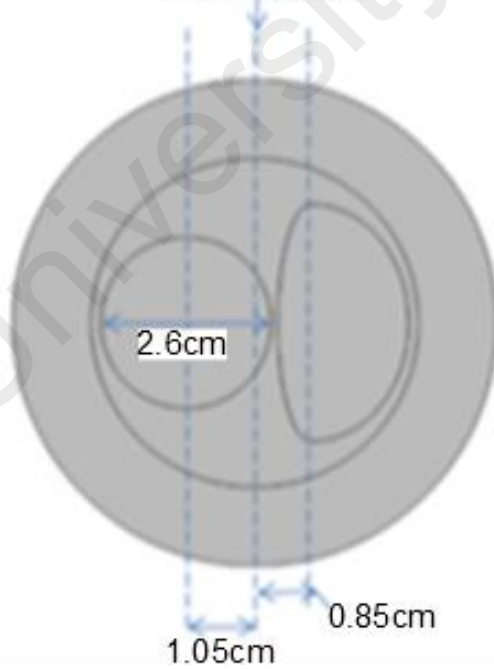
The LV geometry was created which composed of endocardium, epicardium, aortic valve (AOV) and mitral valve (MV). The dimension of LV geometry (Figure 5.1) and model framework were based on a recent electro-FSI implementation (Bakir, Al-Abed, Lovell, & Dokos, 2017). The geometry was constructed using two half prolate ellipsoids, with a major axis of 7 cm, minor axis of 2.5 cm and wall thickness of 1.2 cm. The aortic valve opening area is 5.3 cm<sup>2</sup> while the mitral valve opening area is 5.6 cm<sup>2</sup>. The LV geometrical (Lang et al., 2015) and valve dimensions (Kaplan et al., 2000; Westaby, Karp, Blackstone, & Bishop, 1984) were chosen based on measurements from the published literature on healthy human. A 1-cm diameter cylinder with an isotropic behaviour was used to define the LV apex region in order to prevent singularities in the fibre direction (Bakir et al., 2017; Nordsletten et al., 2011). In this study, a total of five LV geometries (Figure 5.1) were constructed to describe the initial LV geometry of healthy and MI cases.

### LV isometric view



### LV top view

Centre (0,0,0)



### Mitral valve top view

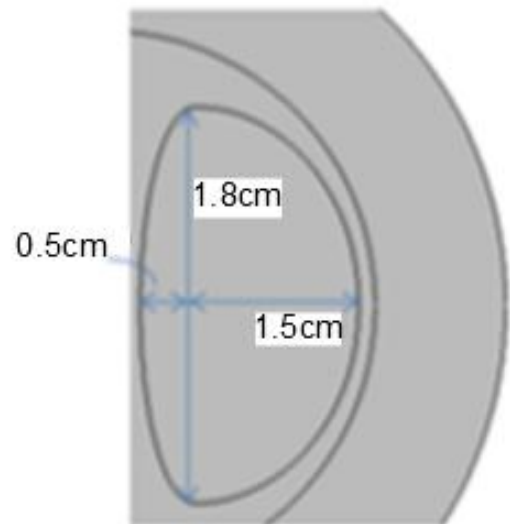


Figure 5.1: LV geometry and dimensions

For simplification, the contribution of the right ventricle and the Purkinje fibre in the original formulation in (Bakir et al., 2017) were excluded. The closed-loop circulation was replaced by a three-element Windkessel as described below. Four groups of physics were employed in the simulation: (1) electrophysiology, (2) excitation-contraction coupling, (3) solid mechanics, and (4) fluid mechanics.

### 5.3.2 Electrophysiology

The propagation of electrical impulse across the myocardium was replicated using the Nash and Panfilov model (Nash & Panfilov, 2004), with slight modification to retain unit consistency by adding a constant  $\beta$  (Bakir et al., 2017). The transmembrane potential or activation variable,  $V$  and conduction of a slow inward current or known as recovery variable,  $R$  that manipulates the recovery of  $V$  were defined in Equations 5.1 and 5.2.

$$\beta C_m \frac{\partial V}{\partial t} = \nabla \cdot (\underline{\underline{\sigma}} \nabla \vec{V}) - \dots$$

$$\beta k_1 k_2 c (V - B) \left( \frac{V - B}{A} - a \right) \left( \frac{V - B}{A} - 1 \right) - \dots$$

$$\beta k_2 c R (V - B)$$
(5.1)

$$\frac{\partial R}{\partial t} = \left( \varepsilon_0 + \frac{\mu_1 R}{\frac{V - B}{A} + \mu_2} \right) \left( -R - k_1 \frac{V - B}{A} \left( \frac{V - B}{A} - a - 1 \right) \right)$$
(5.2)

where the parameters  $\beta = 160000 \text{ m}^{-1}$ ,  $C_m = 0.01 \text{ Fm}^{-2}$ ,  $k_1 = 8$ ,  $k_2 = 100 \text{ s}^{-1}$ ,  $c = 0.01 \text{ Fm}^{-2}$ ,  $A = 0.1 \text{ V}$ ,  $B = -0.08 \text{ V}$ ,  $a = 0.1$ ,  $\varepsilon_0 = 0.2 \text{ s}^{-1}$ ,  $\mu_1 = 20 \text{ s}^{-1}$ ,  $\mu_2 = 0.3$ . The initial value of  $V$  is  $-0.08 \text{ V}$  and initial value of  $R$  is  $0.02$ . The conductivity tensor,  $\underline{\underline{\sigma}}$  (S/m), in Equation 5.1 is calculated from the Equation 5.3

$$\underline{\underline{\sigma}} = \sigma_f (\vec{F} \otimes \vec{F}) + \sigma_s (\vec{S} \otimes \vec{S}) + \sigma_n (\vec{N} \otimes \vec{N}) \quad (5.3)$$

where  $\vec{F}$  represents fibre vector,  $\vec{S}$  represents normal-to-sheet vector,  $\vec{N}$  represents normal vector. The conductivity was anisotropic such that the largest conductivity was in the fibre direction ( $\sigma_f$ ), followed by sheet direction ( $\sigma_s$ ) and normal-to-sheet direction ( $\sigma_n$ ). The value of  $\sigma_f$  is 0.8 S/m and the ratio of  $\sigma_f : \sigma_s : \sigma_n$  was 4: 2: 1. The derivation of  $\underline{\underline{\sigma}}$  can be found in Appendix C. To initiate action potentials, a 2 ms supra-threshold stimulus pulse current was applied at the endocardium at two-thirds the height of the LV distal from the apex.

### 5.3.3 Solid mechanics

The LV fibre varied continuously across the myocardium, oriented from +60° at the epicardium to -60° at the endocardium (Figure 5.2) and the sheet angle was from -45° to 45°. These fibre angles were defined based on the local circumferential direction.

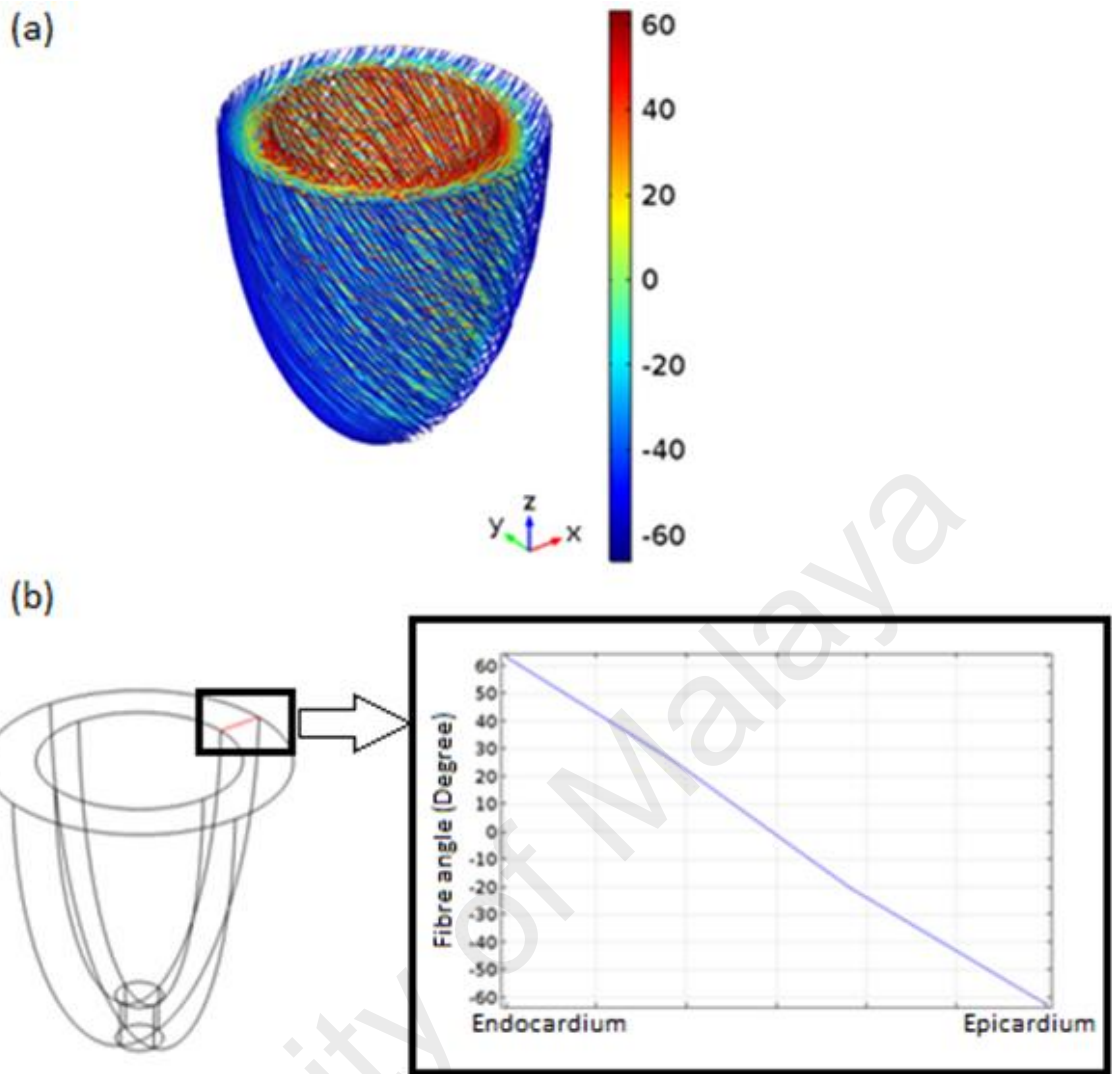


**Figure 5.2: Results of fibre orientation in (a) 3D LV geometry where the colour legend represents fibre angle, (b) fibre angle across the myocardium (myocardial location was indicated by the red line in LV geometry)**

The myocardium was modelled with the nearly incompressible Holzapfel-Ogden hyperelastic material with transverse isotropic behaviour, where the fibre direction was stiffer than the sheet and normal-to-sheet directions (Holzapfel & Ogden, 2009), and volumetric strain-energy (Doll & Schweizerhof, 1999). The strain energy function,  $\psi_s$ , of the myocardium is defined in Equation 5.4.

$$\Psi_s = \Psi_{\text{isotropic}} + \Psi_{\text{fiber}} + \Psi_{\text{vol}} \quad (5.4)$$

where each of the strain energy component was derived as in Equations 5.5 to 5.7.

$$\Psi_{\text{isotropic}} = \frac{a_i}{2b_i} \exp[b_i(I_1 - 3)] \quad (5.5)$$

$$\Psi_{\text{fiber}} = \frac{a_f}{2b_f} \exp[b_f(I_{4f} - 1)^2 - 1] \quad (5.6)$$

$$\Psi_{\text{vol}} = \frac{\kappa(J - 1) \ln(J)}{2} \quad (5.7)$$

where  $a_i$  is 2.28 kPa,  $b_i$  is 9.726,  $a_f$  is 1.685 kPa,  $b_f$  is 15.779,  $\kappa$  is 250 kPa. These parameters were taken previous study (Holzapfel & Ogden, 2009) that performed optimization by fitting to biaxial load experiment measurements. In this implementation, the  $b_i$  value was reduced to 1.945 in order to have the filling pattern in Figure 5.3. The variables  $I_1$  is the first invariant of isochoric elastic right Cauchy-Green tensor,  $\underline{\underline{C}}$ , whilst  $I_{4f} = \vec{F} \cdot (\underline{\underline{CF}})$ .  $J$  is the determinant of the deformation gradient tensor,  $\underline{\underline{F}}$ . In order to ensure material stability,  $I_{4f}$  was set to zero when  $I_{4f} < 0$ . This is to account for the assumption that the fibre does not contribute significantly to the material property during compression as noted in the original Holzapfel and Ogden formulation (Holzapfel & Ogden, 2009). To prevent fibre singularity at the apex, an isotropic behaviour ( $\Psi_{\text{isotropic}}$ ) was assumed at the LV apex where the anisotropic components of the hyperelastic material were discarded.

To ease convergence and reduce non-physiologic oscillation, a Rayleigh damping under was added with  $\alpha_r = 100$  1/s and  $\beta_r = 0.01$  s, similar to the values in previous study (Fritz, Wieners, Seemann, Steen, & Dössel, 2014). Without the damping effect, the heart

appears “dancing” during diastole. The model was set to “inertial included” for structural transient behaviour. The base is held fixed in position.

### 5.3.4 Excitation-contraction coupling

In order to couple the electrical and mechanical behaviour of the model, an active stress,  $T_a$  (kPa) was added to the second Piola Kirchoff stress tensor,  $\underline{\underline{T}}$ , along the fibre, sheet, and normal-to-sheet directions.  $T_a$  was obtained using the single ODE phenomenological model modified by Göktepe and Kuhl (Göktepe & Kuhl, 2010).  $T_a$  along sheet and normal-to-sheet directions was 40% of fibre direction (Usyk, Mazhari, & McCulloch, 2000), as shown in Equation 5.8

$$\underline{\underline{T}} = \frac{\partial \psi_s}{\partial \underline{\underline{E}}} + T_a (\vec{F} \otimes \vec{F}) + 0.4T_a (\vec{S} \otimes \vec{S}) + 0.4T_a (\vec{N} \otimes \vec{N}) \quad (5.8)$$

where  $\underline{\underline{E}}$  is the Green-Lagrange strain tensor while  $\psi_s$  is the strain energy function of myocardium. In the apex with isotropic properties, the apex is assumed to be contracting isotropically at  $T_a$ .

### 5.3.5 Fluid mechanics

The blood in the heart was modelled as incompressible and exhibiting laminar flow using the Navier-Stokes formulations (Cheng et al., 2005; Dahl et al., 2012). A no-slip wall was assumed at the surface at LV base excluding inlet and outlet, while the endocardial wall was set as the fluid-solid interface. The deformation of blood domain was handled by a moving mesh formulation to allow the fluid domain mesh to move as the myocardium deforms.

### 5.3.6 Boundary conditions at inlet and outlet

The mitral valve surface was designated as the inlet and the aortic valve surface was the outlet. During diastole, a time-varying left atrial pressure ( $P_{LA}$ ) was applied as the

inlet boundary condition, which was adjusted till a desired transmitral filling velocity (Figure 5.3) based on previously reported clinical observations on healthy subjects (Abe et al., 2013; Nagueh et al., 2009) was obtained. The inflowing blood passed through a fictitious 50 cm tube length numerically appended to the mitral valve orifice. Blood would flow into the LV when  $P_{LA}$  exceeded the LV pressure ( $P_{LV}$ ) (diastole).

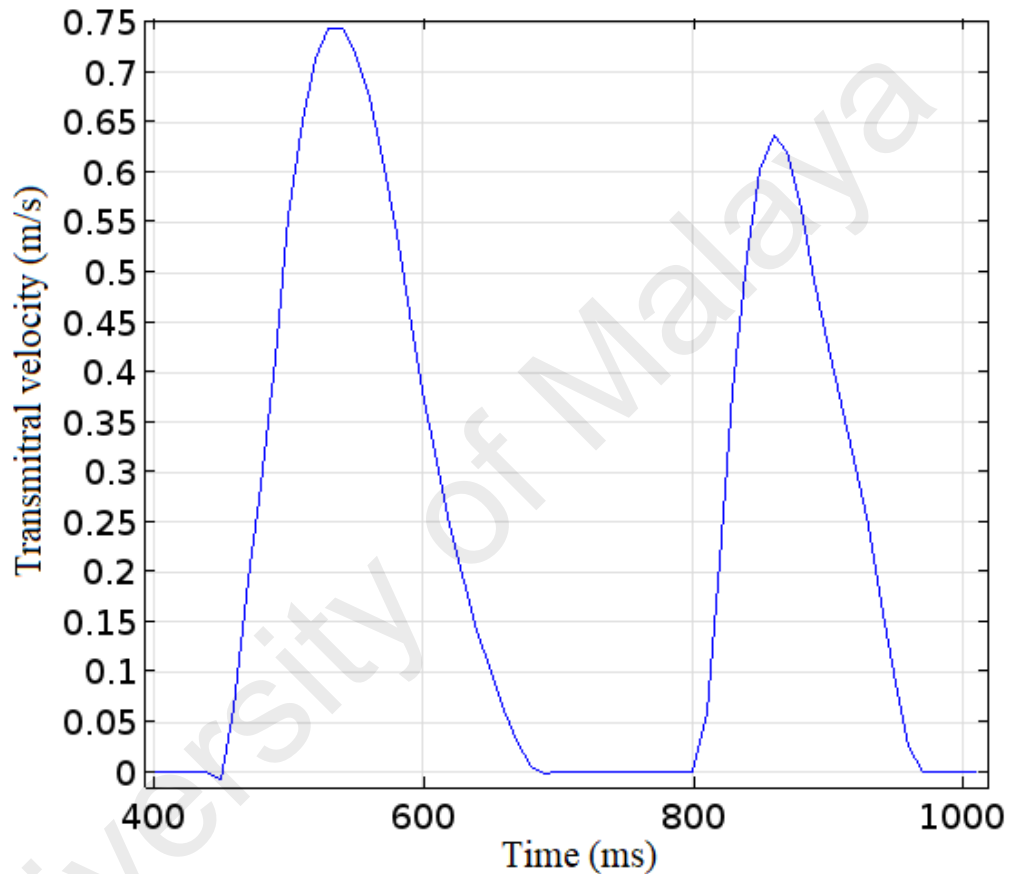


**Figure 5.3: Inflow velocity waveform at mitral valve of healthy LV**

Meanwhile, the LV outlet was connected to a three-element Windkessel model, where blood would flow out from the aortic valve when the aortic pressure ( $P_{aorta}$ ) was greater than the systemic pressure ( $P_{systemic}$ ) in the Windkessel model (systole), as described in Equation 5.9

$$Q_{aorta} = C \frac{dP_{systemic}}{dt} + \frac{P_{systemic}}{R_{systemic}} \quad (5.9)$$

where the parameter values of the Windkessel model were as follows:  $C = 5.81 \text{ ml} \cdot \text{mmHg}^{-1}$ ,  $R_{aorta} = 0.06 \text{ mmHg} \cdot \text{s} \cdot \text{ml}^{-1}$  and  $R_{systemic} = 1 \text{ mmHg} \cdot \text{s} \cdot \text{ml}^{-1}$  (Bakir et al., 2017; Lim et al., 2010; Simaan, Ferreira, Chen, Antaki, & Galati, 2009; Watanabe et al., 2004), while the initial value of  $P_{systemic}$  was set to 89 mmHg (Bakir et al., 2017; Guyton, 1986). The flow rates through the mitral ( $Q_{mitral}$ ) and aortic valves ( $Q_{aorta}$ ) were defined in Equations 5.10 and 5.11,

$$Q_{mitral} = \begin{cases} \frac{P_{mitral} - P_{LV}}{R_{mitral}} & , P_{mitral} > P_{LV} \\ 0 & , P_{mitral} \leq P_{LV} \end{cases} \quad (5.10)$$

$$Q_{aorta} = \begin{cases} \frac{P_{aorta} - P_{systemic}}{R_{aorta}} & , P_{aorta} > P_{systemic} \\ 0 & , P_{aorta} \leq P_{systemic} \end{cases} \quad (5.11)$$

where  $R_{mitral}$  was the mitral valve resistance (set to  $0.008 \text{ mmHg} \cdot \text{s} \cdot \text{ml}^{-1}$ ), and  $R_{aorta}$  was the aortic valve resistance (set to  $0.06 \text{ mmHg} \cdot \text{s} \cdot \text{ml}^{-1}$ ). The parameter values of the valve resistances as well as the Windkessel model were fixed across models in order not to influence the comparison results among the models.

### 5.3.7 Infarct models

All infarcts were modelled as round shape and extended across the full thickness of the LV. The infarcts were located at mid-height of LV, at a distance from base and apex to avoid boundary effects (Leong et al., 2017). The infarct size was defined as the percentage ratio of the infarcted region to the myocardial wall volume of the LV. The different sizes of infarcts (10% vs. 20%) and infarct multiplicity (single infarct vs. two

opposite infarcts or known as multiple infarcts in this thesis) were incorporated into the infarct models. The appearance of different infarct characteristics was shown in Figure 5.4.

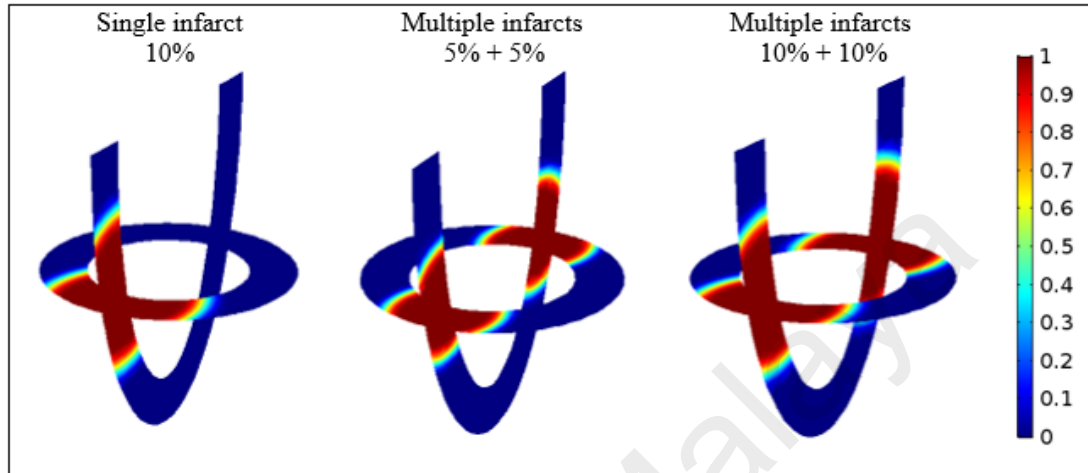


**Figure 5.4: Constructed infarct LVs with varying infarct size and multiplicity. The red and blue colours represent infarct and remote regions respectively, whilst colour in between the two indicates border zone.**

To account for lower electrical conductivity of the infarct regions, conductivity parameters in (Bakir et al., 2017) were tuned such that the ratio of conduction velocity from infarct ( $\sigma_f = 0.025$  S/m) to healthy regions ( $\sigma_f = 2$  S/m) matched the experimental results from a previous study (Abd-Elmoniem et al., 2012). The infarct was also assumed to be non-contractile ( $T_a = 0$  kPa) (Gao et al., 2014). The border zones were transition regions that inherited properties changing from infarct to healthy regions. The material properties of healthy region was based on previous study (Holzapfel & Ogden, 2009) that performed optimization by fitting to biaxial load experiment measurements. The passive material properties of the infarct and border zones were modelled to be three times stiffer than the remote region (Hiesinger et al., 2012; Leong et al., 2017). The stress-strain relationships of healthy and infarct regions were compared in Figure 5.5.

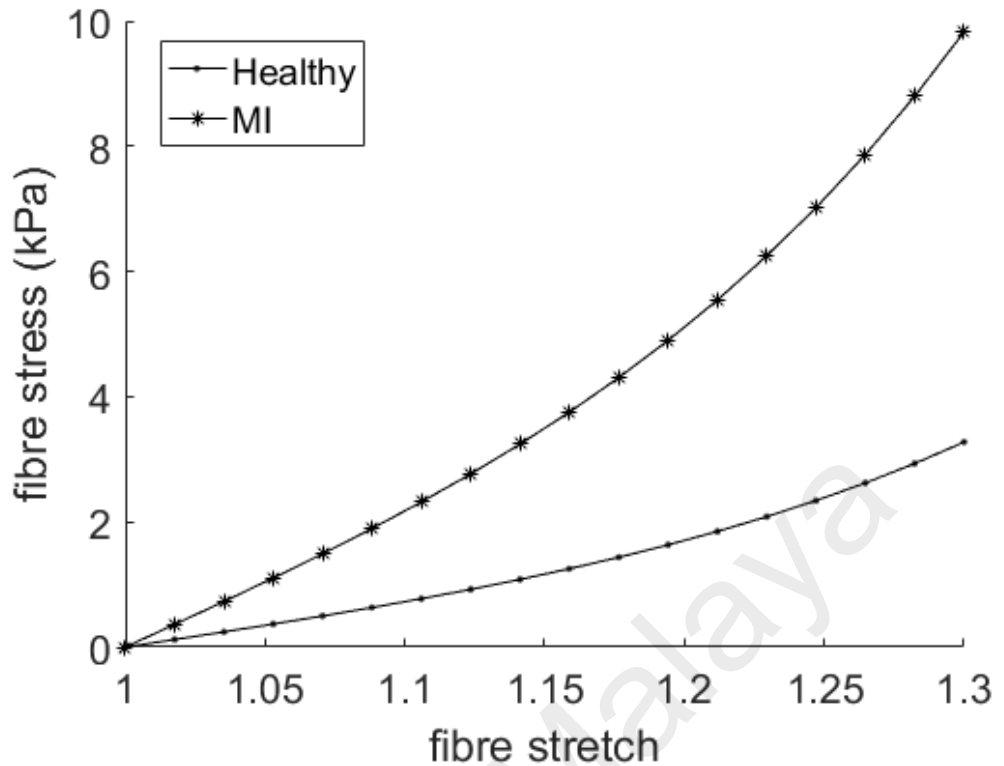


**Figure 5.5: Comparison of stress-strain curves under uniaxial tension along fibre direction for healthy and MI LV.**

To study the effects of RECVm in MI patients, the contraction strength ( $T_a$ ) of the healthy region in an infarcted LV was elevated so that it achieved the same LVEF as in healthy LV.

### 5.3.8 Simulation models

Four diseased LV models that had different MI parameters (i.e. LV size, infarct multiplicity, LVMD, and RECVm) were constructed. A healthy LV model was also produced to serve as baseline comparison. Thus, a total of 5 individual LV models were simulated in this study: healthy model, NEF-5+5, REF-5+5, REF-10 and REF-10+10. The term “NEF” was used to indicate infarct LV with normal ejection fraction while “REF” was used to indicate infarct LV with a reduced ejection fraction. Table 5.1

summarises the settings of the FSI models. The LV dimensional and functional parameters in Table 5.1 were comparable to previously published clinical studies on healthy subjects (Cain et al., 2009) and MI patients (Chang et al., 2009; Nucifora et al., 2010; Zhang et al., 2013).

**Table 5.1: Model settings in FSI simulation**

Model	Total infarct size (%)	ESV (mL)	EDV (mL)	LVEF (%)	Peak systolic velocity (m/s)	SDI (%)	EDP (mmHg)	E-peak (m/s)	A-peak (m/s)	E/A ratio
Healthy LV	N/A	70	151	54	1.5	5.81	11	0.74	0.64	1.2
NEF-5+5	10	70	151	54	1.7	8.87	13	0.70	0.70	1.0
REF-5+5	10	79	151	48	1.3	9.82	13	0.79	0.60	1.3
REF-10	10	79	151	48	1.3	9.58	13	0.78	0.61	1.3
REF-10+10	20	89	151	41	1.1	11.49	15	0.73	0.79	0.8

NEF = normal ejection fraction. REF = Reduced ejection fraction. REF-10 had single infarct while the other infarcted LV models (NEF-5+5, REF-5+5 and REF-10+10) had multiple infarcts. ESV, End-Systolic Volume; EDV, End-Diastolic Volume; LVEF, Left Ventricular Ejection Fraction; SDI, Systolic Dyssynchrony Index; and, EDP, End Diastolic Pressure.

### 5.3.9 Discretisation and implementation

The LV geometry was discretised whereby the blood flow domain had finer mesh than the myocardial wall domain. The mesh independent test was performed in healthy model with element sizes of 6.5 mm, 6.1 mm, 5.7 mm, 5.3 mm and 4.9 mm in blood flow domain. The meshes were considered sufficient when the differences of average wall displacement, LV volume, LV pressure and flow-energetic indices (DI, E' and W') were less than 3% in filling phase. Considering the computational efficiency and mesh size of 5.7 mm yielded converged results, the 5.7 mm was chosen for all subsequent simulations. A total of 44,509 elements with an average mesh size of 5.7 mm in blood flow domain, and 5.9 mm in wall domain, were used in the present study.

The simulation was performed using finite element fully-coupled FSI and Partial Differential Equation modules in COMSOL (v5.2, COMSOL AB, Sweden). The Navier-Stokes and myocardial constitutive equations were solved using PARDISO solver with

backward difference formulation method. The absolute tolerance level was set at  $5 \times 10^{-4}$ , with a time-step of 20 ms in diastole and 2 ms in systole (Bakir et al., 2017).

The simulation process was indicated in Figure 5.6. At first, the initial LV geometry was filled with blood-flow volume from the original zero-stress configuration until a desired EDV was achieved. Subsequently, the electrical stimulus was initiated to generate action potential that spread across LV from apex towards base. Then, the simulation starts with a systole, followed by a diastole. The simulation was run for three cycles until a steady PV loop and flow-energetic results were obtained. It took 25 hours to solve for a full cycle using an Intel(R) Core (TM) i7-2600 3.40GHz processor with 32GB RAM.

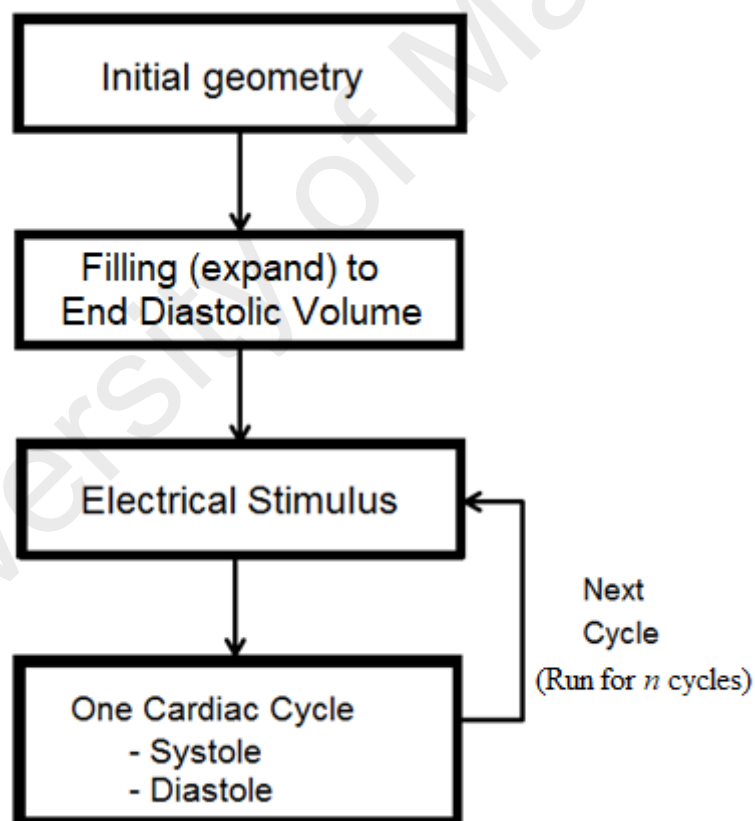


**Figure 5.6: Flow chart of simulation process where  $n$  was 3 cycles in this study.**

### 5.3.10 3D assessment of flow energetic indices

The formulation of flow-energetics was based on previous 2D studies (Agati et al., 2014; Chan et al., 2018), where the energy dissipation index (DI), KE fluctuation index (E') and vorticity fluctuation index (W') were calculated as dimensionless indices. The 2D formulation was extended to 3D in this study.

The DI describes the viscous EL within blood flow and was calculated using Equation 5.12,

$$DI = \frac{T_c \int \int EL dV dt}{\int \int KE dV dt} \quad (5.12)$$

In the DI formulation, KE (kg/ms<sup>2</sup>) is defined by Equation 5.13,

$$KE = \frac{\rho}{2} (v_x^2 + v_y^2 + v_z^2) \quad (5.13)$$

and EL (kg/ms<sup>3</sup>) is the viscous EL calculated by Equation 5.14,

$$EL = \mu \left\{ \begin{array}{l} 2 \left[ \left( \frac{\partial v_x}{\partial x} \right)^2 + \left( \frac{\partial v_y}{\partial y} \right)^2 + \left( \frac{\partial v_z}{\partial z} \right)^2 \right] + \dots \\ \left( \frac{\partial v_x}{\partial y} + \frac{\partial v_y}{\partial x} \right)^2 + \left( \frac{\partial v_z}{\partial y} + \frac{\partial v_y}{\partial z} \right)^2 + \left( \frac{\partial v_x}{\partial z} + \frac{\partial v_z}{\partial x} \right)^2 - \dots \\ \frac{2}{3} \left( \frac{\partial v_x}{\partial x} + \frac{\partial v_y}{\partial y} + \frac{\partial v_z}{\partial z} \right)^2 \end{array} \right. \quad (5.14)$$

where  $T_c$  is cardiac cycle duration (s),  $\rho$  is blood density (1060 kg/m<sup>3</sup>),  $\mu$  is blood viscosity (0.0035 Pa.s) while  $v_x$ ,  $v_y$  and  $v_z$  are blood flow velocity components (m/s).

E' represents the degree of KE fluctuations and is calculated by using Equation 5.15,

$$E' = \frac{\frac{\rho}{2} \int_T \int_{LV} \left[ (v_x - v_{x0})^2 + (v_y - v_{y0})^2 + (v_z - v_{z0})^2 \right] dV dt}{\int_T \int_{LV} KE dV dt} \quad (5.15)$$

while  $W'$  defines the degree of vorticity fluctuations and the calculation is based on Equation 5.16,

$$W' = \frac{\int_T \int_{LV} (\omega - \omega_0)^2 dV dt}{\int_T \int_{LV} \omega^2 dV dt} \quad (5.16)$$

where  $\omega$  is the vorticity,  $v_{x0}$ ,  $v_{y0}$ ,  $v_{z0}$  and  $\omega_0$  are the phase-averaged velocity (m/s) and vorticity (1/s).

### 5.3.11 Vortex identification and assessments

The vortical region was detected using  $\lambda_2$ -criterion (Jeong & Hussain, 1995) and visualised as isosurfaces throughout the cardiac cycle. A threshold of  $\lambda_2 < \lambda_{\text{threshold}}$  was applied to decrease the vortical region so that the significant vortex seen visually could be presented (Loerakker, Cox, Van Heijst, De Mol, & Van De Vosse, 2008). The same  $\lambda_{\text{threshold}}$  ( $-300 \text{ s}^{-2}$ ) was used in all cases for comparison. The vortex parameters evaluated included volume, depth, circulation and KE. Vortex volume was the 3D vortex volume normalised with the LV volume. Vortex depth was the distance between the vortex centre and LV base that was normalised to the LV axis length. Vortex circulation was the integral of the vorticity magnitude within vortical region, normalised to the vorticity magnitude in the LV chamber. Vortex KE was the KE entrained in the vortical region normalised to LV KE. All these vortex flow parameters were dimensionless. The mean vortex flow parameters were expressed as a time-average during systole, diastole and a full cardiac cycle.

### **5.3.12 Myocardial assessment of Systolic Dyssynchrony Index (SDI)**

The Systolic Dyssynchrony Index (SDI) was used to characterise the homogeneity of myocardial contraction or mechanical dyssynchrony extent in LV (Delgado et al., 2008). A total of 2750 points were equally distributed in the myocardium, spanning 1cm from under the fixed base to apex. In the assessment, the systolic fibre strain of these myocardial points was calculated and the standard deviation of TPS-SD among all myocardial points was evaluated. SDI was expressed as a percentage of TPS-SD in duration of the cardiac cycle (Delgado et al., 2008). The greater the SDI value, the higher degree of LVMD.

## **5.4 Results**

### **5.4.1.1 Assessment of LV dyssynchrony**

Figure 5.7 illustrates the fibre strain (Green-Lagrange strain) distribution in a healthy LV and infarcted LV (represented by REF-5+5) during end systole and end diastole. Healthy LV demonstrated homogeneous fibre strain across the endocardium, whereby the muscle fibres would contract (negative strain) during systole (Figure 5.7a) and relax during diastole (Figure 5.7c). On the other hand, a heterogeneous fibre strain was seen distributed across an infarcted LV, particularly within the dead tissue. The movement of muscle fibres in the infarct contradicted those in remote regions, where they lengthen (positive strain) instead of shortening during systole (Figure 5.7b), and the least expansion (fibres relaxing) was observed within the infarct during diastole (Figure 5.7d).

In SDI assessment (Table 5.1), the healthy LV had the smallest SDI (5.81%) while all infarcted LVs demonstrated greater SDI due to their feature that caused a heterogeneous myocardial contraction. The effects of RECVm could slightly improve LVMD. Therefore, NEF-5+5 (which was affected by RECVm) had the lowest SDI value (8.87%) among all the infarct models because the contraction of remote regions in that

myocardium was more homogenous. The SDI value was comparable with REF-5+5 (9.82%) and REF-10 (9.58%), both of which had the same LVEF and infarct size. The LV with the largest infarct (REF-10+10) demonstrated the highest degree of LVMD (SDI = 11.49%).

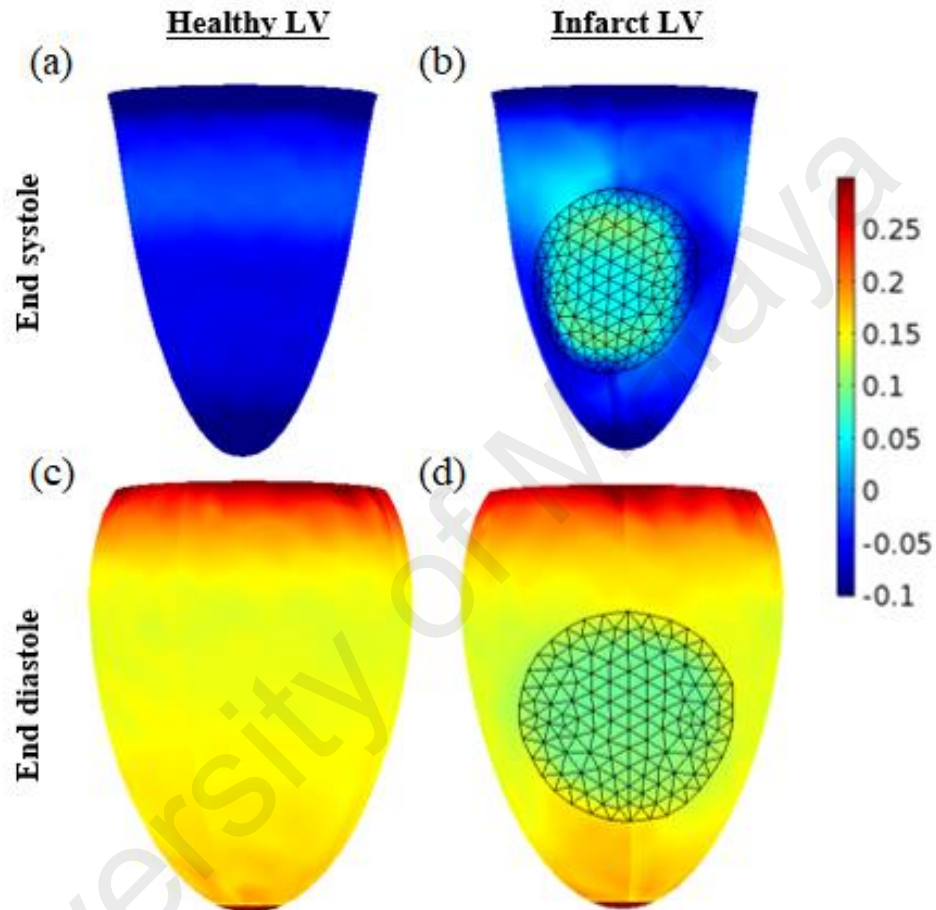


**Figure 5.7: Endocardial Green-Lagrange fibre strain in healthy and infarct LV (REF-5+5) during end systole (a, b) and end diastole (c, d). Negative strain represents muscle fibre shortening while positive strain represents fibre lengthening. Black grid on endocardium indicates infarct.**

#### 5.4.1.2 Vortex evolution

Figure 5.8 showed the vortex evolution in healthy and infarcted LVs (represented by REF-10+10) at different intervals of a cardiac cycle. In healthy LV, a vortex formed beneath the mitral inlet, along with a high velocity inflow jet during E-wave deceleration. The vortex kept growing while propagating into the LV cavity (Figure 5.8a). Later, in

diastasis, no inflow was coming into the LV because atrioventricular pressure was in equilibrium. The large diastolic vortex was progressing towards the apical region (Figure 5.8b) and slowly weakening. In late diastole, a new smaller vortex formed at the LV base due to atrial contraction (A-wave), which then continued moving into the LV cavity (Figure 5.8c). The diastolic vortex remained in the LV chamber and travelled towards the aortic outlet during systole (Figure 5.8d). The vortex continued to shrink along with flow ejection, and eventually disappeared in late systole.

The vortex evolution in all infarct models were similar to the healthy LV. However, due to the infarct appearance that reduced the heart chamber compliance, the vortex in REF-5+5 and REF-10 were smaller and propagated slower than those in healthy LV, especially in E-deceleration and mid-systole, whereas REF-10+10 had the smallest vortex that moved the slowest. In REF-10+10, a small diastolic vortex formed during E-wave deceleration (Figure 5.8e), which had limited growth in diastasis (Figure 5.8f). Then another vortex formed in late diastole due to atrial contraction (Figure 5.8g), which had comparable size to its early diastolic vortex (Figure 5.8e) in order to compensate the early diastolic filling. The late diastolic vortex persisted into systole but travelled slowly from mid-height of the LV towards the aortic outlet in mid-systole (Figure 5.8h).

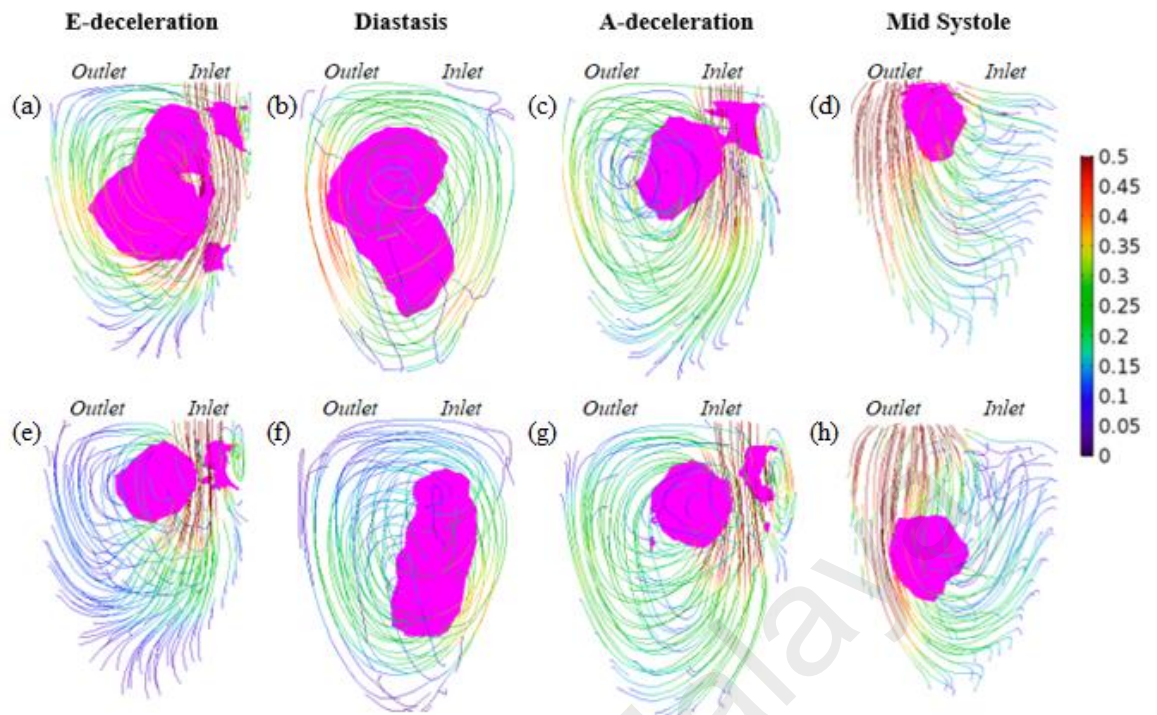


**Figure 5.8: Vortex evolution in healthy (a-d) and REF-10+10 (e-h) in LVOT view. The 3D vortex is visualised by magenta isosurfaces ( $\lambda_2 = -300 \text{ s}^{-2}$ ) and the colour map represents the magnitude of velocity streamline (m/s).**

#### 5.4.1.3 Viscous energy dissipation

Figure 5.9 shows the comparison of vortex appearance (Figure 5.9a-c) and spatial distribution of endocardial viscous EL (Figure 5.9d-f) in LVOT view at mid-systole of REF-5+5, REF-10 and REF-10+10. In all LV models, most of the high viscous EL happened at the area with high flow velocity i.e. close to inlet during diastole and outlet during systole (Figure 5.9a-c vs. Figure 5.9d-f). In addition, the high flow velocity region also appeared adjacent to the vortex core, where its recirculating motion also caused high viscous EL at the endocardium. The observation of high endocardial viscous EL was more significant when the vortex core was located near the infarct (Figure 5.9f). In LV with weakest systolic function (REF-10+10), about 50% of the total endocardial viscous EL occurred within its infarct, while in all other infarct models, it was 30% only. By having comparable flow velocity and infarct size, however, more flow disturbance and greater

viscous EL were noticed in the LV with multiple infarcts (REF-5+5) compared with a single infarct (REF-10), especially at regions between the two infarcted areas (Figure 5.9g).

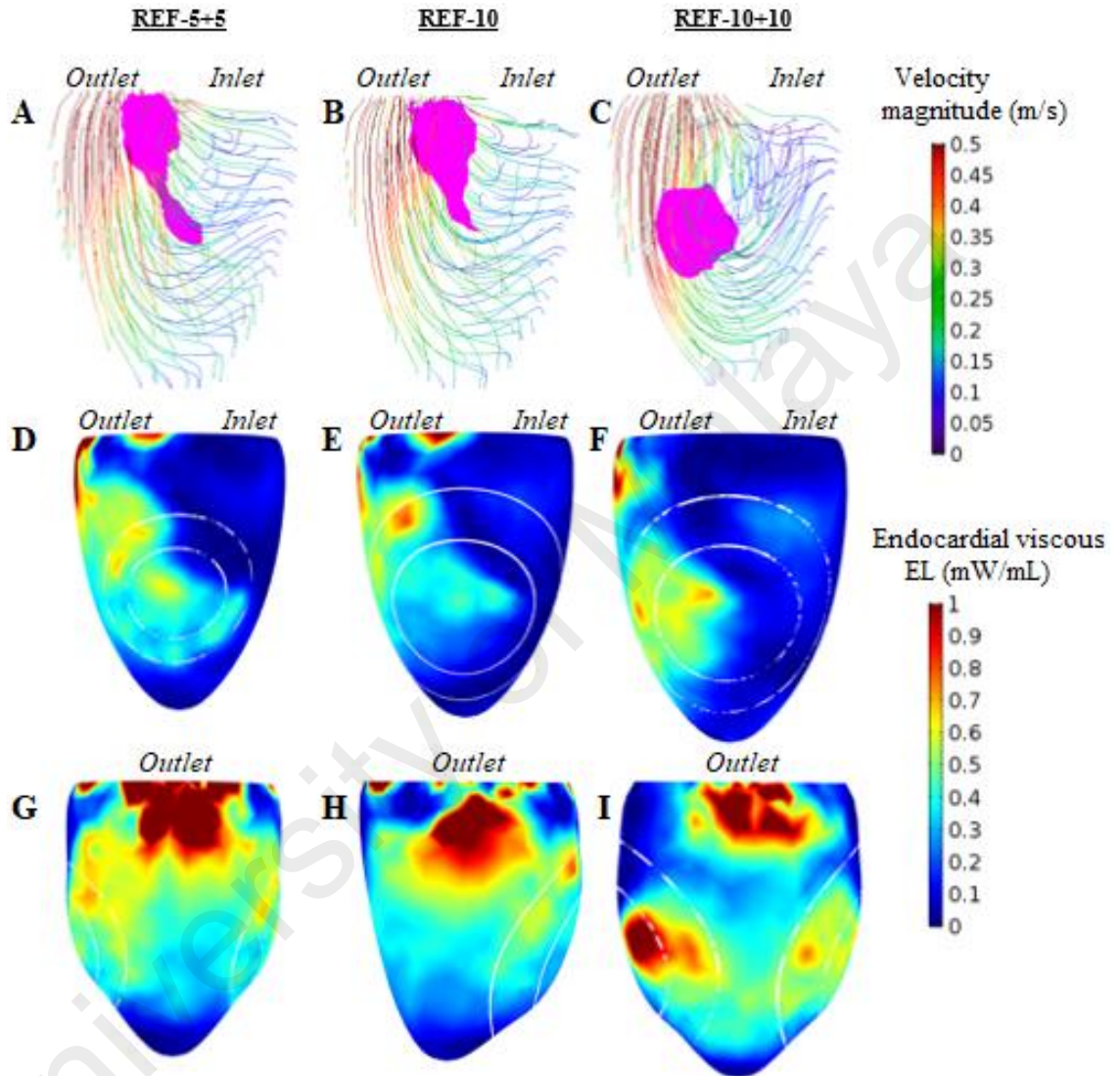


**Figure 5.9:** Vortex appearance with velocity streamlines in front view (a-c) and endocardial viscous EL (d-i) in REF-5+5, REF-10 and REF-10+10 during mid-systole. The endocardial viscous EL is shown in front view (d-f) and sagittal view (g-i). White circular lines on endocardium indicates infarct region. Colour maps represent velocity magnitude (m/s) (top) and endocardial viscous EL (mW/mL) (bottom). Vortex is visualised by magenta colour isosurfaces ( $\lambda_2 = -300 \text{ s}^{-2}$ )

#### 5.4.1.4 Analysis of flow energetic indices (DI, E' and W')

Figure 5.10 indicated the percentage differences of intraventricular flow-energetic indices (DI, E' and W') between healthy LV and each infarct model during systole and diastole. Overall, the infarct appearance contributed to excessive DI in both systole and diastole, except in REF-10+10. A substantial increment in DI was found in the NEF-5+5 and REF-5+5 cases. The LV model with a single infarct (REF-10) presented a significantly lower DI than the multiple infarcts cases (REF-5+5).

In terms of E', only the LV with RECVI (NEF-5+5) showed greater systolic E' than healthy LV, whereas the other infarct models had much lower E' coincidentally with their weaker LVEF. In diastole, the E' demonstrated an inverse trend to the systolic E'. The lowest diastolic E' was found in the LV with strong systolic function (NEF-5+5), while the LV with weakest LVEF (REF-10+10) had the greatest diastolic E'. The W' had similar trend to E' in systole and diastole, predominantly the NEF-5+5 had the greatest systolic W', but the lowest diastolic W' as a result of RECVI. In diastole, there is no remarkable difference in W' between the healthy LV and other infarct models.

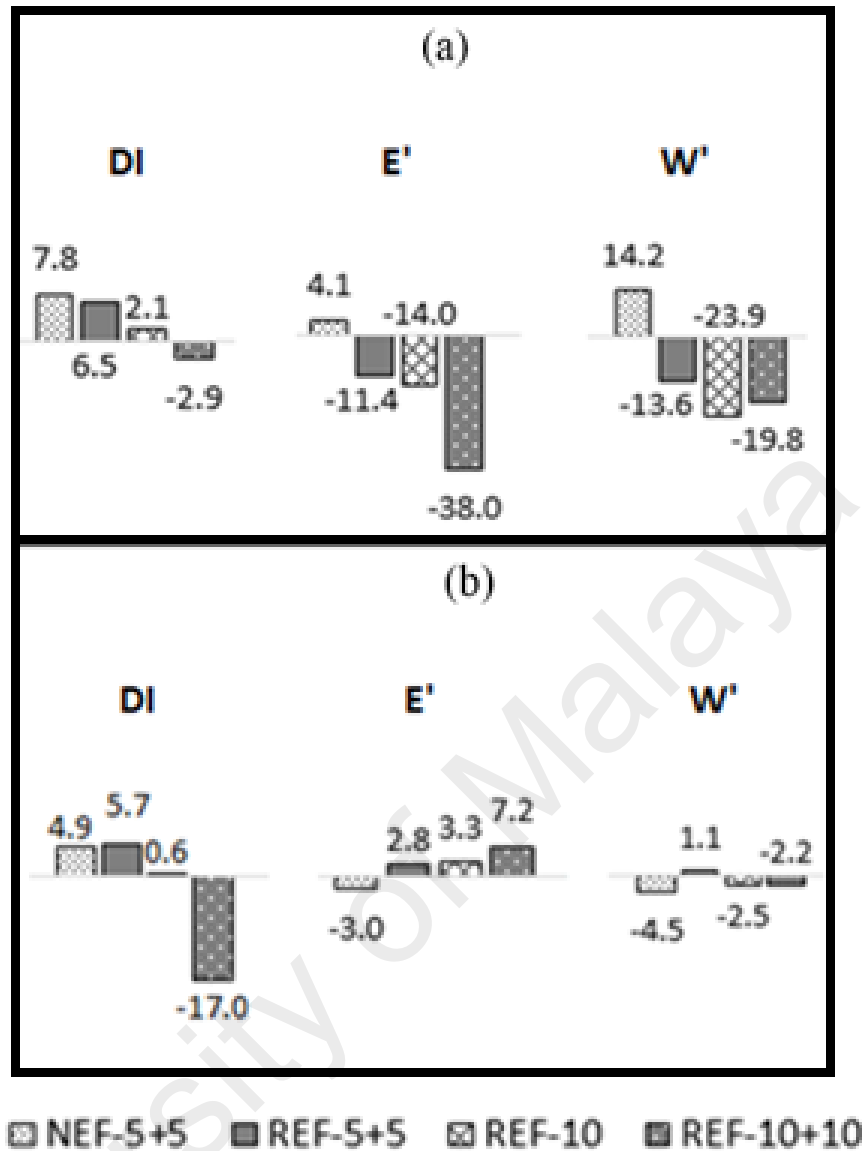


**Figure 5.10: Percentage difference of intraventricular flow energetic indices (DI, E' and W') between healthy LV and each infarct model in systole (a) and diastole (b).**

#### 5.4.1.5 Correlations among vortex, flow energetics and LVEF

Figure 5.11 showed strong correlation between E', LVEF and vortex during systole and diastole. In systole, there was a very strong correlation between E' and LVEF ( $R^2=0.982$ ) as indicated in Figure 5.11a. Higher systolic E' was expected in LV with stronger LVEF. Surprisingly, there was also a strong correlation between systolic E' and diastolic E' ( $R^2 = 0.970$ ), as shown in Figure 5.11b. During diastole, strong negative relationships were noted between E' and vortex KE ( $R^2 = 0.960$ ) (Figure 5.11c) as well

as  $E'$  and vortex depth ( $R^2 = 0.876$ ) (Figure 5.11d). Lower diastolic  $E'$  was acquired when the energetic vortex propagated deeper into LV cavity during diastole.

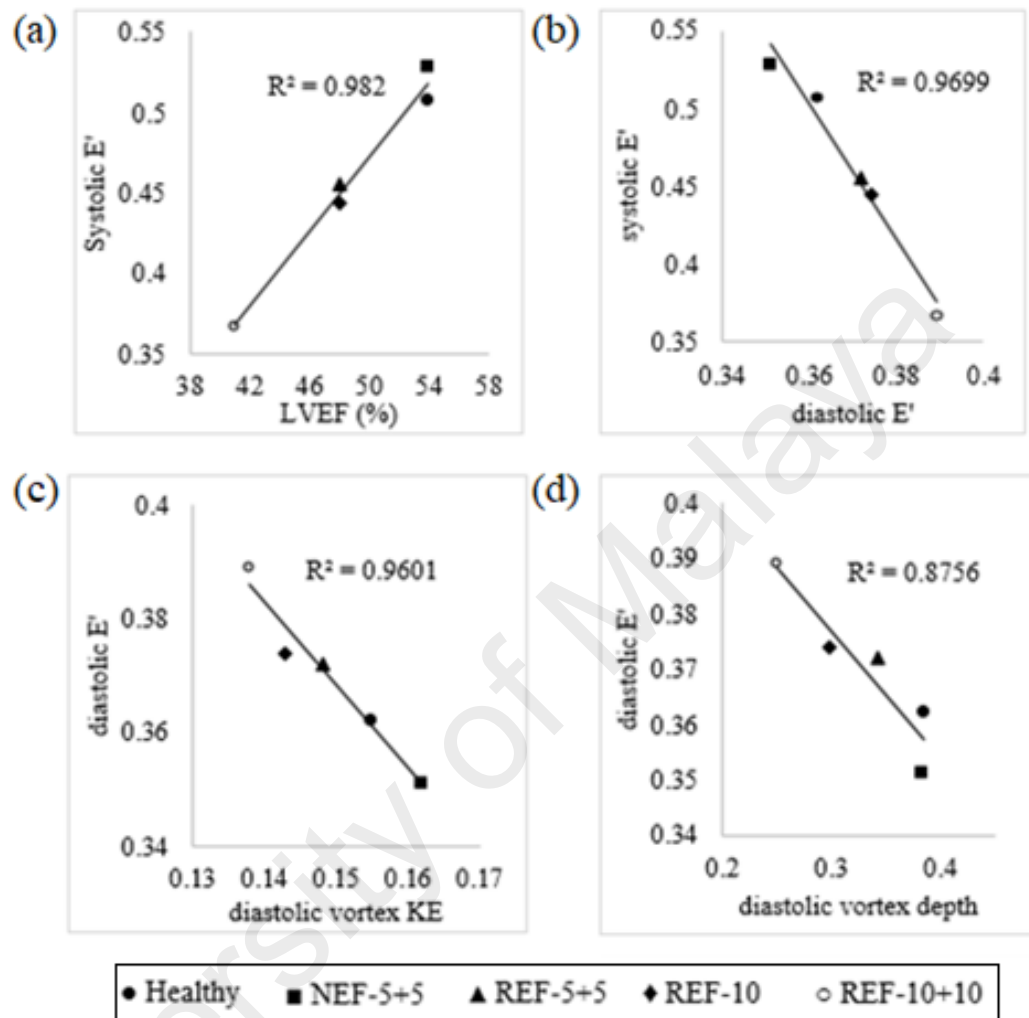


**Figure 5.11: Relationships among  $E'$ , LVEF and vortex during systole (a, b) and diastole (c, d).**

## 5.5 Discussion

This computational study analyses the underlying relationship between MI parameters (infarct size, infarct multiplicity, LVMD, and RECV) and intraventricular vortex and flow-energetic indices. The results in this study agreed with previous findings where myocardial fibre strains were not uniform across all infarct models because of the regional heterogeneity caused by the infarct (Gao et al., 2014; Leong et al., 2017). The SDI results (SDI in healthy = 5.8%; SDI in infarcted LV = 8.9 – 11.5%) were comparable with earlier studies which acquired the SDI using real-time three-dimensional echocardiography

(RT3DE). Based on the assessment of 60 healthy volunteers and 84 heart disease patients, Soliman et al. (Soliman et al., 2009) reported a mean SDI value of 4.1% in healthy volunteers, 13.4% for heart disease patients. In another study on 23 AMI patients, a mean SDI value of 8.1% was reported (Delgado et al., 2008). The intraventricular 3D vortex evolution was similar to a recent imaging study of healthy LVs (Elbaz et al., 2014). The vortex evolution concurred with earlier imaging studies (Hong et al., 2008; Zhang et al., 2013) that the vortex evolves more rapidly in the healthy LV than infarct models.

This study showed that the presence of infarct could lead to higher DI value. In the results, all infarct models had higher DI than healthy LVs, except the weakest LV with the largest infarct (REF-10+10). The infarct did not actively contract or relax, but neighbouring remote muscles had to compensate its loss of function during systole and diastole (Figure 5.7). Thus, this conflicting myocardial movement had led to a waste of mechanical work (Watanabe et al., 2004). The wasted energy was immediately transferred as flow frictional EL (Elbaz et al., 2017) and revealed as viscous EL (Figure 5.9d-f). Besides infarct, a high viscous EL and DI value at the endocardium could also be caused by the presence of a vortex, which would induce friction in blood flow, especially at the blood-wall interface (Elbaz et al., 2017; Pedrizzetti & Domenichini, 2005). When the effects of the infarct and vortex were combined, the viscous EL and DI values would be significantly augmented, particularly at the infarct site, as seen in Figure 5.9f. By having analogous LVMD, the results showed that DI values were around two-times higher in LVs with multiple infarcts. In the present study, the region of contact between infarct and strong vortex was larger in LVs with multiple infarcts, thus vortex-infarct interaction was enhanced. In addition, high viscous EL and DI could also be caused by the appearance of multiple infarcts, which caused more flow disturbance, especially in between two infarcts (Figure 5.9g).

Although REF-10+10 had the highest degree of LVMD (reflected by SDI), it demonstrated the smallest DI in both systole and diastole (Figure 5.10). As observed in Figure 6, REF-10+10 had the lowest intraventricular velocity, which caused a low blood-wall frictional EL, producing smaller viscous EL and DI values. Unlike other infarct models, which had stronger LVEF, REF-10+10 showed greater DI within its infarct rather than beneath the inlet and outlet. This was caused by the poor flow acceleration at the inlet and outlet of REF-10+10. The slow vortex propagation prolonged its residence at mid-height LV, which was adjacent to the infarct. On the contrary, NEF-5+5 demonstrated the greatest DI among all infarct models although it had the lowest degree of LVMD. At the same time, it had the most vigorous intraventricular flow acceleration. Akiyama et al. (2017) reported strong correlation between viscous EL to flow acceleration. The findings suggested that the vigorous intraventricular flow acceleration could precede LVMD in amplifying DI in infarcted LVs.

In terms of KE flow fluctuation indices ( $E'$ ), the results showed that only RECV (NEF-5+5) demonstrated an excessive  $E'$ , while the rest of the infarct models had much lower  $E'$  than healthy LV during systole (Figure 5.10a). However, the opposite phenomenon was observed during diastole (Figure 5.10b). In a recent echo-PIV study, PNEF were found to have augmented  $E'$  in a full cardiac cycle and this was interpreted as an undesirable flow turbulence that led to excessive EL (Agati et al., 2014). In another CFD study, which found substantial flow fluctuations in healthy LV, Chnafa et al. (2016) proposed that flow fluctuation itself was not a sign of pathology, unless there was also significant EL. In this study, flow-energetic indices (DI,  $E'$  and  $W'$ ) were separated into systole and diastole values. Additionally, the individual correlation between flow-energetic indices and different factors were analysed. Based on the findings in this study, the existence of higher level of systolic  $E'$  is believed to be able to characterise the energetic flow acceleration in systole. This is supported by a strong relationship between

$E'$  and LVEF in that cardiac phase (Figure 5.11a). Due to the presence of infarct, a more forceful systolic flow (greater systolic  $E'$ ) was generated by RECVF to expel the same amount of blood as a healthy model. This would explain why NEF-5+5 demonstrated a stronger flow acceleration and  $E'$  than healthy LV during systole (Figure 5.10a).

In diastole, a high diastolic  $E'$  value is proposed to signify inefficient blood filling. Diastolic  $E'$  had been observed to have a strong inverse relationship with vortex KE (Figure 5.11c) and depth during diastole (Figure 5.11d). This suggested that an energetic diastolic vortex could enhance LV filling process by pulling the incoming flow into the LV cavity (Bermejo et al., 2014) as observed in NEF-5+5 and healthy LV, which demonstrated high vortex KE and depth during diastole. Interestingly, NEF-5+5 released more systolic and stored more diastolic vortex KE than the healthy model. This also suggested the vortex's role in systolic-diastolic coupling to maintain cardiac output (Abe et al., 2013; Kojima et al., 2012). Yoshida et al. (2006) reported that the absence of an inertia force in late systolic flow could lead to impaired diastolic filling. In conjunction with the proposed roles of  $E'$  in systole and diastole, it is hypothesized the LV systolic-diastolic coupling mechanism could be indicated by the connection between systolic  $E'$  and diastolic  $E'$ . Coincidentally, all LV models demonstrated an opposite trend of systolic  $E'$  to the diastolic  $E'$  (Figure 5.10). Meanwhile, a remarkable inverse correlation was noted between systolic  $E'$  and diastolic  $E'$  (Figure 5.11b).

The high systolic  $W'$  is interpreted as an evolution of the energetic vortex during systole because of its similar trend to systolic  $E'$ . However, unlike  $E'$ , there was no strong correlation between  $W'$  and other factors, including LVEF and vortex. On the other hand, as observed in REF-10+10, a large infarct caused the weakest systolic  $E'$  and  $W'$  due to the sluggish intraventricular flow and its inactive vortex.

### 5.5.1 Clinical implications

There has been immense interest in the evaluation of blood flow dynamics in cardiac function analysis for their ability to provide independent and prognostic information over conventional measures (Bahlmann et al., 2013; Hong et al., 2013; Pedrizzetti et al., 2014). The present study reveals the underlying relationship between MI, vortex and flow energetics using a 3D electro-FSI model. The findings show that the existence of vigorous flow acceleration, dyssynchrony in LV motion and vortex-infarct interaction was the culprits behind excessive viscous energy dissipation in early MI. In all patients, excessive viscous EL and DI was observed in regions adjacent to the infarct, especially when they come into contact with strong vortices. Previous studies have reported that substantial viscous energy dissipation would diminish intraventricular flow efficiency, leading to a progressively weakened cardiac function and adverse LV remodelling (Mangual et al., 2013; Pedrizzetti & Sengupta, 2015).

Although viscous energy dissipation inside the LV cavity is considered small as compared to the LV stroke work, this study showed a substantial regional viscous energy loss near the infarct-vortex interaction region. In a previous simulation study (Leong et al., 2017), localized high fibre stress, impaired myocardial energy efficiency and elevated energy expenditure has been found at the border zone (surrounding the infarct area), leading to infarct extension and LV remodelling. It is believed that regional elevation of the viscous energy loss nearby the infarct region may increase the work requirement of the border zone tissues during cardiac contraction, thus augmenting the oxygen consumption to activate the additional chemical work. This is further supported by a recent study (Honda et al., 2017) which observed a positive correlation between intraventricular energy loss and serum brain natrium peptide (BNP), predominantly secreted from the ventricles in response to volume or pressure load (Levin, Gardner, & Samson, 1998). In another study, serum BNP levels have been shown to reflect

compensatory mechanism to preserve heart function (Koch, Zink, & Singer, 2006). Thus, any interventions that aim to inhibit extension of the infarct area, such as polymer injection (Nelson, Ma, Fujimoto, Hashizume, & Wagner, 2011) and patching (Dor, 2001), or to improve homogeneity in cardiac contraction, such as cardiac resynchronization therapy (Bleeker et al., 2006), are believed to help minimize energy dissipation and delay the corresponding LV remodelling events.

In addition, the present study revealed that systolic DI is a better early indicator for flow abnormality in MI patients as compared to systolic  $E'$ . Instead of being a negative measure of LV functional efficiency as proposed in a previous study (Agati et al., 2014), our study indicated that systolic  $E'$  characterizes energetic flow acceleration in systole and is strongly correlated to LVEF. On the contrary, based on the results of this study, high diastolic  $E'$  signifies impaired diastolic blood filling in MI patients. It could therefore be used as a potential early indicator for progressive diastolic impairment in MI patients, particularly in those with arrhythmia whose diastolic function assessment is difficult to be performed using Doppler echocardiography (Henein & Lindqvist, 2015).

## **5.6 Conclusion**

This study investigated the impact of infarct size, infarct multiplicity, LVMD and RECVI on flow-energetic indices and vortex flow. The RECVI and infarct multiplicity would induce excessive DI in the LV due to LVMD, systolic flow acceleration and vortex-infarct interaction. Instead of creating undesired flow turbulence, high systolic  $E'$  suggested the existence of an energetic flow acceleration while high diastolic  $E'$  implied inefficient vortex dynamics. Additionally, the infarcted LV with normal LVEF could be differentiated from a healthy LV through an excessive systolic DI value.

## CHAPTER 6: CONCLUSION AND RECOMMENDATIONS

The main findings related to the research objectives and their contributions are summarised in this chapter. Furthermore, recommendations on future work are also presented.

### 6.1 Summary and conclusion

This thesis has proposed several Vp measurement techniques and recommended the most consistent Vp measurement techniques (i.e. AV method) to be used for Vp analysis. With the use of 2D PC-MRI that has higher dimensional spatial-temporal data than the conventional Vp measurement using 1D CMMD, the findings of this study showed that the Vp measurement was affected by both the inflow jet direction and measurement positions. The Vp results acquired from the proposed AV method presented good correlation with the isovolumic relaxation myocardial strain rate. In addition, notable difference in mean Vp was observed between healthy subjects and MI patients using the AV method at one-half distance. Therefore, the use of AV method based on mean forward flow, at the one-half distance between the MLT-inflow and the apex was recommended for assessing diastolic dysfunction given varying LV sizes and inflow jet directions. As such, the proposed AV method was used for Vp analysis in the following objective to quantify Vp (as one of the intraventricular flow variables) among all healthy and MI patients.

Based on the 2D image analysis, this thesis has evaluated the intraventricular flow variables, including Vp, flow-energetic indices and vortex parameters in 20 healthy subjects and 30 MI patients. This study systematically collates and correlates the intraventricular flow variables with myocardial abnormality (based on LV wall motion and dyssynchrony) and LVEF in MI patients. No significant differences in intraventricular flow variables between the healthy group and MI patients with normal

LVEF, whereas considerable reductions in  $E'$  and vortex KE were found in the MI patients with reduced LVEF. In multivariate analysis, only vortex KE and infarct size were significantly related to LVEF. Furthermore, vortex KE was correlated negatively with DI. This 2D flow analysis study highlights that the flow energetic indices have limited applicability as early predictors of LV progressive dysfunction, whereas the vortex KE could be scrutinized as an alternative to LV performance.

In order to understand the pathophysiology of MI, the flow analysis based on clinical images could be restricted due to high variability in MI patient characteristics and the existence of various confounding factors. Therefore this study has incorporated a generic 3D FSI models with varying MI parameters, including infarct sizes, infarct multiplicity, LVMD, and RECVL to study the impacts of individual MI parameters on intraventricular flow for LV dysfunction. Based on the investigation, the RECVL and infarct multiplicity was found to induce excessive DI due to LVMD and systolic flow acceleration as well as the vortex-infarct interaction. Instead of creating an undesired flow turbulence, high systolic  $E'$  suggested the existence of an energetic flow acceleration while high diastolic  $E'$  implied an inefficient vortex dynamics. Additionally, the infarcted LV with normal LVEF could be differentiated from a healthy LV through an excessive systolic DI value.

## **6.2 Recommendation for future studies**

The present study proposed potential flow indicators based on findings from the collected data. However, the analysis of the present study was based on a small number of subjects and uneven gender distribution (less female patients) although gender difference has been reported to be unrelated to intraventricular flow (Mego et al., 1998). Moreover, the analysis of this study used multi-slice PC-MRI which only involved 2D in-plane flow fields and vortex and the out-of-plane swirling flow motion was neglected. In future, data from a larger population and even gender distribution are to be collected

in order to further verify the preliminary results and draw more concrete conclusions. Further improvement of the flow analysis using 3D flow fields is to be studied with the use of 4D flow MRI (Callaghan et al., 2016; Elbaz et al., 2017).

The pathophysiology of MI is complicated and is associated with many physiological changes, such as stroke volume, heart rate and EDV, that could also affect the flow energetic indices in the LV (Vasudevan et al., 2017). However, the model formulation in this thesis focuses on key parameters directly related to the infarct, including LV mechanical dyssynchrony, infarct size, infarct multiplicity and regional enhancement contractility at the viable myocardium, to investigate the causal relationship between these variables and the intraventricular flow variables through structural and flow dynamics changes. Therefore, while EDV was fixed across all models to isolate the effect of LV size, most other variables, including SV and wall motion, were allowed to change naturally according to the simulation scenario. Future works can be done by considering the effect of the other possible scenarios that could occur in MI.

In the model implementation, the LV base of the FSI model was fixed in place. This fixed LV base could lead to a remarkably high stress near the LV fixed basal plane. However, the regional stress distribution at the other area of the myocardium were not affected. Therefore, in this study, the hemodynamics within 1cm under the basal plane was excluded from result analysis. In addition, the mitral and aortic valves were modelled as a fixed opening orifice instead of flexible valve leaflets. Nevertheless, the vortex evolution and velocity streamlines showed concurrence with results from clinical studies (Hong et al., 2008; Zhang et al., 2013) because the intraventricular flow field was predominantly determined by the formation of a diastolic filling jet at the inlet (Krittian, Janoske, Oertel, & Böhlke, 2010). In future, the incorporation of asymmetric mitral valve leaflets (Dahl et al., 2012) and adding both mitral and aortic valve tracts into the FSI

model are required for pragmatic mitral valve dynamics as well as accurate stress distribution near LV base.

The electrical activation was simplified where the impulse conduction through Purkinje fibre network was neglected. However, our activation profile was agreed to human isolated heart (Durrer et al., 1970). The complete electrical impulse conduction through Purkinje fibre network (Bakir et al., 2017) can be considered in future studies. Instead using a patient-specific geometry, the present study used a generalised geometry for model investigation, which does not accurately represent the LV outflow tract. Nonetheless, the findings on intraventricular flow velocity and vortex evolution were in line with the results of published clinical studies (Abe et al., 2013; Elbaz et al., 2014; Zhang et al., 2013). Simulations using generalized models are much less computationally expensive and allow global predictions of cardiac function. For accurate model validation, future work are to be carried out with the use of patient-specific geometry with optimised model formulation and clinical data to predict disease progression.

## REFERENCES

- Abd-Elmoniem, K. Z., Tomas, M. S., Sasano, T., Soleimanifard, S., Vonken, E.-J. P., Youssef, A., Agarwal, H., Dimaano, V. L., Calkins, H., & Stuber, M. (2012). Assessment of distribution and evolution of Mechanical dyssynchrony in a porcine model of myocardial infarction by cardiovascular magnetic resonance. *Journal of Cardiovascular Magnetic Resonance*, *14*(1), 1.
- Abe, H., Caracciolo, G., Kheradvar, A., Pedrizzetti, G., Khandheria, B. K., Narula, J., & Sengupta, P. P. (2013). Contrast echocardiography for assessing left ventricular vortex strength in heart failure: a prospective cohort study. *European Heart Journal–Cardiovascular Imaging*, *14*(11), 1049-1060.
- Agati, L., Cimino, S., Tonti, G., Cicogna, F., Petronilli, V., De Luca, L., Iacoboni, C., & Pedrizzetti, G. (2014). Quantitative analysis of intraventricular blood flow dynamics by echocardiographic particle image velocimetry in patients with acute myocardial infarction at different stages of left ventricular dysfunction. *European Heart Journal - Cardiovascular Imaging*, *15*(11), 1203-1212.
- Akiyama, K., Maeda, S., Matsuyama, T., Kainuma, A., Ishii, M., Naito, Y., Kinoshita, M., Hamaoka, S., Kato, H., Nakajima, Y., Nakamura, N., Itatani, K., & Sawa, T. (2017). Vector flow mapping analysis of left ventricular energetic performance in healthy adult volunteers. *BMC Cardiovascular Disorders*, *17*(1), 21.
- Applegate, E. (2011). *The Anatomy and Physiology Learning System* S. Epstein (Ed.)
- Arefin, M. S., & Morsi, Y. S. (2014). Fluid structure interaction (FSI) simulation of the left ventricle (LV) during the early filling wave (E-wave), diastasis and atrial contraction wave (A-wave). *Australasian Physical and Engineering Sciences in Medicine*, *37*(2), 413-423.
- Arvidsson, P. M., Kovács, S. J., Töger, J., Borgquist, R., Heiberg, E., Carlsson, M., & Arheden, H. (2016). Vortex ring behavior provides the epigenetic blueprint for the human heart. *Scientific Reports*, *6*, 22021.
- Athanasuleas, C. L., Buckberg, G. D., Stanley, A. W. H., Siler, W., Dor, V., Di Donato, M., Menicanti, L., Almeida de Oliveira, S., Beyersdorf, F., Kron, I. L., Suma, H., Kouchoukos, N. T., Moore, W., McCarthy, P. M., Oz, M. C., Fontan, F., Scott, M. L., & Accola, K. A. (2004). Surgical ventricular restoration in the treatment of congestive heart failure due to post-infarction ventricular dilation. *Journal of the American College of Cardiology*, *44*(7), 1439-1445.
- Baccani, B., Domenichini, F., Pedrizzetti, G., & Tonti, G. (2002). Fluid dynamics of the left ventricular filling in dilated cardiomyopathy. *Journal of Biomechanics*, *35*(5), 665-671.
- Bahlmann, E., Gerds, E., Cramariuc, D., Gohlke-Baerwolf, C., Nienaber, C. A., Wachtell, K., Seifert, R., Chambers, J. B., Kuck, K. H., & Ray, S. (2013). Prognostic Value of Energy Loss Index in Asymptomatic Aortic Stenosis. *Circulation*.

- Bakir, A. A., Al-Abed, A., Lovell, N. H., & Dokos, S. (2017, 11-15 July 2017). *A generic cardiac biventricular fluid-electromechanics model*. Paper presented at the 2017 39th Annual International Conference of the IEEE Engineering in Medicine and Biology Society (EMBC).
- Bellhouse, B. (1972). Fluid mechanics of a model mitral valve and left ventricle. *Cardiovascular Research*, 6(2), 199-210.
- Bermejo, J., Benito, Y., Alhama, M., Yotti, R., Martinez-Legazpi, P., Del Villar, C. P., Perez-David, E., Gonzalez-Mansilla, A., Santa-Marta, C., Barrio, A., Fernandez-Aviles, F., & Del Alamo, J. C. (2014). Intraventricular vortex properties in nonischemic dilated cardiomyopathy. *American Journal of Physiology-Heart and Circulatory Physiology*, 306(5), H718-729.
- Bird, R. B., Stewart, W. E., & Lightfoot, E. N. (2002). *Transport phenomena*.
- Bleeker, G. B., Holman, E. R., Steendijk, P., Boersma, E., van der Wall, E. E., Schalij, M. J., & Bax, J. J. (2006). Cardiac resynchronization therapy in patients with a narrow QRS complex. *Journal of the American College of Cardiology*, 48(11), 2243-2250.
- Buss, S. J., Breuninger, K., Lehrke, S., Voss, A., Galuschky, C., Lossnitzer, D., Andre, F., Ehlermann, P., Franke, J., & Taeger, T. (2015). Assessment of myocardial deformation with cardiac magnetic resonance strain imaging improves risk stratification in patients with dilated cardiomyopathy. *European Heart Journal-Cardiovascular Imaging*, 16(3), 307-315.
- Cain, P. A., Ahl, R., Hedstrom, E., Ugander, M., Allansdotter-Johnsson, A., Friberg, P., & Arheden, H. (2009). Age and gender specific normal values of left ventricular mass, volume and function for gradient echo magnetic resonance imaging: a cross sectional study. *BMC Medical Imaging*, 9(1), 2.
- Calkoen, E. E., Marsan, N. A., Bax, J. J., van den Boogaard, P. J., Roest, A. A., de Roos, A., & Westenberg, J. J. (2015). High temporal velocity encoded MRI for the assessment of left ventricular inflow propagation velocity: Comparison with color M-mode echocardiography. *Journal of Magnetic Resonance Imaging*, 42(5), 1297-1304.
- Callaghan, F. M., Kozor, R., Sherrah, A. G., Vallely, M., Celermajer, D., Figtree, G. A., & Grieve, S. M. (2016). Use of multi - velocity encoding 4D flow MRI to improve quantification of flow patterns in the aorta. *Journal of Magnetic Resonance Imaging*, 43(2), 352-363.
- Carlsson, M., Heiberg, E., Toger, J., & Arheden, H. (2012). Quantification of left and right ventricular kinetic energy using four-dimensional intracardiac magnetic resonance imaging flow measurements. *American Journal of Physiology-Heart and Circulatory Physiology*, 302(4), H893-H900.
- Chahal, N. S., Lim, T. K., Jain, P., Chambers, J. C., Kooner, J. S., & Senior, R. (2012). Population-based reference values for 3D echocardiographic LV volumes and ejection fraction. *Journal of the American College of Cardiology: Cardiovascular Imaging*, 5(12), 1191-1197.

- Chan, B. T., Abu Osman, N. A., Lim, E., Chee, K. H., Abdul Aziz, Y. F., Abed, A. A., Lovell, N. H., & Dokos, S. (2013). Sensitivity analysis of left ventricle with dilated cardiomyopathy in fluid structure simulation. *PloS One*, 8(6), e67097.
- Chan, B. T., Yeoh, H. K., Liew, Y. M., Dokos, S., Al Abed, A., Chee, K. H., Aziz, Y. F. A., Sridhar, G. S., Chinna, K., & Lim, E. (2018). Quantitative analysis of intraventricular flow-energetics and vortex in ischaemic hearts. *Coronary Artery Disease*, 29(4), 316-324.
- Chang, S.-A., Chang, H.-J., Choi, S. I., Chun, E. J., Yoon, Y. E., Kim, H.-K., Kim, Y.-J., Choi, D.-J., Sohn, D.-W., & Helm, R. H. (2009). Usefulness of left ventricular dyssynchrony after acute myocardial infarction, assessed by a tagging magnetic resonance image derived metric, as a determinant of ventricular remodeling. *The American Journal of Cardiology*, 104(1), 19-23.
- Charonko, J. J., Kumar, R., Stewart, K., Little, W. C., & Vlachos, P. P. (2013). Vortices formed on the mitral valve tips aid normal left ventricular filling. *Annals of Biomedical Engineering*, 41(5), 1049-1061.
- Chen, S., Yuan, J., Qiao, S., Duan, F., Zhang, J., & Wang, H. (2014). Evaluation of left ventricular diastolic function by global strain rate imaging in patients with obstructive hypertrophic cardiomyopathy: a simultaneous speckle tracking echocardiography and cardiac catheterization study. *Echocardiography*, 31(5), 615-622.
- Cheng, Y., Oertel, H., & Schenkel, T. (2005). Fluid-structure coupled CFD simulation of the left ventricular flow during filling phase. *Annals of Biomedical Engineering*, 33(5), 567-576.
- Ching, S. M., Chia, Y. C., Chong, W. P., & Jalalian, M. (2014). Determinants of left ventricular hypertrophy among elderly hypertensive in Malaysia. *Asia Life Sciences*, 23(1), 1-9.
- Chnafa, C., Mendez, S., & Nicoud, F. (2016). Image-based simulations show important flow fluctuations in a normal left ventricle: what could be the implications? *Annals of Biomedical Engineering*, 44(11), 3346-3358.
- Cohn, J. N., Ferrari, R., & Sharpe, N. (2000). Cardiac remodeling—concepts and clinical implications: a consensus paper from an international forum on cardiac remodeling. *Journal of the American College of Cardiology*, 35(3), 569-582.
- Coronary Artery Disease*. (2015). In J. T. Willerson & J. David R. Homes (Series Eds.),
- D'cruz, I. A., & Sharaf, I. S. (1991). Patterns of Flow Within the Dilated Cardiomyopathy Left Ventricle: Color Flow Doppler Observations. *Echocardiography*, 8(2), 227-231.
- Dahl, S. K., Vierendeels, J., Degroote, J., Annerel, S., Hellevik, L. R., & Skallerud, B. (2012). FSI simulation of asymmetric mitral valve dynamics during diastolic filling. *Computer Methods in Biomechanics and Biomedical Engineering*, 15(2), 121-130.

- De Boeck, B. W., Oh, J. K., Vandervoort, P. M., Vierendeels, J. A., Aa, R. P., & Cramer, M. J. M. (2005). Colour M - mode velocity propagation: a glance at intra - ventricular pressure gradients and early diastolic ventricular performance. *European Journal of Heart Failure*, 7(1), 19-28.
- Delgado, V., Sitges, M., Vidal, B., Silva, E., Azqueta, M., Tolosana, J. M., Mont, L., Paré, C., & Brugada, J. (2008). Assessment of Left Ventricular Dyssynchrony by Real-Time Three-Dimensional Echocardiography. *Revista Española de Cardiología (English Edition)*, 61(08), 825-834.
- Doenst, T., Spiegel, K., Reik, M., Markl, M., Hennig, J., Nitzsche, S., Beyersdorf, F., & Oertel, H. (2009). Fluid-dynamic modeling of the human left ventricle: methodology and application to surgical ventricular reconstruction. *The Annals of Thoracic Surgery*, 87(4), 1187-1195.
- Doll, S., & Schweizerhof, K. (1999). On the Development of Volumetric Strain Energy Functions. *Journal of Applied Mechanics*, 67(1), 17-21.
- Domenichini, F., & Pedrizzetti, G. (2011). Intraventricular vortex flow changes in the infarcted left ventricle: numerical results in an idealised 3D shape. *Computer Methods in Biomechanics and Biomedical Engineering*, 14(01), 95-101.
- Doost, S. N., Ghista, D., Su, B., Zhong, L., & Morsi, Y. S. (2016). Heart blood flow simulation: a perspective review. *Biomedical engineering online*, 15(1), 101.
- Dor, V. (2001). The endoventricular circular patch plasty ("Dor procedure") in ischemic akinetic dilated ventricles. *Heart Failure Reviews*, 6(3), 187-193.
- Durrer, D., Van Dam, R. T., Freud, G., Janse, M., Meijler, F., & Arzbaecher, R. (1970). Total excitation of the isolated human heart. *Circulation*, 41(6), 899-912.
- Dyverfeldt, P., Kvitting, J. P., Sigfridsson, A., Engvall, J., Bolger, A. F., & Ebbers, T. (2008). Assessment of fluctuating velocities in disturbed cardiovascular blood flow: in vivo feasibility of generalized phase-contrast MRI. *Journal of Magnetic Resonance Imaging*, 28(3), 655-663.
- Dyverfeldt, P., Sigfridsson, A., Kvitting, J. P. E., & Ebbers, T. (2006). Quantification of intravoxel velocity standard deviation and turbulence intensity by generalizing phase-contrast MRI. *Magnetic Resonance in Medicine*, 56(4), 850-858.
- Einav, S., & Bluestein, D. (2004). Dynamics of Blood Flow and Platelet Transport in Pathological Vessels. *Annals of the New York Academy of Sciences*, 1015(1), 351-366.
- Elbaz, M. S., Calkoen, E. E., Westenberg, J. J., Lelieveldt, B. P., Roest, A. A., & van der Geest, R. J. (2014). Vortex flow during early and late left ventricular filling in normal subjects: quantitative characterization using retrospectively-gated 4D flow cardiovascular magnetic resonance and three-dimensional vortex core analysis. *Journal of Cardiovascular Magnetic Resonance*, 16(1), 78.
- Elbaz, M. S., van der Geest, R. J., Calkoen, E. E., de Roos, A., Lelieveldt, B. P., Roest, A. A., & Westenberg, J. J. (2017). Assessment of viscous energy loss and the

association with three-dimensional vortex ring formation in left ventricular inflow: In vivo evaluation using four-dimensional flow MRI. *Magnetic Resonance in Medicine*, 77(2), 794-805.

Eriksson, J., Bolger, A. F., Ebbers, T., & Carlhäll, C.-J. (2012). Four-dimensional blood flow-specific markers of LV dysfunction in dilated cardiomyopathy. *European Heart Journal—Cardiovascular Imaging*, 14(5), 417-424.

Flachskampf, F. A., Biering-Sørensen, T., Solomon, S. D., Duvernoy, O., Bjerner, T., & Smiseth, O. A. (2015). Cardiac imaging to evaluate left ventricular diastolic function. *JACC: Cardiovascular Imaging*, 8(9), 1071-1093.

Fritz, T., Wieners, C., Seemann, G., Steen, H., & Dössel, O. (2014). Simulation of the contraction of the ventricles in a human heart model including atria and pericardium. *Biomechanics and Modeling in Mechanobiology*, 13(3), 627-641.

Fukuda, N., Itatani, K., Kimura, K., Ebihara, A., Negishi, K., Uno, K., Miyaji, K., Kurabayashi, M., & Takenaka, K. (2014). Prolonged vortex formation during the ejection period in the left ventricle with low ejection fraction: a study by vector flow mapping. *Journal of Medical Ultrasonics*, 41(3), 301-310.

Fung, Y. C. (1997). *Biomechanics: Circulation* (2nd ed.): Springer.

Gaasch, W. H., & Zile, M. R. (2011). Left ventricular structural remodeling in health and disease: with special emphasis on volume, mass, and geometry. *Journal of the American College of Cardiology*, 58(17), 1733-1740.

Gao, H., Carrick, D., Berry, C., Griffith, B. E., & Luo, X. (2014). Dynamic finite-strain modelling of the human left ventricle in health and disease using an immersed boundary-finite element method. *The IMA journal of applied mathematics*, 79(5), 978-1010.

Garcia, D., del Álamo, J. C., Tanné, D., Yotti, R., Cortina, C., Bertrand, É., Antoranz, J. C., Pérez-David, E., Rieu, R., & Fernández-Avilés, F. (2010). Two-dimensional intraventricular flow mapping by digital processing conventional color-Doppler echocardiography images. *Medical Imaging, IEEE Transactions on*, 29(10), 1701-1713.

Garcia, M. J., Ares, M. A., Asher, C., Rodriguez, L., Vandervoort, P., & Thomas, J. D. (1997). An index of early left ventricular filling that combined with pulsed Doppler peak E velocity may estimate capillary wedge pressure. *Journal of the American College of Cardiology*, 29(2), 448-454.

Garcia, M. J., Thomas, J. D., & Klein, A. L. (1998). New Doppler echocardiographic applications for the study of diastolic function. *Journal of the American College of Cardiology*, 32(4), 865-875.

Gharib, M., Rambod, E., Kheradvar, A., Sahn, D. J., & Dabiri, J. O. (2006). Optimal vortex formation as an index of cardiac health. *Proceedings of the National Academy of Sciences*, 103(16), 6305.

- Göktepe, S., & Kuhl, E. (2010). Electromechanics of the heart: a unified approach to the strongly coupled excitation–contraction problem. *Computational Mechanics*, 45(2-3), 227-243.
- González-Vilchez, F., Ayuela, J., Ares, M., Mata, N. S., González, A. G., & Durán, R. M. (2002). Comparison of Doppler echocardiography, color M-mode Doppler, and Doppler tissue imaging for the estimation of pulmonary capillary wedge pressure. *Journal of the American Society of Echocardiography*, 15(10), 1245-1250.
- Gürel, E., Prinz, C., Van Casteren, L., Gao, H., Willems, R., & Voigt, J.-U. (2016). The impact of function-flow interaction on left ventricular efficiency in patients with conduction abnormalities: a particle image velocimetry and tissue Doppler study. *Journal of the American Society of Echocardiography*, 29(5), 431-440.
- Guyton, A. C. (1986). *Textbook of Medical Physiology*. WB Saunders, Philadelphia, 298-299.
- Halley, C. M., Houghtaling, P. L., Khalil, M. K., Thomas, J. D., & Jaber, W. A. (2011). Mortality rate in patients with diastolic dysfunction and normal systolic function. *Archives of Internal Medicine*, 171(12), 1082-1087.
- Hashimoto, I., Li, X., Bhat, A. H., Jones, M., Zetts, A. D., & Sahn, D. J. (2003). Myocardial strain rate is a superior method for evaluation of left ventricular subendocardial function compared with tissue Doppler imaging. *Journal of the American College of Cardiology*, 42(9), 1574-1583.
- Heiberg, E., Sjögren, J., Ugander, M., Carlsson, M., Engblom, H., & Arheden, H. (2010). Design and validation of Segment—freely available software for cardiovascular image analysis. *BMC Medical Imaging*, 10(1), 1.
- Henein, M. Y., & Lindqvist, P. (2015). Assessment of Left Ventricular Diastolic Function by Doppler Echocardiography. *Cardiac Failure Review*, 1(2), 87-89.
- Hiesinger, W., Brukman, M. J., McCormick, R. C., Fitzpatrick, J. R., Frederick, J. R., Yang, E. C., Muenzer, J. R., Marotta, N. A., Berry, M. F., Atluri, P., & Woo, Y. J. (2012). Myocardial tissue elastic properties determined by atomic force microscopy after stromal cell–derived factor 1 $\alpha$  angiogenic therapy for acute myocardial infarction in a murine model. *The Journal of Thoracic and Cardiovascular Surgery*, 143(4), 962-966.
- Holzapfel, G. A., & Ogden, R. W. (2009). Constitutive modelling of passive myocardium: a structurally based framework for material characterization. *Philosophical Transactions of the Royal Society A: Mathematical Physical and Engineering Sciences*, 367(1902), 3445-3475.
- Honda, T., Itatani, K., Takanashi, M., Kitagawa, A., Ando, H., Kimura, S., Oka, N., Miyaji, K., & Ishii, M. (2017). Exploring energy loss by vector flow mapping in children with ventricular septal defect: Pathophysiologic significance. *International Journal of Cardiology*, 244, 143-150.

- Hong, G.-R., Kim, M., Pedrizzetti, G., & Vannan, M. A. (2013). Current clinical application of intracardiac flow analysis using echocardiography. *Journal of Cardiovascular Ultrasound*, 21(4), 155-162.
- Hong, G. R., Pedrizzetti, G., Tonti, G., Li, P., Wei, Z., Kim, J. K., Baweja, A., Liu, S., Chung, N., Houle, H., Narula, J., & Vannan, M. A. (2008). Characterization and quantification of vortex flow in the human left ventricle by contrast echocardiography using vector particle image velocimetry. *JACC Cardiovasc Imaging*, 1(6), 705-717.
- Hor, K. N., Gottliebson, W. M., Carson, C., Wash, E., Cnota, J., Fleck, R., Wansapura, J., Klimeczek, P., Al-Khalidi, H. R., & Chung, E. S. (2010). Comparison of magnetic resonance feature tracking for strain calculation with harmonic phase imaging analysis. *Journal of the American College of Cardiology: Cardiovascular Imaging*, 3(2), 144-151.
- Houliind, K., Schroeder, A. P., Stødkilde-Jørgensen, H., Paulsen, P. K., Egeblad, H., & Pedersen, E. M. (2002). Intraventricular dispersion and temporal delay of early left ventricular filling after acute myocardial infarction. Assessment by magnetic resonance velocity mapping. *Magnetic Resonance Imaging*, 20(3), 249-260.
- Hsu, E., Muzikant, A., Matulevicius, S., Penland, R., & Henriquez, C. (1998). Magnetic resonance myocardial fiber-orientation mapping with direct histological correlation. *American Journal of Physiology-Heart and Circulatory Physiology*, 274(5), H1627-H1634.
- Ie, E. H., Vletter, W. B., Folkert, J., Nette, R. W., Weimar, W., Roelandt, J. R., & Zietse, R. (2003). Preload dependence of new Doppler techniques limits their utility for left ventricular diastolic function assessment in hemodialysis patients. *Journal of the American Society of Nephrology*, 14(7), 1858-1862.
- Jeong, J., & Hussain, F. (1995). On the identification of a vortex. *Journal of fluid mechanics*, 285, 69-94.
- Kanski, M., Arvidsson, P. M., Töger, J., Borgquist, R., Heiberg, E., Carlsson, M., & Arheden, H. (2015). Left ventricular fluid kinetic energy time curves in heart failure from cardiovascular magnetic resonance 4D flow data. *Journal of Cardiovascular Magnetic Resonance*, 17(1), 111.
- Kaplan, S. R., Bashein, G., Sheehan, F. H., Legget, M. E., Munt, B., Li, X.-N., Sivarajan, M., Bolson, E. L., Zeppa, M., & Archa, M. (2000). Three-dimensional echocardiographic assessment of annular shape changes in the normal and regurgitant mitral valve. *American Heart Journal*, 139(3), 378-387.
- Kasner, M., Gaub, R., Sinning, D., Westermann, D., Steendijk, P., Hoffmann, W., Schultheiss, H.-P., & Tschöpe, C. (2010). Global strain rate imaging for the estimation of diastolic function in HFNEF compared with pressure-volume loop analysis. *European Journal of Echocardiography*, 11(9), 743-751.
- Kempny, A., Fernández-Jiménez, R., Orwat, S., Schuler, P., Bunck, A. C., Maintz, D., Baumgartner, H., & Diller, G.-P. (2012). Quantification of biventricular myocardial function using cardiac magnetic resonance feature tracking,

endocardial border delineation and echocardiographic speckle tracking in patients with repaired tetralogy of fallot and healthy controls. *Journal of Cardiovascular Magnetic Resonance*, 14(1), 1-14.

Khalafvand, S. S., Hung, T.-K., Ng, E. Y.-K., & Zhong, L. (2015). Kinematic, Dynamic, and Energy Characteristics of Diastolic Flow in the Left Ventricle. *Computational and Mathematical Methods in Medicine*, 2015, 701945.

Khalafvand, S. S., Ng, E. Y.-K., Zhong, L., & Hung, T.-K. (2012). Fluid-dynamics modelling of the human left ventricle with dynamic mesh for normal and myocardial infarction: preliminary study. *Computers in Biology and Medicine*, 42(8), 863-870.

Khoury, S. J., Maly, G. T., Suh, D. D., & Walsh, T. E. (2004). A practical approach to the echocardiographic evaluation of diastolic function. *Journal of the American Society of Echocardiography*, 17(3), 290-297.

Kilner, P. J., Yang, G. Z., Wilkes, A. J., Mohiaddin, R. H., Firmin, D. N., & Yacoub, M. H. (2000). Asymmetric redirection of flow through the heart. *Nature*, 404(6779), 759-761.

Kim, W. Y., Walker, P. G., Pedersen, E. M., Poulsen, J. K., Oyre, S., Houlind, K., & Yoganathan, A. P. (1995). Left ventricular blood flow patterns in normal subjects: a quantitative analysis by three-dimensional magnetic resonance velocity mapping. *Journal of the American College of Cardiology*, 26(1), 224-238.

Koch, A., Zink, S., & Singer, H. (2006). B-type natriuretic peptide in paediatric patients with congenital heart disease. *European Heart Journal*, 27(7), 861-866.

Kojima, T., Kameyama, T., Nakajima, H., Khmyrova, E., Kurokawa, T., & Saijo, Y. (2012, Aug. 28 2012-Sept. 1 2012). *Evaluation of vortex flow in left ventricle by echo-dynamography and phase contrast magnetic resonance angiography*. Paper presented at the 2012 Annual International Conference of the IEEE Engineering in Medicine and Biology Society.

Kowallick, J. T., Kutty, S., Edelmann, F., Chiribiri, A., Villa, A., Steinmetz, M., Sohns, J. M., Staab, W., Bettencourt, N., Unterberg-Buchwald, C., Hasenfuß, G., Lotz, J., & Schuster, A. (2014). Quantification of left atrial strain and strain rate using Cardiovascular Magnetic Resonance myocardial feature tracking: a feasibility study. *Journal of Cardiovascular Magnetic Resonance*, 16(1), 1-9.

Krittian, S., Janoske, U., Oertel, H., & Böhlke, T. (2010). Partitioned fluid–solid coupling for cardiovascular blood flow. *Annals of Biomedical Engineering*, 38(4), 1426-1441.

Lang, R. M., Badano, L. P., Mor-Avi, V., Afilalo, J., Armstrong, A., Ernande, L., Flachskampf, F. A., Foster, E., Goldstein, S. A., & Kuznetsova, T. (2015). Recommendations for cardiac chamber quantification by echocardiography in adults: an update from the American Society of Echocardiography and the European Association of Cardiovascular Imaging. *Journal of the American Society of Echocardiography*, 28(1), 1-39. e14.

- Leong, C.-N., Lim, E., Andriyana, A., Al Abed, A., Lovell, N. H., Hayward, C., Hamilton-Craig, C., & Dokos, S. (2017). The role of infarct transmural extent in infarct extension: A computational study. *International Journal for Numerical Methods in Biomedical Engineering*, 33(2).
- Levin, E. R., Gardner, D. G., & Samson, W. K. (1998). Natriuretic peptides. *New England Journal of Medicine*, 339(5), 321-328.
- Liew, Y., McLaughlin, R., Chan, B., Aziz, Y. A., Chee, K., Ung, N., Tan, L., Lai, K., Ng, S., & Lim, E. (2015). Motion corrected LV quantification based on 3D modelling for improved functional assessment in cardiac MRI. *Physics in Medicine and Biology*, 60(7), 2715.
- Lim, E., Dokos, S., Cloherty, S. L., Salamonsen, R. F., Mason, D. G., Reizes, J. A., & Lovell, N. H. (2010). Parameter-optimized model of cardiovascular–rotary blood pump interactions. *IEEE Transactions on Biomedical Engineering*, 57(2), 254-266.
- Loerakker, S., Cox, L., Van Heijst, G., De Mol, B., & Van De Vosse, F. (2008). Influence of dilated cardiomyopathy and a left ventricular assist device on vortex dynamics in the left ventricle. *Computer Methods in Biomechanics and Biomedical Engineering*, 11(6), 649-660.
- Long, Q., Merrifield, R., Xu, X., Kilner, P., Firmin, D., & Yang, G. (2008). Subject-specific computational simulation of left ventricular flow based on magnetic resonance imaging. *Proceedings of the Institution of Mechanical Engineers. Part H: Journal of Engineering in Medicine*, 222(4), 475-485.
- Mangual, J. O., Kraigher-Krainer, E., De Luca, A., Toncelli, L., Shah, A., Solomon, S., Galanti, G., Domenichini, F., & Pedrizzetti, G. (2013). Comparative numerical study on left ventricular fluid dynamics after dilated cardiomyopathy. *Journal of Biomechanics*, 46(10), 1611-1617.
- Mego, D. M., DeGeare, V. S., Nottestad, S. Y., Lamanna, V. P., Oneschuk, L. C., Rubal, B. J., & Zabalgaitia, M. (1998). Variation of flow propagation velocity with age. *Journal of the American Society of Echocardiography*, 11(1), 20-25.
- Moody, W. E., Taylor, R. J., Edwards, N. C., Chue, C. D., Umar, F., Taylor, T. J., Ferro, C. J., Young, A. A., Townend, J. N., & Leyva, F. (2015). Comparison of magnetic resonance feature tracking for systolic and diastolic strain and strain rate calculation with spatial modulation of magnetization imaging analysis. *Journal of Magnetic Resonance Imaging*, 41(4), 1000-1012.
- Mooi, C. S., Chin, C. Y., Ahmad, W. A. W., & Jalalian, M. (2012). Prevalence of left ventricular diastolic dysfunction among hypertensive adults in Klang Valley, Malaysia. *Life Science Journal*, 9(3), 713-719.
- Morris, P. D., Narracott, A., von Tengg-Kobligh, H., Soto, D. A. S., Hsiao, S., Lungu, A., Evans, P., Bressloff, N. W., Lawford, P. V., & Hose, D. R. (2016). Computational fluid dynamics modelling in cardiovascular medicine. *Heart*, 102(1), 18-28.

- Nagueh, S. F., Appleton, C. P., Gillebert, T. C., Marino, P. N., Oh, J. K., Smiseth, O. A., Waggoner, A. D., Flachskampf, F. A., Pellikka, P. A., & Evangelista, A. (2009). Recommendations for the evaluation of left ventricular diastolic function by echocardiography. *Journal of the American Society of Echocardiography*, 22(2), 107-133.
- Nash, M. P., & Panfilov, A. V. (2004). Electromechanical model of excitable tissue to study reentrant cardiac arrhythmias. *Progress in Biophysics and Molecular Biology*, 85(2-3), 501-522.
- Nelson, D. M., Ma, Z., Fujimoto, K. L., Hashizume, R., & Wagner, W. R. (2011). Intramyocardial biomaterial injection therapy in the treatment of heart failure: Materials, outcomes and challenges. *Acta biomaterialia*, 7(1), 1-15.
- Nesser, H.-J., Mor-Avi, V., Gorissen, W., Weinert, L., Steringer-Mascherbauer, R., Niel, J., Sugeng, L., & Lang, R. M. (2009). Quantification of left ventricular volumes using three-dimensional echocardiographic speckle tracking: comparison with MRI. *European Heart Journal*, 30(13), 1565-1573.
- Nguyen, V.-T., Wibowo, S. N., Leow, Y. A., Nguyen, H.-H., Liang, Z., & Leo, H. L. (2015). A patient-specific computational fluid dynamic model for hemodynamic analysis of left ventricle diastolic dysfunctions. *Cardiovascular Engineering and Technology*, 6(4), 412-429.
- Nordsletten, D., McCormick, M., Kilner, P. J., Hunter, P., Kay, D., & Smith, N. P. (2011). Fluid-solid coupling for the investigation of diastolic and systolic human left ventricular function. *International Journal for Numerical Methods in Biomedical Engineering*, 27(7), 1017-1039.
- Nucifora, G., Delgado, V., Bertini, M., Marsan, N. A., Van de Veire, N. R., Ng, A. C., Siebelink, H. M., Schalij, M. J., Holman, E. R., Sengupta, P. P., & Bax, J. J. (2010). Left ventricular muscle and fluid mechanics in acute myocardial infarction. *American Journal of Cardiology*, 106(10), 1404-1409.
- Ogunyankin, K. O. (2011). Assessment of left ventricular diastolic function: the power, possibilities, and pitfalls of echocardiographic imaging techniques. *Canadian Journal of Cardiology*, 27(3), 311-318.
- Pasipoularides, A. (2015). Mechanotransduction mechanisms for intraventricular diastolic vortex forces and myocardial deformations: part 1. *Journal of Cardiovascular Translational Research*, 8(1), 76-87.
- Pasipoularides, A., Shu, M., Shah, A., Womack, M. S., & Glower, D. D. (2003). Diastolic right ventricular filling vortex in normal and volume overload states. *American Journal of Physiology-Heart and Circulatory Physiology*, 284(4), H1064-H1072.
- Pedrizzetti, G., & Domenichini, F. (2005). Nature optimizes the swirling flow in the human left ventricle. *Physical Review Letters*, 95(10), 108101.
- Pedrizzetti, G., La Canna, G., Alfieri, O., & Tonti, G. (2014). The vortex-an early predictor of cardiovascular outcome? *Nature Reviews Cardiology*, 11(9), 545-553.

- Pedrizetti, G., & Sengupta, P. P. (2015). Vortex imaging: new information gain from tracking cardiac energy loss. *European Heart Journal Cardiovascular Imaging*, 16(7), 719-720.
- Peskin, C. S. (1977). Numerical analysis of blood flow in the heart. *Journal of Computational Physics*, 25(3), 220-252.
- Plein, S., Ridgway, J. P., & Greenwood, J. P. (2011). *Cardiovascular MR Manual*: Springer.
- Roes, S. D., Kelle, S., Kaandorp, T. A., Kokocinski, T., Poldermans, D., Lamb, H. J., Boersma, E., van der Wall, E. E., Fleck, E., & de Roos, A. (2007). Comparison of myocardial infarct size assessed with contrast-enhanced magnetic resonance imaging and left ventricular function and volumes to predict mortality in patients with healed myocardial infarction. *American Journal of Cardiology*, 100(6), 930-936.
- Saber, N. R., Wood, N. B., Gosman, A., Merrifield, R. D., Yang, G.-Z., Charrier, C. L., Gatehouse, P. D., & Firmin, D. N. (2003). Progress towards patient-specific computational flow modeling of the left heart via combination of magnetic resonance imaging with computational fluid dynamics. *Annals of Biomedical Engineering*, 31(1), 42-52.
- Sato, M., Toyama, T., Kasama, S., Hoshizaki, H., Oshima, S., & Kurabayashi, M. (2017). Left Ventricular Mechanical Dyssynchrony after Acute Myocardial Infarction Assessed by CardioGRAF Analysis is a Predictor of Subsequent Cardiac Events. *Annals of Nuclear Cardiology*, 3(1), 20-28.
- Schenkel, T., Malve, M., Reik, M., Markl, M., Jung, B., & Oertel, H. (2009). MRI-based CFD analysis of flow in a human left ventricle: methodology and application to a healthy heart. *Annals of Biomedical Engineering*, 37(3), 503-515.
- Schuster, A., Stahnke, V.-C., Unterberg-Buchwald, C., Kowallick, J., Lamata, P., Steinmetz, M., Kutty, S., Fasshauer, M., Staab, W., & Sohns, J. (2015). Cardiovascular magnetic resonance feature-tracking assessment of myocardial mechanics: intervender agreement and considerations regarding reproducibility. *Clinical Radiology*, 70(9), 989-998.
- Scollan, D. F., Holmes, A., Winslow, R., & Forder, J. (1998). Histological validation of myocardial microstructure obtained from diffusion tensor magnetic resonance imaging. *The American journal of physiology*, 275(6 Pt 2), H2308-2318.
- Sengupta, P. P., Khandheria, B. K., Korinek, J., Jahangir, A., Yoshifuku, S., Milosevic, I., & Belohlavek, M. (2007). Left ventricular isovolumic flow sequence during sinus and paced rhythms - New insights from use of high-resolution Doppler and ultrasonic digital particle imaging velocimetry. *Journal of the American College of Cardiology*, 49(8), 899-908.
- Sengupta, P. P., Pedrizetti, G., Kilner, P. J., Kheradvar, A., Ebberts, T., Tonti, G., Fraser, A. G., & Narula, J. (2012). Emerging trends in CV flow visualization. *Journal of the American College of Cardiology: Cardiovasc Imaging*, 5(3), 305-316.

- Seo, Y., Ishizu, T., Enomoto, Y., Sugimori, H., Yamamoto, M., Machino, T., Kawamura, R., & Aonuma, K. (2009). Validation of 3-dimensional speckle tracking imaging to quantify regional myocardial deformation. *Circulation: Cardiovascular Imaging*, 2(6), 451-459.
- Simaan, M. A., Ferreira, A., Chen, S., Antaki, J. F., & Galati, D. G. (2009). A dynamical state space representation and performance analysis of a feedback-controlled rotary left ventricular assist device. *IEEE Transactions on Control Systems Technology*, 17(1), 15-28.
- Soliman, O. I. I., van Dalen, B. M., Nemes, A., Zwaan, H. B. v. d., Vletter, W. B., ten Cate, F. J., Theuns, D. A. M. J., Jordaens, L. J., & Geleijnse, M. L. (2009). Quantification of Left Ventricular Systolic Dyssynchrony by Real-Time Three-Dimensional Echocardiography. *Journal of the American Society of Echocardiography*, 22(3), 232-239.
- Son, J.-W., Park, W.-J., Choi, J.-H., Houle, H., Vannan, M. A., Hong, G.-R., & Chung, N. (2012). Abnormal left ventricular vortex flow patterns in association with left ventricular apical thrombus formation in patients with anterior myocardial infarction. *Circulation Journal*, 76(11), 2640-2646.
- Steding-Ehrenborg, K., Arvidsson, P. M., Töger, J., Rydberg, M., Heiberg, E., Carlsson, M., & Arheden, H. (2015). Determinants of kinetic energy of blood flow in the four-chambered heart in athletes and sedentary controls. *American Journal of Physiology-Heart and Circulatory Physiology*, 310(1), H113-H122.
- Stewart, K. C., Kumar, R., Charonko, J. J., Ohara, T., Vlachos, P. P., & Little, W. C. (2011). Evaluation of LV diastolic function from color M-mode echocardiography. *JACC: Cardiovascular Imaging*, 4(1), 37-46.
- Stugaard, M., Koriyama, H., Katsuki, K., Masuda, K., Asanuma, T., Takeda, Y., Sakata, Y., Itatani, K., & Nakatani, S. (2015). Energy loss in the left ventricle obtained by vector flow mapping as a new quantitative measure of severity of aortic regurgitation: a combined experimental and clinical study. *European Heart Journal-Cardiovascular Imaging*, 16(7), 723-730.
- Sundareswaran, K. S., Haggerty, C. M., De Zélicourt, D., Dasi, L. P., Pekkan, K., Frakes, D. H., Powell, A. J., Kanter, K. R., Fogel, M. A., & Yoganathan, A. P. (2012). Visualization of flow structures in Fontan patients using 3-dimensional phase contrast magnetic resonance imaging. *The Journal of Thoracic and Cardiovascular Surgery*, 143(5), 1108-1116.
- Tang, D., Yang, C., Geva, T., & Pedro, J. (2010). Image-based patient-specific ventricle models with fluid-structure interaction for cardiac function assessment and surgical design optimization. *Progress in Pediatric Cardiology*, 30(1), 51-62.
- Usyk, T., Mazhari, R., & McCulloch, A. (2000). Effect of laminar orthotropic myofiber architecture on regional stress and strain in the canine left ventricle. *Journal of elasticity and the physical science of solids*, 61(1-3), 143-164.
- Van Dantzig, J. M., Delemarre, B. J., Bot, H., Koster, R. W., & Visser, C. A. (1995). Doppler left ventricular flow pattern versus conventional predictors of left

- ventricular thrombus after acute myocardial infarction. *Journal of the American College of Cardiology*, 25(6), 1341-1346.
- van den Boogaard, P. J., Marsan, N. A., Bax, J. J., de Roos, A., & Westenberg, J. J. (2013). Left ventricular inflow propagation velocity for diastolic function testing: head-to-head comparison between velocity-encoded MRI and color M-mode Doppler echocardiography. *Journal of Cardiovascular Magnetic Resonance*, 15(Suppl 1), P54.
- Vasudevan, V., Low, A. J. J., Annamalai, S. P., Sampath, S., Poh, K. K., Totman, T., Mazlan, M., Croft, G., Richards, A. M., & de Kleijn, D. P. (2017). Flow dynamics and energy efficiency of flow in the left ventricle during myocardial infarction. *Biomechanics and Modeling in Mechanobiology*, 16(5), 1503-1517.
- Walker, P. G., Cranney, G. B., Scheidegger, M. B., Waseleski, G., Pohost, G. M., & Yoganathan, A. P. (1993). Semiautomated method for noise reduction and background phase error correction in MR phase velocity data. *Journal of Magnetic Resonance Imaging*, 3(3), 521-530.
- Wang, J., Khoury, D. S., Thohan, V., Torre-Amione, G., & Nagueh, S. F. (2007). Global Diastolic Strain Rate for the Assessment of Left Ventricular Relaxation and Filling Pressures. *Circulation*, 115(11), 1376-1383.
- Wang, Y., Ma, R., Ding, G., Hou, D., Li, Z., Yin, L., & Zhang, M. (2016). Left ventricular energy loss assessed by vector flow mapping in patients with prediabetes and type 2 diabetes mellitus. *Ultrasound in Medicine and Biology*, 42(8), 1730-1740.
- Watanabe, H., Sugano, T., Sugiura, S., & Hisada, T. (2004). Finite element analysis of ventricular wall motion and intra-ventricular blood flow in heart with myocardial infarction. *JSME International Journal Series C Mechanical Systems, Machine Elements and Manufacturing*, 47(4), 1019-1026.
- Watanabe, H., Sugiura, S., & Hisada, T. (2008). The looped heart does not save energy by maintaining the momentum of blood flowing in the ventricle. *American Journal of Physiology-Heart and Circulatory Physiology*, 294(5), H2191-H2196.
- Westaby, S., Karp, R. B., Blackstone, E. H., & Bishop, S. P. (1984). Adult human valve dimensions and their surgical significance. *The American Journal of Cardiology*, 53(4), 552-556.
- Wong, K. K., Kelso, R. M., Worthley, S. G., Sanders, P., Mazumdar, J., & Abbott, D. (2009). Cardiac flow analysis applied to phase contrast magnetic resonance imaging of the heart. *Annals of Biomedical Engineering*, 37(8), 1495-1515.
- World Health Organization. (2015). *Country Statistics and global health estimates*.
- Wu, Y., & Wu, E. X. (2009). MR study of postnatal development of myocardial structure and left ventricular function. *Journal of Magnetic Resonance Imaging*, 30(1), 47-53.
- Yoshida, T., Ohte, N., Narita, H., Sakata, S., Wakami, K., Asada, K., Miyabe, H., Saeki, T., & Kimura, G. (2006). Lack of Inertia Force of Late Systolic Aortic Flow Is a

Cause of Left Ventricular Isolated Diastolic Dysfunction in Patients With Coronary Artery Disease. *Journal of the American College of Cardiology*, 48(5), 983.

Zafari, A. M., Reddy, S., Jeroudi, A., & Garas, S. (2012). Myocardial infarction. *Medscape reference*.

Zajac, J., Eriksson, J., Dyverfeldt, P., Bolger, A. F., Ebbers, T., & Carlhäll, C. J. (2015). Turbulent kinetic energy in normal and myopathic left ventricles. *Journal of Magnetic Resonance Imaging*, 41(4), 1021-1029.

Zhang, H., Liu, L., Chen, L., Ma, N., Zhou, L., Liu, Y., Li, Z., Liu, C., Hou, R., & Zhu, S. (2013). The evolution of intraventricular vortex during ejection studied by using vector flow mapping. *Echocardiography*, 30(1), 27-36.

Zhong, Y., Liu, Y., Wu, T., Song, H., Chen, Z., Zhu, W., Cai, Y., Zhang, W., Bai, W., Tang, H., & Rao, L. (2016). Assessment of Left Ventricular Dissipative Energy Loss by Vector Flow Mapping in Patients With End-Stage Renal Disease. *Journal of Ultrasound in Medicine*, 35(5), 965-973.

University of Malakya

## LIST OF PUBLICATIONS AND PAPERS PRESENTED

### Journal articles:

1. **Bee Ting Chan**, Hak Koon Yeoh, Yih Miin Liew, Yang Faridah Abdul Aziz, Ganiga Srinivasaiah Sridhar, Christian Hamilton-Craig, David Platts, Einly Lim. (2017). Left ventricular flow propagation velocity measurement: Is it cast in stone? *Medical & Biological Engineering & Computing*, **55**(10): 1883-1893.
2. **Bee Ting Chan**, Hak Koon Yeoh, Yih Miin Liew, Socrates Dokos, Amr Al Abed, Kok Han Chee, Yang Faridah Abdul Aziz, Ganiga Srinivasaiah Sridhar, Karuthan Chinna, Einly Lim. (2018). Quantitative analysis of intraventricular flow-energetics and vortex in ischemic hearts. *Coronary Artery Disease*, **29**(4): 316-324.
3. **Bee Ting Chan**, Azam Ahmad Bakir, Amr Al Abed, Socrates Dokos, Chin Neng Leong, Ean Hin Ooi, Einly Lim. Impact of Myocardial Infarction on Intraventricular Vortex and Flow Energetics using Fluid Structure Simulation. *International Journal for Numerical Methods in Biomedical Engineering*. (Under Review).

### Proceedings:

1. **Bee Ting Chan**, Hak Koon Yeoh, Yih Miin Liew, Yang Faridah Abdul Aziz, Kok Han Chee, Ganiga Srinivasaiah Sridhar, Zhen-Vin Lee, Einly Lim. (2016). Quantitative analysis of intraventricular flow dynamics in patients with ischemic heart disease. Oral presentation at *the 16th International Conference on Biomedical Engineering (ICBME 2016)* in National University of Singapore, Singapore.